Supramolecularly Engineered Nanobiocatalysts

Application to Cofactor Independent Oxidoreductase Biocatalysis in Organic Solvents

Inauguraldissertation

zur

Erlangung der Würde eines Doktors der

Philosophie vorgelegt der

Philosophisch-Naturwissenschaftlichen Fakultät der

Universität Basel

von

Jenny Alexandra Sahlin

Basel, 2024

Genehmigt von der Philosophisch-Naturwissenschaftlichen Fakultät

auf Antrag von

Erstbetreuer: Prof. Dr. Patrick Shahgaldian

Zweitbetreuerin: Prof. Dr. Cornelia Palivan

externer Experte: Prof. Dr. Harald Gröger

Basel, den 22. März 2022

Prof. Dr. Marcel Mayor

Dekan

To my parents

Acknowledgements

At this point, I would like to acknowledge those people who helped me in various ways during my time as a PhD student and shape this thesis into what it is. And despite how I may seem in person, in writing I am not a person of many words, I apologise in advance for that.

First and foremost, I would like to thank my supervisor, Prof. Patrick Shahgaldian for giving me the opportunity to work on this project and for valuable advice in the preparation of this thesis. I am grateful for the trust he had in me, the support he gave me when I needed it and the independence he allowed me when I craved it.

I am very grateful to Prof. Cornelia Palivan for stepping in as supervisor for me in this thesis. And I would like to thank the late Prof. Wolfgang Meier for supporting me earlier during my PhD. I would also like to acknowledge Prof. Harald Gröger for agreeing to be part of the final steps of my PhD thesis.

I would like to give special thanks to Daniela Tobler, Jan Bergsch, Chasper Puorger and Boris Kolvenbach. You have all helped me in various ways, from problematic ÄKTA systems (apparently not everything from Sweden is extraordinary) to expression issues. Without your valuable input, there would have been significantly fewer enzymes present within this thesis. I would also like to thank Andy Büttler for teaching me all the tips and tricks when it comes to GC measurements.

I would like to acknowledge all the members of the Shahgaldian group for their support in various ways during the years. It was a pleasure to get to know you all and work with you. Therefore, thank you, Magda, Amir, Congyu, Manon, Ajmal, Caro, Tala and Karen. Additionally, I would like to thank Nicole for the practical support in the lab for my final experiments. I would like to thank the people from INOFEA and Perseo for sharing the lab with us during these past years. So thank you, Lars, Anna, Emilie and Rita.

I would like to give a special thanks to the people who helped me proofread this thesis, Yasmin, Amir, and especially Magda. Without whom, there most likely would not have been any thesis at all to read.

I am eternally grateful to my parents. In particular, my mother for always believing in me and for all the encouragement during the last months of this challenging period. Thanks to you I was reminded that “Just idag är jag stark”.

And most importantly of all, thanks to my dearest Claude. Thanks for caring for me after a hard day in the lab, thanks for teaching me when my chemistry knowledge was too limited, thanks for re-teaching me when I later forgot it all, thanks for waiting patiently for me all late evenings in the lab, thanks for being my most overqualified and lowest paid lab assistance ever, even when my experimental plan had been too ambitious or when everything just went to hell (as it usually did), thanks for joining me in the lab on weekends, thanks for keeping me well-nourished, thanks for being you, thanks for everything.

Abstract

For further advancements in industrial catalysis, enzymes play an important role. Currently, there are numerous examples of industrial biocatalysis. However, when it comes to biocatalysis in organic solvents, cofactor-dependent oxidoreductase enzymes experience implementation difficulties. These enzymes often display reduced stability in organic solvents and their cofactors that are needed in stoichiometric amounts are strictly water soluble. Therefore, the synthesis and application of a novel nanobiocatalyst system for cofactor-independent oxidoreductase catalysis in organic solvents was investigated.

The nanobiocatalyst utilised mesoporous silica nanoparticles as a carrier, of which the mesopores could be exploited as an aqueous reservoir for the cofactor of the enzymes. The mesoporous core particle possessed radial pore channels with large pore size, allowing for a greater volume in which the cofactor could be contained. The inner core was surrounded by a second layer with reduced porosity, serving as a support for the immobilisation of the enzymes while also restricting the immobilisation to the particle's surface. However, still allowing the diffusion of cofactor from the reservoir to the enzyme. The immobilised enzymes were shielded in a protecting organosilica layer grown at the surface of the nanoparticles with a controlled thickness completely covering the enzymes. The produced nanobiocatalysts were characterised by the means of scanning electron and cryogenic transmission electron microscopy to visualise the structure of the obtained nanobiocatalyst. The catalytic properties of the produced nanobiocatalysts were explored by catalysing the reduction of several relevant substrates in different organic solvents (methyl *tert*-butyl ether, ethyl acetate, toluene and heptane) with increasing hydrophobicity, in the absence of additional cofactor. The preserved catalytic properties of the nanobiocatalyst provided evidence of effective cofactor recycling, despite the lack of external cofactor. This inspired further implementation of the produced nanobiocatalyst within a continuous flow reactor for the transformation of the hydrophobic ketone benzylacetone to 4-phenyl-2-butanol with self-sustained cofactor recycling.

Table of Contents

List of figures

List of tables

Abbreviations

3D-MSN	Three-dimensional dendritic mesoporous nanoparticle
ADH	Alcohol dehydrogenase
AmDH	Amine dehydrogenase
API	Active pharmaceutical ingredient
APTES	(3-aminopropyl)triethoxysilane
a_w	Water activity
BS(PEG)5	PEGylated bis(sulfosuccinimidyl)suberate
cryoEM	Cryogenic transmission electron microscopy
CTAB	Cetrimonium bromide
CTAC	Cetrimonium chloride
DLS	Dynamic light scattering
ee	Enantiomeric excess
ER	Ene-reductase
EtOAc	Ethyl acetate
FOYE	Ene-reductase of old yellow enzyme type from *"Ferrovum"* sp. JA12
His-tag	Polyhistidine sequence/tag
***i*-PrOH**	2-Propanol, isopropanol
IRED	Imine reductase
KRED	Ketoreductase
LysNTA	Nα,Nα-Bis(carboxymethyl)-L-lysine
MSN	Mesoporous silica nanoparticle
MSN-NH_2	Amino-functionalised mesoporous silica nanoparticles
$MSN_{Co\text{-}Enz}$	MSNs with two co-immobilised enzymes through affinity
$MSN_{BS(PEG)5\text{-}Enz}$	MSNs with enzyme immobilised through BS(PEG)5
$MSN_{EGS\text{-}Enz}$	MSNs with enzyme immobilised through EGS

$MSN_{EGS\text{-}Enz\text{-}OrgS}$	MSNs with enzyme immobilised through EGS with organosilica layer
MSN_{Enz}	MSNs with enzyme immobilised, linker unspecified
$MSN_{G\text{-}Enz}$	MSNs with enzyme immobilised through glutaraldehyde
$MSN_{NTA\text{-}Enz}$	MSNs with enzyme immobilised through affinity
$MSN_{NTA\text{-}Enz\text{-}OrgS}$	MSNs with enzyme immobilised through affinity with organosilica layer
MTBE	Methyl-tert-butyl-ether
$NADP^+$	Nicotinamide adenine dinucleotide phosphate
NTA	Nitrilotriacetic acid
PDI	Polydispersity index
RedAm	Reductive aminase from *Aspergillus oryzae*
SEM	Field-emission scanning electron microscopy
SyADH	Secondary alcohol dehydrogenase from *Sphingobium yanoikuyae*
TEM	Transmission electron microscopy
TEOS	Tetraethyl orthosilicate
TeSADH	Secondary dehydrogenase from *Thermoanaerobacter ethanolicus*

Chapter 1

Introduction

1 Introduction

Our society is facing major environmental and resource scarcity issues and the development of more sustainable manufacturing is of high importance. In this context, biocatalysis has a pivotal role in the design of new and efficient chemical production. The use of biocatalysis to synthesise industrially relevant molecules has gone through a significant development during the past decades. This thesis focuses on the synthesis and application of a novel nanobiocatalyst system for cofactor-independent oxidoreductase catalysis in organic solvents. This introductory chapter gives an overview of the progress and innovation in biocatalysis as well as key concepts targeted within this thesis.

1.1 Biocatalysis: a historical point of view

The earliest examples of biocatalysis can be found as early as 6000 BC when Sumerians and Babylonians brewed beer (*1*). In 1833, Anselme Payen and Jean Persoz, two French industrial chemists, found out that an ethanolic extract of barley seeds, when transferred to an aqueous environment, was degrading starch into simple sugars. Payen and Persoz named this active substance, which came to represent the first example of a purified enzyme, diastase (*2*). However, the authors recognised this active substance to be a *ferment* and did not understand its acellular nature. For the term *enzyme*, we needed to wait another fifty years until 1877, when Wilhelm Kühne, a German physiologist, demonstrated the distinction between bacteria and enzymes and coined the term.

The concept of catalyst was introduced by Jakob Berzelius, a Swedish chemist, in 1836 as a substance that increases the rate of a reaction without being consumed. He also quickly hypothesised that enzymes were such catalysts. In 1897 cell-free fermentation was discovered and in 1926 it was determined that enzymes were a kind of protein (*3*). The 1950s have seen great advances in our perception of protein structure. Indeed in 1958 the first three-dimensional structures of proteins, namely myoglobin and hemoglobin, were solved by single-crystal X-ray crystallography by John Kendrew and Max Perutz respectively, at the University of Cambridge (*4*).

During the 1950s came also the first reports of enzyme immobilisation (*5*, *6*) and since 1972 Bayer has been using an immobilised penicillin acylase for the synthesis of 6-aminopenicillanic acid an important building block for the synthetic antibiotic's ampicillin and amoxycillin. This reaction had previously been done with a tedious chemical process. The enzyme process was

simpler and more environmentally friendly, however, to use the soluble enzyme was expensive. By immobilising the enzyme, the reaction became more economically feasible.

During the nineteenth century, there was an ongoing dispute regarding enzymes and fermentation. “Vitalists” claimed that, due to failed attempts of isolation of the enzyme responsible for fermentation, such complex reactions needed a “life-force” for successful transformation. Enzymes were thought to only be able to carry out “simple” hydrolysis reactions (*3, 7*). Luckily, the vitalists were wrong, and a large number of biocatalytic reactions taking place in acellular systems have been discovered.

Several other advancements within enzymology and biocatalysis have occurred which is also reflected in the annual market value of this business. Figure 1.1 is a graph where the estimated global enzyme sales are plotted versus time (*8*). This is an effect of the increased interest and possibilities with biocatalysis.

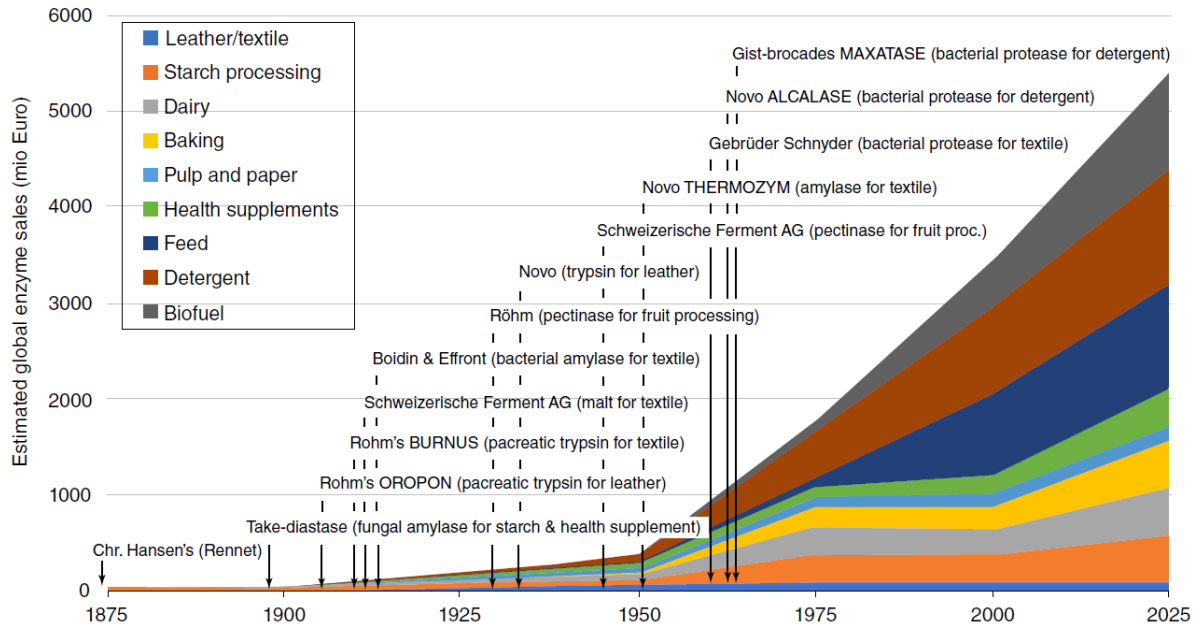

Figure 1.1. Estimated global enzyme sales. From 1875 to 2025 and historical events for the enzyme business. Reprinted with permission from Industrial Enzyme Applications, 2019. Copyright 2019 Wiley-VCH.

The biocatalyst

Biocatalysis has developed into an attractive alternative to traditional organic synthesis (*9*). Consequently, the application of biocatalysis to industrial catalysis has increased significantly over the past two decades (*8, 10, 11*). Therefore, the rate at which new biocatalysts are being developed has increased. An ideal biocatalyst should display high turnover rates, substrate selectivity when needed or promiscuity for other applications. For example, when using

biocatalysts in detergents a highly promiscuous enzyme is favourable, so that a large variety of stains (i.e., substrates) can be targeted. However, for the production of active pharmaceutical ingredients (API) or fine chemicals high substrate specificity and enantioselectivity are needed to obtain the correct enantiomers for these delicate applications. With the increasing complexity of products needed for industrial applications for such API and fine chemicals, biocatalysis has become a key player in enantioselective catalysis (*12*-*15*). Additionally, the enzyme needs to be stable under process conditions including, temperature and process environment. Hence, the development of a broad range of biocatalysts is needed, each adapted to the specific process. There are several advantages to using enzymes as catalysts instead of other catalysts. Processes can be simplified owing to enzymes' regio- and chemoselectivity and thus avoid protection and deprotection steps. Moreover, multistep synthesis can be reduced to a one-step process (*9*). This can be achieved either by using an enzyme that catalyses several chemical steps or by utilising multiple enzymes for a cascade reaction. The latter is possible thanks to enzymes' compatibility with each other in regard to similar reaction conditions and narrow substrate scope (*16*).

Biocatalysts can be divided into two different groups, the use of whole living cells, typically within fermentation, or the free enzyme. The latter can then be further divided into two classes, either dead/resting whole cells containing the enzyme of interest or isolates of the target enzyme (*17*). The advantage assigned to whole-cell catalysis is that no enzyme purification is needed which reduces the preparation cost. However, it usually also brings a need for more extensive workup due to larger volumes, low productivity due to low concentration tolerance and an increased risk for side reactions due to the metabolism of the organism (*16*). Such drawbacks can be avoided by using the isolated enzyme. This thesis describes the preparation of nanobiocatalysts belonging to the isolated enzyme group of biocatalysts and therefore the focus of this introductory part is done accordingly.

1.2.1 Biocatalysis and sustainability

In 1998 Anastas and Warner published their book *Green Chemistry: Theory and practice* in which they introduced the twelve principles of green (i.e. more sustainable) chemistry (*18*). These principles are the following:

1. Waste prevention
2. Atom economy
3. Less hazardous chemical synthesis

4. Designing safer chemicals
5. Safer solvents and auxiliaries
6. Design for energy efficiency
7. Use of renewable feedstocks
8. Reduce derivatives
9. Catalytic rather than stochiometric reagents
10. Design for product degradation
11. Real-time analysis for pollution prevention
12. Safer chemistry for accident prevention.

These principles serve as guidelines for the design of new greener chemical syntheses. Biocatalysis coheres with ten principles, number four and ten, are not relevant since they refer to the final product rather than to the process (*11*).

Enzymes easily adhere to principle seven, since they can be produced from renewable feedstocks (*11*). Principle nine calls for increased use of catalytic reagents in favour of stochiometric reagents, however many current catalysts are based on precious transition metals (*e.g.*, rhodium, palladium, platinum, ruthenium, iridium, gold, silver and osmium) (*19, 20*). The scarcity of these metals in combination with their increasing and fluctuating prices makes enzymes gain pivotal importance as catalysts (*21-23*). Moreover, biocatalysis can often be done at ambient temperature and atmospheric pressure. The previously discussed shortening of synthetic routes also reduces the amount of waste generated from biocatalysis (*24*).

1.2.2 Biocatalysis in organic solvents

For sustainability reasons, catalysis in organic solvents is not desirable. However, it still provides beneficial properties not achievable in aqueous environments. Situations, where biocatalysis in organic solvents provides positive aspects, are increased solubility of nonpolar substrates, reduced water-dependent side reactions, elimination of microbial contamination, the application of enzymes directly in current chemical processes and easier product recovery (*25, 26*). However, biocatalysis in an organic solvent is often hindered due to the incompatibility of enzymes with this non-physiological environment. Enzymes frequently display reduced activity, poor stability and deactivation in organic solvents.

A critical parameter of the solvent effect on the enzymes catalytic properties is the hydrophobicity of the solvent and its relation to the enzymatic activity (*27-29*). Solvents with log*P* values of ≥ 2 have been shown to cause minor enzyme distortion allowing the enzyme to

retain its enzymatic activity. This has been connected to a low capability of these solvents to strip the enzyme of "structural water" that is bound to the enzyme surface and crucial to the enzyme for performing catalysis. On the contrary, solvents with log*P* values of < 2 are polar enough to remove these structurally bound water molecules and, therefore, limit the catalytic properties of the enzyme due to the loss of molecular flexibility.

The effect of the organic solvent on the enzyme is also dependent on the enzyme itself since the water requirement for enzymes varies. A way to measure an enzyme's water requirement is with the media's water activity (a_w). The different water requirements of enzymes can be met by adjusting the a_w. For example, lipases can typically survive with a_w values of 0.0-0.2, while oxidoreductases need higher a_w values of 0.1-0.7 to maintain their catalytic properties (*30*).

A lot of efforts have been put into improving enzymatic catalysis in organic solvents. Examples of strategies employed for stabilising enzymes in organic solvents include chemical modification, solvent additives, protein engineering and enzyme immobilisation (*31*).

1.2.3 Biocatalysis and oxidoreductases

Oxidoreductases are enzymes catalysing the transfer of electrons from one molecule (the reductant or electron donor) to another (the oxidant, or electron acceptor). Oxidoreductases account for almost a third of all enzymatic activities registered in the Braunschweig Enzyme Database, BRENDA (Figure 1.2), thus, being a large enzyme class of pivotal importance (*32*).

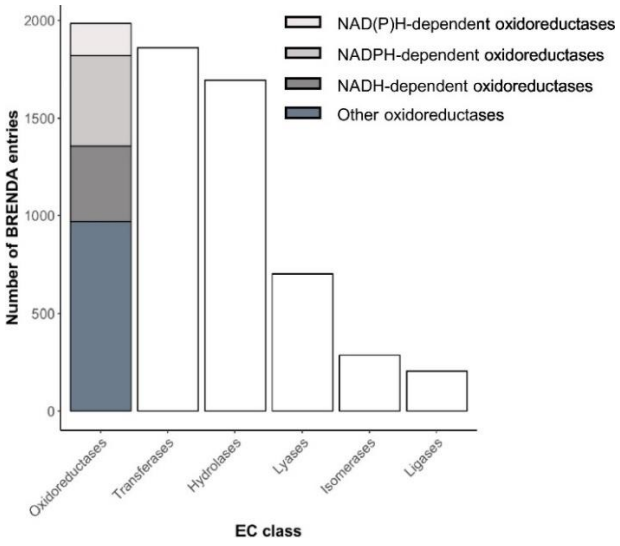

Figure 1.2. Distribution of enzyme activities registered in BRENDA. Reprinted from Biochim. Biophys. Acta, 2018, 1866, 327-347.

Oxidoreductases can act on a broad range of substrates such as ketones, alcohols, amines, and alkenes, some of which are shown in Figure 1.3.

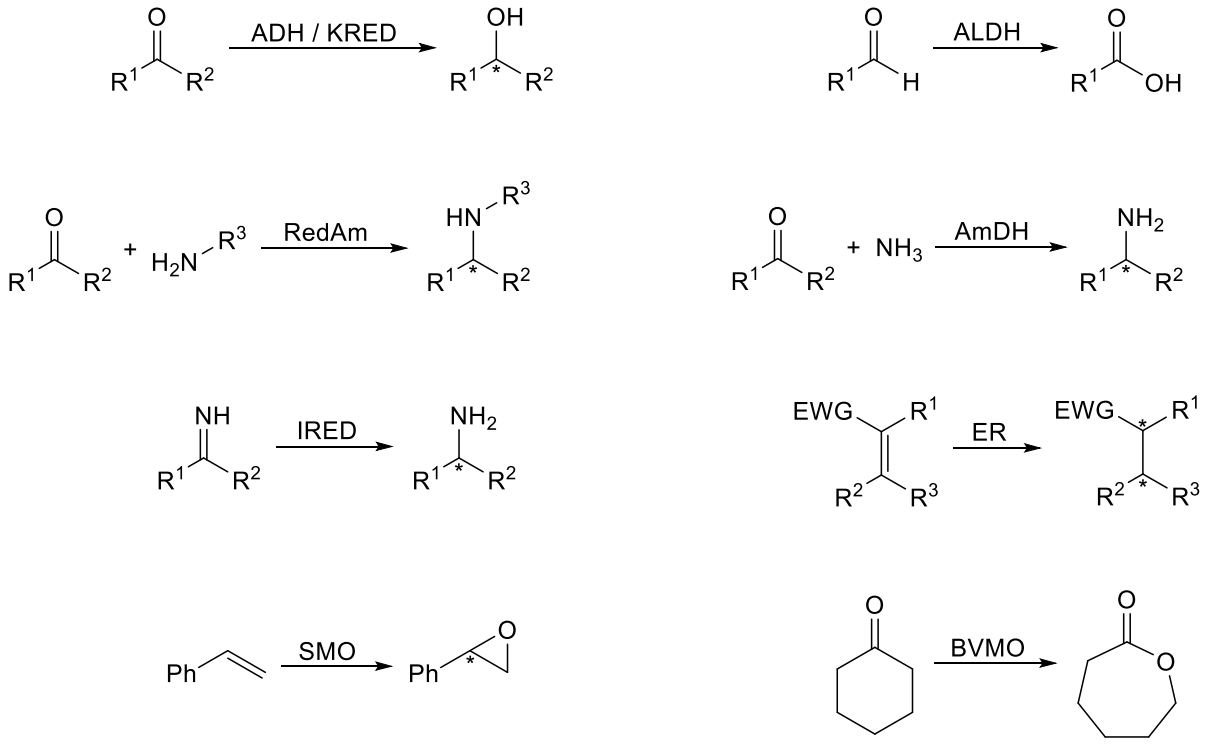

Figure 1.3. Examples of oxidoreductase catalysed reactions. Enzymes presented: alcohol dehydrogenase (ADH), ketoreductase (KRED), aldehyde dehydrogenase (ALDH), reductive aminase (RedAm), amine dehydrogenase (AmDH), imine reductase (IRED), ene-reductase (ER), styrene monooxygenase (SMO) and Baeyer-Villiger monooxygenase (BVMO).

Oxidoreductases have gained considerable interest in organic chemistry for their capability of asymmetric reduction of carbonyls to chiral alcohols or reductive amination. As an example, a ketoreductase (KRED) was employed as a key step in the synthesis of atorvastatin, which is the active ingredient of a cholesterol-lowering drug, with 96 % isolate yield and >99.5 % enantiomeric excess (ee) (*33*) (Figure 1.4).

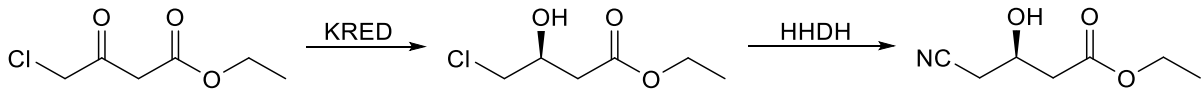

Figure 1.4. Synthetic route to atorvastatin. Catalysed with KRED and halohydrin dehalogenase (HHDH).

Another KRED was reported for catalysing a key intermediate in the synthesis of montelukast with 97.2 % yield and >99.9 % ee. Montelukast is a leukotriene receptor antagonist used for medication of asthma (*34*) (Figure 1.5).

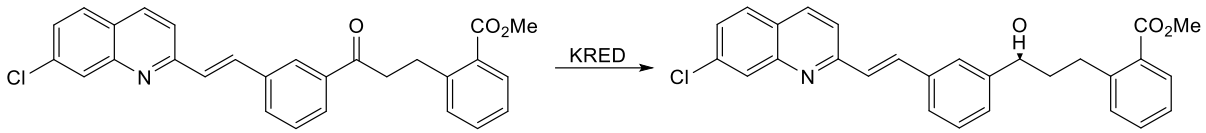

Figure 1.5. Synthetic route to montelukast sodium with KRED.

1.2.3.1 Biocatalysis and cofactors

Many oxidoreductases are dependent on cofactors for the electron transfer. This exchange is achieved by hydride transfer during catalysis. The most commonly used cofactors are nicotinamide adenine dinucleotide phosphate ($NADP^+$ or NAD^+) and their reduced form NADPH or NADH. As seen in Figure 1.2 NAD(P)H dependent oxidoreductases represent over 50 % of all oxidoreductase activities in BRENDA. The challenge with cofactors is that they are relatively expensive and needed in stoichiometric amounts for the catalytic reaction. This has restricted the widespread use of oxidoreductases as a biocatalyst. Cofactor recycling has proven to be the solution to this issue, by adding a second substrate, a cosubstrate, that can be used to regenerate the cofactor to its original oxidation state. This can be achieved using two enzymes for the reaction, one catalysing the reduction of the substrate of interest while oxidising the cofactor. The second enzyme can then reduce the cofactor and oxidise its own substrate. Alternatively, the main enzyme can also independently catalyse the reduction of the cofactor and oxidation of the cosubstrate if the cosubstrate is a fitting substrate for the enzyme as well. An illustration of these two recycling variants can be seen in Figure 1.6.

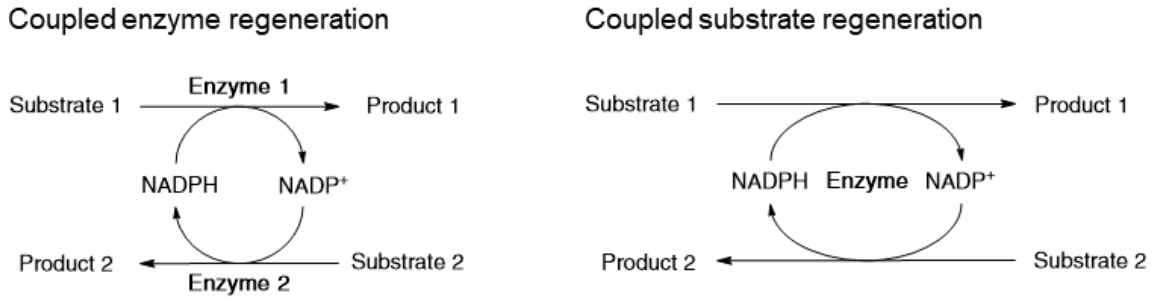

Figure 1.6. Two alternatives to cofactor recycling. Coupled enzyme regeneration is a two-enzyme approach with one enzyme responsible for each substrate/product pair. Coupled substrate regeneration is a one enzyme approach where the enzyme recycles the cofactor by itself using the second substrate/product pair.

There are numerous studies where scientists have applied cofactor recycling strategies to overcome the limitation of stochiometric amounts of cofactor required for many oxidoreductases. For coupled enzyme regenerations have for example the following enzymes

been employed: glucose dehydrogenase with glucose as substrate, formate dehydrogenase with formate as substrate, glucose-6-phosphate dehydrogenase with glucose-6-phosphate as substrate or alcohol dehydrogenase (ADH) with isopropanol (*i*-PrOH) as substrate (*23*, *35*, *36*). The latter has also been used for the coupled substrate regeneration by catalysing both the main reaction and the regeneration reaction.

Another strategy to overcome the stochiometric cofactor need is by biocatalytic hydrogen borrowing. When two NADPH/$NADP^+$ dependent reactions are combined, of which one is a substrate oxidation and the other a reduction of the formed intermediate the cofactor is recycled over the whole process. This was reported by Mutti *et al.* (*37*) and Montgomery *et al.* (*38*) where ADH was combined with either an amine dehydrogenase (AmDH) or a reductive aminase (RedAm) for synthesis of amines from alcohols. (Figure 1.7)

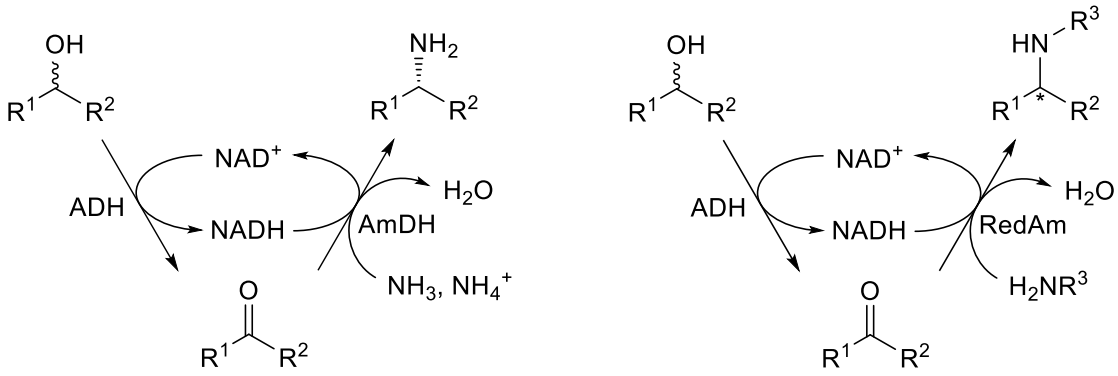

Figure 1.7. Biocatalytic hydrogen borrowing using ADH and AmDH or RedAm.

Even with a functioning cofactor recycling system, oxidoreductase catalysis in organic solvents is, however, a major challenge due to the polarity of the cofactors. Cofactors are not soluble in non-polar organic solvents and alternative solutions for bringing the cofactor to the enzyme in such environments are needed.

1.3 Biocatalyst development

There are several approaches for developing new biocatalysts. In the following chapter three of the main strategies are described i.e., discovery of novel enzymes, engineering of existing enzymes and enzyme immobilisation for stabilisation or improved properties.

1.3.1 Enzyme discovery

One way for finding new possible biocatalysts is by searching for novel enzymes with a new range of properties. This can be done by isolating new organisms and with the use of

metagenomics isolate novel enzymes from these organisms. With the development of high-throughput screening, modern bioinformatic tools and rational genome mining the probability of finding new enzymes can be increased (*39*).

For example, Scholtissek *et al.* reported the identification of an ene-reductase (ER) from an acidophilic iron-oxidizing betaproteobacterium by genome mining. This enzyme showed to have a close phylogenetic relationship with ER from mesophilic organism, however it exhibits increase in its thermostability (*40*). Yoshida *et al.* reported the finding of microorganisms harbouring poly(ethylene terephthalate) (PET) degradability properties found at PET bottle recycling sites. From these organisms, they could isolate a novel enzyme responsible for the PET degradation that they named PETase, a PET hydrolase (*41*). Aleku et al. reported the discovery of a reductive aminase (RedAm) through sequence similarity to known imine reductases on their quest to identify new enzymes for the production of chiral amines. The enzyme discovered were shown to catalyse the reductive coupling of a variety of carbonyls to primary and secondary amines with high conversion (>98 %) and high enantioselectivity (>98%) (*42*).

The discovery of novel enzymes is one way to create new biocatalysts and can also be further combined with other strategies for easier and more efficient implementation.

1.3.2 Protein engineering

The most established way for improving or introducing new catalytic properties to enzymes is through protein engineering. This is done by genetically altering the enzyme and followed by recombinant protein expression. There are two major approaches for introducing genetic variations, rational protein design or directed evolution, additionally, is a combination of these approaches common (*43, 44*). In Figure 1.8 are the different strategies presented.

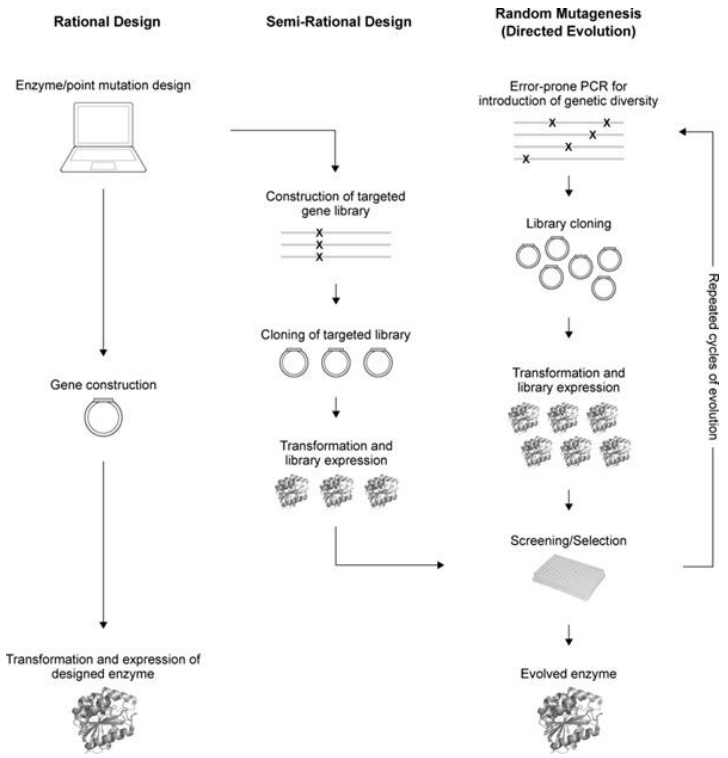

Figure 1.8 Sequence for protein engineering for biocatalysis. The three strategies; rational design, directed evolution or semi-rational design are presented. Reprinted from ChemBioChem, 2016, 17, 197-203.

In rational design are mutations of specific amino acids introduced by site-directed mutagenesis. The mutations are made with knowledge of the protein structure and function to for example increase the stability of the enzyme or commonly alter the active site of the enzyme to modify its promiscuity or enantioselectivity. Ziegelmann-Fjeld *et al.* reported an example of a mutated ADH where the active site of the enzyme had been modified to accommodate larger substrates (*45*). Further mutations have been conducted to the same ADH and Musa *et al.* reported a change in enantioselectivity of the enzyme by altering the shape of the active site (*46*). Cui et al. reported an experiment where strategic mutations had been done at the surface of a lipase to enhance the enzymes resistance in organic solvents. They found that mutating amino acids to increase the hydration of the enzyme increased its resistance towards organic solvents (Figure 1.9) (*47*).

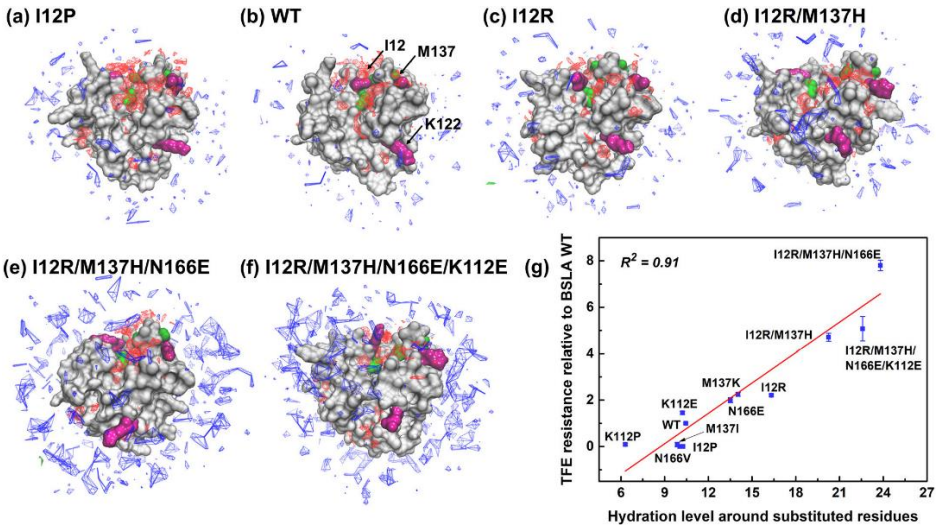

Figure 1.9. Representation of hydration levels around native enzyme and mutants. Increased resistant against solvent with increasing hydration levels around the enzyme. Reprinted with permission from ACS Catal., 2020, 10, 14847-14856. Copyright 2020 American Chemical Society.

In directed evolution, extensive prior knowledge of the enzyme is not necessary. Instead, it usually begins with the creation of a mutated library of the gene created by employing error-prone PCR. The enzymes encoded by the genes are produced and screened for specific properties. The genes with the desired properties are selected and can then be subjected to further mutation cycles to acquire more beneficial mutations (*48*). One example is the enzyme cytochrome P450 which has been used extensively for directed evolution to expand their catalytic scope (*49, 50*). They have also been engineered to improve their solvent stability (*51*).

Within protein engineering, also new fusion protein constructs can be designed. Recently, Hartley *et al.* reported an approach with engineered enzymes that retain and recycle their cofactors. This was achieved by expressing the enzymes like a fusion protein with a bridge between each enzyme on which a linker could be attached. The linker allowed the connection of the cofactor to the whole module. This engineered enzyme complex was then successfully used for continuous flow catalysis (*52*).

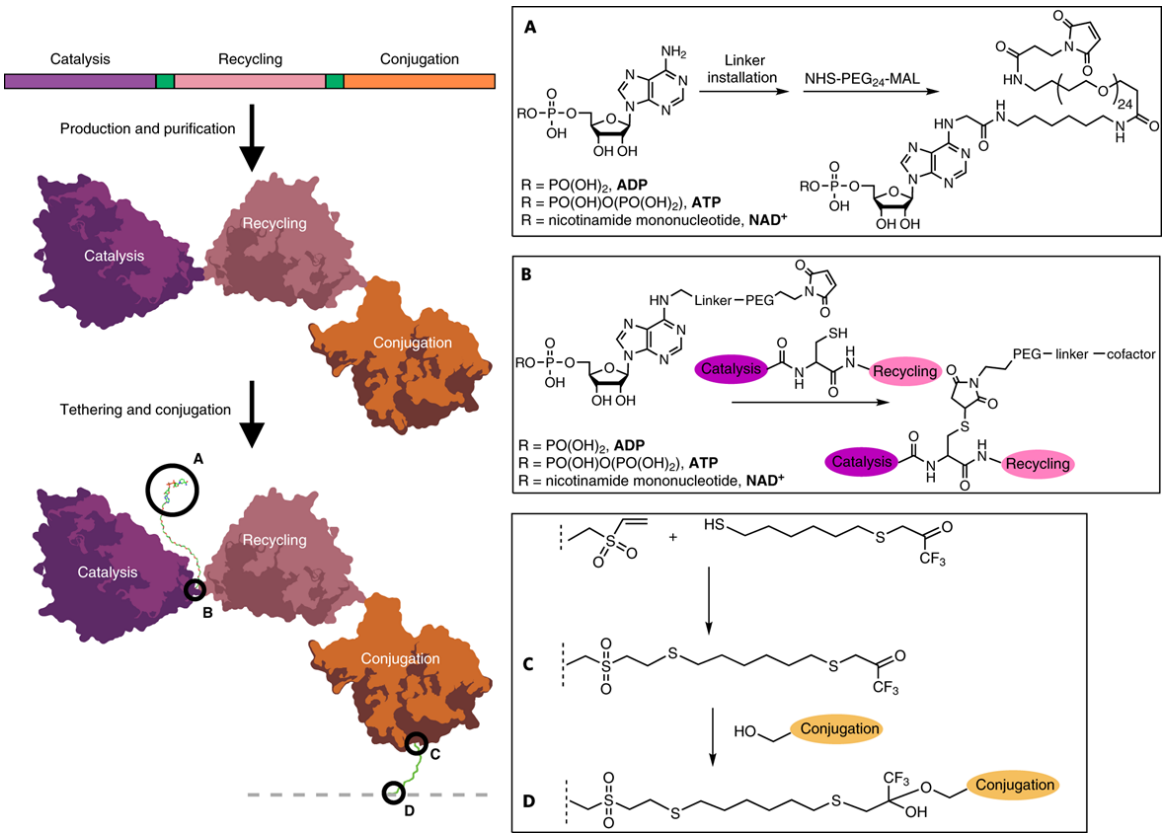

Figure 1.10. Fusion protein complex retaining its cofactor. (Reproduced with permission from Nat. Cal., 2019, 2, 1006-1015. Copyright 2019 Springer Nature).

Protein engineering have been a successful and highly important factor for developing new biocatalysts. However, even with improved solvent stability and new catalytic properties there are challenges with implementation of the soluble enzyme for industrial purposes. For example, soluble enzymes are typically not recovered at the end of the process, this leads to high costs for the continuous addition of new enzyme.

1.3.3 Enzyme immobilisation and protection

Another strategy employed for developing and preparing biocatalysts is through enzyme immobilisation. There are several advantages to using immobilised enzymes for biocatalysis. The most obvious one is the easier handling of the enzyme since the enzyme can be considered a solid rather than a liquid (*53*). This allows for straightforward removal of the enzyme from the reaction solution allowing for both the biocatalysts' reuse and a significantly reduced risk of protein contamination in the final product. Additionally, a solid biocatalyst can easily be retained within a reactor as well as used for continuous flow catalysis (*54*). Furthermore, enzyme immobilisation may reduce the enzyme's sensitivity to changes in the environment,

hence increasing its stability (*55*). Moreover, immobilisation may increase the activity, improve the selectivity and specificity of the immobilised enzyme (*56*, *57*).

There are three major strategies for enzyme immobilisation: entrapment of the enzyme within a matrix/polymer network, cross-linked enzymes and immobilisation to an inert carrier (*58*). (Figure 1.11)

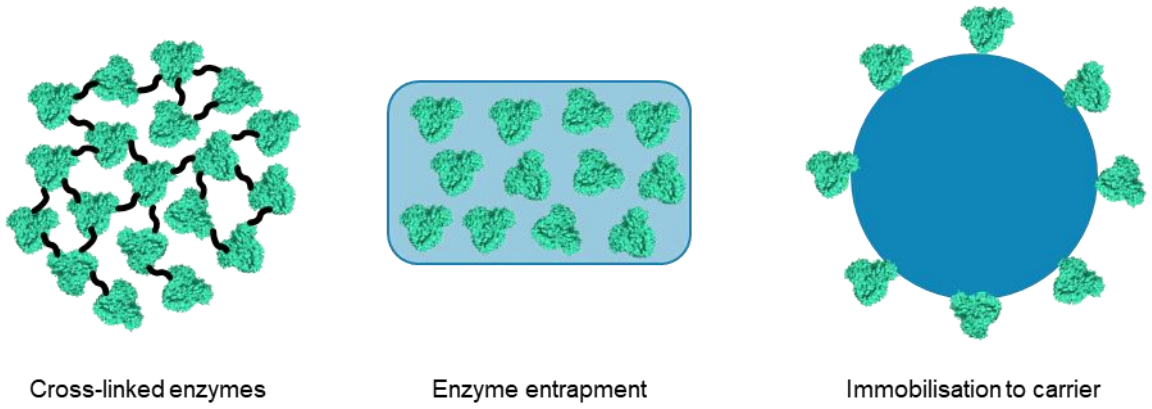

Figure 1.11. Schematic representation of three different immobilisation strategies. Enzymes are represented in green. Crosslinker between enzymes are represented in black. Turquoise represents entrapment material or carrier.

1.3.3.1 Cross-linked enzymes

The preparation of cross-linked enzymes is a carrier-free immobilisation strategy. There are several types of such biocatalysts. Their general preparation strategy is by cross-linking enzymes prepared in different ways. Some of the most common types are cross-linked dissolved enzymes (CLEs), cross-linked enzyme aggregates (CLEAs) and cross-linked enzyme crystals (CLECs) (*59*). CLEs have been shown to possess increased thermostability of the enzyme but have also displayed several drawbacks such as low mechanical stability and poor reproducibility (*59*). CLECs were first described in 1964 (*60*) and have created robust and highly active biocatalysts. They were further commercialised for biocatalysis in the 1990s (*61*, *62*) however suffered from the drawback of the need to crystallise the enzyme prior to preparation (*63*). Figure 1.11 A and B displays examples of crystallised enzymes. CLEAs were developed in order to avoid the need for crystallisation of the enzyme and instead replace it with precipitation before crosslinking (*64*). This gave biocatalysts with comparable activity as CLECs but without the hurdle of crystallisation (*64*, *65*). CLEAs have been successfully used

for several catalytic purposes (*66-68*)(Figure 1.11 C) however, low mechanical resistance has limited their widespread use for industrial biocatalytic purposes (*69*).

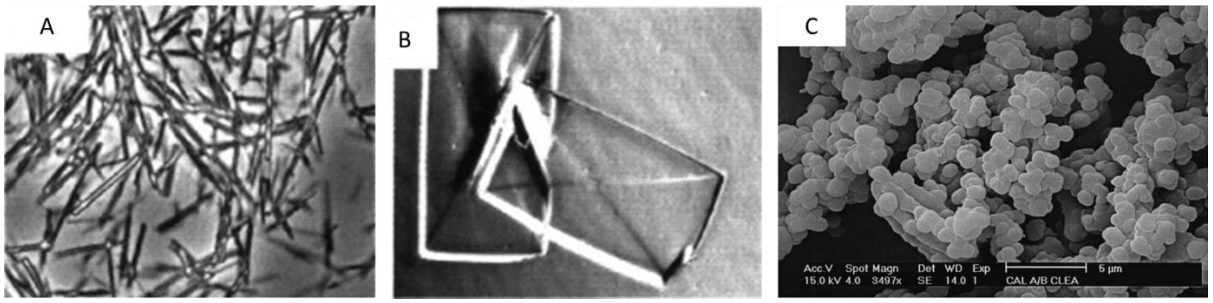

Figure 1.12 Enzyme crystals and CLEAs. A, Enzyme crystals of ADH from *Thermoanaerobacter ethanolicus*. B, Enzyme crystals of penicillin acylase from *E. coli.* (A and B are reproduced with permission from Angew. Chem. Int. Ed., 2021, 40, 2204-2222. Copyright 2001 John Wiley and Sons). C, CLEA particles of lipase A/B from *Candida antarctica*. (Reproduced with permission from Biotechnol. Bioeng., 2004, 87, 754-762. Copyright 2004 John Wiley and Sons).

1.3.3.2 Enzyme entrapment

The general definition of enzyme immobilisation through entrapment is an irreversible entrapment of the enzyme into a support (*70, 71*). The support should allow for diffusion of substrates or products but retention of the enzyme. Typically, the fabrication of the support is carried out in the presence of the enzyme (*53*). The entrapment material can consist of various materials such as different polymers, sol-gels, composites, or inorganic materials (*70*). An advantage with entrapment is that no chemical modification is done to the enzyme; therefore, limited denaturation of the enzyme occurs. However, the conditions of the material must be tuned against enzyme leaching and restricted mass transfer (*72*). Temiño *et al.* reported a method for entrapment of an ADH and its cofactor within polyvinyl alcohol gel beads. The entrapped enzyme was then successfully used to reduce a series of ketones to their corresponding alcohols in pure hexane (*73*). Musa *et al.* described an entrapment strategy for another ADH and its cofactor into silica-based "Xerogel". The entrapped enzyme was then used for the catalysis of chiral alcohols in various organic solvents in batch mode (*74*).

1.3.3.3 Covalent enzyme immobilisation

The immobilisation of enzymes to a carrier can be done either covalently or non-covalently. Non-covalent immobilisation will be discussed further in chapter 1.3.3.4. The immobilisation of the enzyme can be done to a variety of supports. Similarly, the type of supports used for enzyme immobilisation will be further discussed below in chapter 1.3.3.5. Covalent enzyme

immobilisation has the advantage of fixing the enzyme to the carrier surface, thus further limiting enzyme leaching or protein contamination of the final product (*55*). For covalent enzyme immobilisation, chemical modification of surface available amino acids is commonly used. However, other functional moieties on the surface of the enzyme can also be used. Recently Nazemi *et al.* published a strategy for the immobilisation of glycosylated enzymes. The immobilisation was carried out through covalent binding between a boronate derivative on the carrier to the glycans of the enzymes and yielded stable biocatalysts (*75*).

A wide range of commercially available crosslinkers, possible chemical modifications of the enzyme, and the large variety of possible carriers with their own functional surface have created countless possibilities for choosing the experimental parameters for enzyme immobilisation.

Examples of covalent enzyme immobilisation by utilising the available lysine residues have been reported (*76*). Immobilisation can then be achieved to an amino functionalised carrier by using the homo bifunctional crosslinker glutaraldehyde (*77-79*). The formed imines after the reaction can be further reduced, by e.g. sodium borohydride, to yield the corresponding secondary amine, and to obtain an irreversible immobilisation (*55*). Due to the frequent occurrence of lysine in the sequence of most proteins immobilisation through this amino acid can commonly achieve a multi-point attachment between the enzyme and the carrier. Other reactive groups commonly used for immobilisation through amines are N-hydroxysuccinimide (NHS) esters, which generate a stable amide bond after immobilisation, and epoxides (*55, 80*). However, the reactivity between epoxides and amines is poor. Therefore it is often not possible to achieve a multi-point attachment of the enzyme or high enzyme immobilisation yield without further actions (*81*). Additionally, with lysine typically being distributed over the surface of the enzyme the immobilisation orientation is not controlled which might generate unfavourable positions (*82*). This could lead to reduced enzymatic activity due to restricted access to the enzymes active site. Another amino acid used for immobilisation due to its high nucleophilicity is cysteine (*83*). Compared with lysine, it has a significantly higher reactivity with epoxides and can achieve immobilisation through alkylation, disulphide exchange and by conjugate addition to maleimide (*81, 84*). However, the low abundance of surface available cysteines not already involved in a disulphide bond reduces the possibilities with this amino acid. This can be of advantage as well since a lower number of available cysteines could provide more control of the immobilisation orientation of the enzyme. The amino acids, glutamic acid and aspartic acid, are used for immobilisation however often requires previous activation of the carboxylic acid group with carbodiimides. Even though cysteine and lysine are most commonly used for

bioconjugation, there are many strategies for several other amino acids which allows for more flexibility when designing a biocatalyst (*70*, *85*, *86*). A selection of different enzyme immobilisation reactions are presented in Figure 1.13.

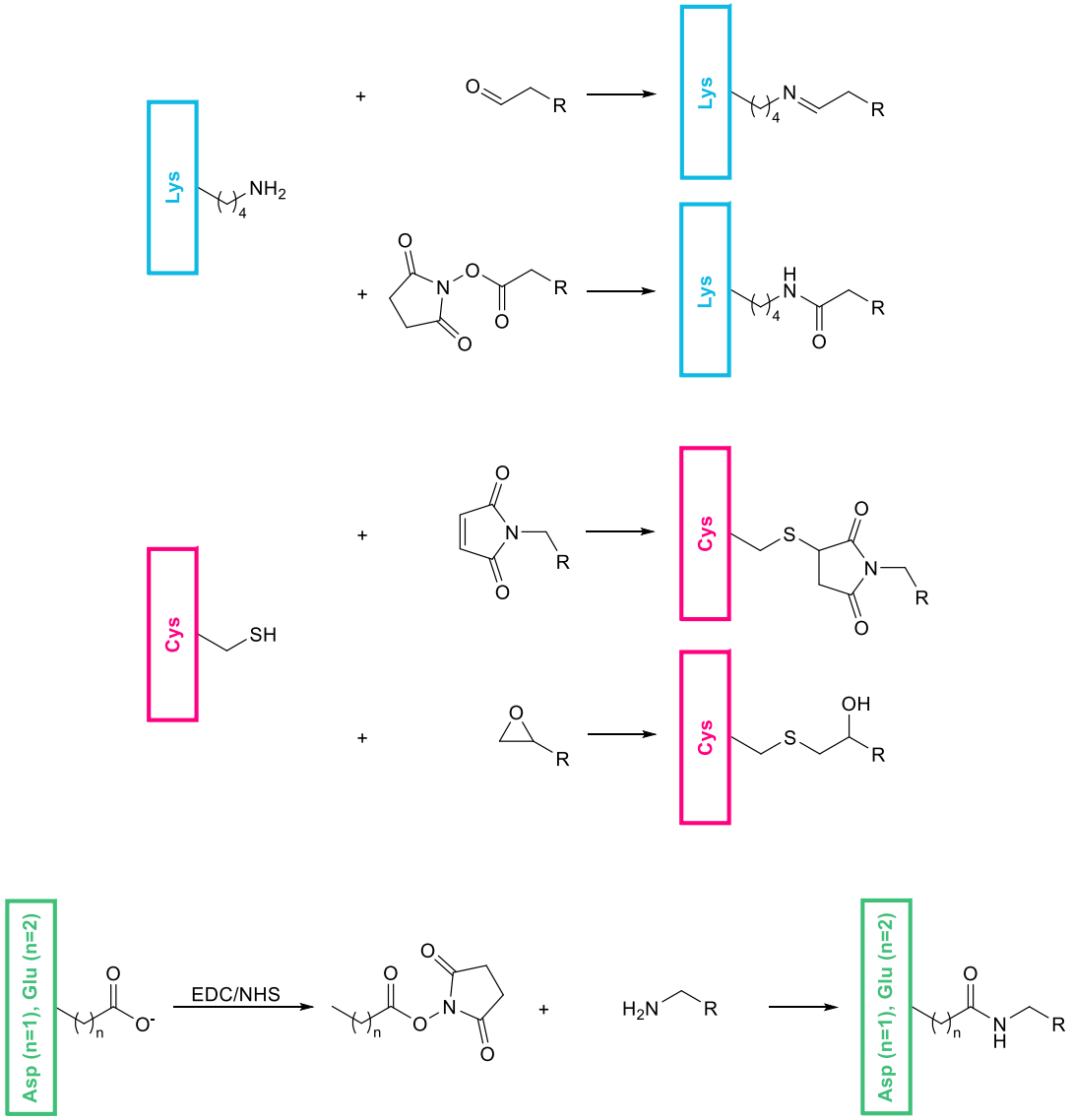

Figure 1.13. A selection of covalent enzyme immobilisation strategies.

1.3.3.4 Non-covalent enzyme immobilisation

For non-covalent enzyme immobilisation the immobilisation of the enzyme occurs through physical adsorption to the surface of the carrier (via van der Waals and hydrophobic interactions), or via ionic or affinity binding (*71*).

Enzyme immobilisation through adsorption can occur via several different strategies. One example are enzymes with large lipophilic area can interact with a hydrophobic carrier through van der Waal forces and changes in entropy. Advantages of adsorption-based immobilisation

include no need for chemical modification of the enzyme, a limited amount of destructive effect on the enzyme and a relatively easy and straightforward immobilisation strategy. However, enzyme leakage is common, particularly in aqueous environments (*55*). Lipases are commonly immobilised via adsorption of their hydrophobic area close to their active site on hydrophobic supports. This leaves the enzyme in an open conformation that is more accessible for efficient catalysis (*56, 87*). A well-known example of non-covalent immobilisation for biocatalytic purposes is the commercially available product Novozym 435, based on immobilisation of lipase B from *Candida antarctica* on a resin (*88*). This product has for examples been successfully used for kinetic resolution in toluene of aromatic cyanohydrin acetates in toluene (*89*).

Another strategy for enzyme immobilisation is affinity binding. It exploits the selectivity between an enzyme and its ligand and this allows for an efficient immobilisation (*90*). This strategy generates orientation controlled immobilisation and a low amount of conformational changes of the enzyme which combined allows for high retention of enzymatic activity (*70*). Fornera *et al.* described an immobilisation strategy of horseradish peroxidase by exploiting the strong affinity between biotin and avidin (*91*). They used a biotinylated version of the enzyme, and they developed a reproducible immobilisation method which generated a stabilized enzyme. Holland-Nell *et al.* compared the site specific and random immobilisation of an aldo/keto reductase. The site-specific immobilisation was done by biotinylation of the enzyme and binding to streptavidin. This generated a biocatalyst with comparable remaining activity with the soluble enzyme and 60-300 fold greater remaining activity compared to the randomly immobilised enzyme (*92*).

Many recombinant enzymes are expressed with a polyhistidine sequence (His-tag) for easy purification of the enzyme through immobilised metal affinity chromatography. The high affinity between the His-tag and the chelated metal ion can also be utilized for immobilisation purposes. This is also a site-specific immobilisation method since the location of the His-tag is known. Zhou *et al.* described a method for immobilisation of organophosphohydrolase on nickel-nitrilotriacetic acid modified mesoporous silica nanoparticles. The Ni^{2+} allowed for the selective immobilisation of the enzyme and the obtained nanobiocatalyst displayed excellent stability and catalytic activity towards the degradation of methyl parathion (*93*). The His-tag immobilisation strategy was also used by Quaglia *et al.* for immobilisation of an ADH to a solid support. The biocatalyst was used for the reduction of aliphatic and aromatic aldehydes and showed enhanced enantioselectivity and high reusability (*94*).

1.3.3.5 Carrier materials for enzyme immobilisation

A wide range of different carrier materials have been used as supports for enzyme immobilisation. The choice of a carrier should be made according to the chemical and practical requirements of the application. The carrier should be insoluble in the reaction conditions as well as chemically and thermally stable. Additionally, their surface or structure needs to provide possibilities for immobilisation. Possible ways for that are by providing reactive functional groups for covalent immobilisation of enzymes, a porous structure, or specific hydrophobic/hydrophilic or charge properties to allow non-covalent immobilisation of the enzyme. Described in this chapter are examples of a selected range of carrier materials that successfully been applied for enzyme immobilisation for biocatalytic purposes.

Different organic polymers are often used as a carrier for enzyme immobilisation. Jermoin developed a new non-covalent immobilisation strategy for two ADHs where the enzymes and their cofactors were absorbed on commercially available superabsorber polymers. The superabsorbed ADH could be used for biotransformations in 10:90 % water:2-propanol (*i*-PrOH) mixtures for productions of chiral alcohols (*95*). This absorption strategy was then further utilized by Heidlindemann *et al.* who combined it with a organocatalyst to create a one pot process where the catalysts are compartmentalized (*96*). The enzyme, an ADH was absorbed into the superabsorber together with its cofactor. An initial aldol reaction catalysed by the organocatalyst was followed by the reduction of the aldol by ADH. This was then run in organic solvents without any need for purification between the two steps and the cofactor could be recycled thanks to the superabsorber. Contente *et al.* used commercially available beads from methacrylic polymer for enzyme immobilisation for a combined covalent and affinity binding. The beads were packed into columns for continuous flow catalysis of amines to chiral alcohols using a transaminase and oxidoreductases with up to >99 % yield and 99 % ee. Cofactor recycling was achieved through a recirculation of the aqueous media (*97*).

Velasco-Lozano *et al.* described a method for co-immobilisation of phosphorylated cofactors and enzymes to natural polymers i.e., porous microbeads of agarose. This allowed for the retention of the cofactor to achieve cofactor recycling in continuous flow catalysis. The system they developed allowed them to perform biotransformations without additional cofactor add-ons *(98)*. A similar approach was reported by Benitez-Mateos *et al.* that co-immobilised a KRED and its cofactor NADPH on agarose beads. The produced biocatalysts achieved 100% conversion and >99 % ee over several reaction cycles (*99*).

Seelajaroen et al. reported the immobilisation of formate dehydrogenase, formaldehyde dehydrogenase and ADH on graphene through covalent immobilisation using EDC-NHS coupling. The final nanobiocatalyst was used for cofactor-free electroreduction of CO_2 to methanol for continuous operation for durations of up to 20 hours (*100*) (Figure 1.14).

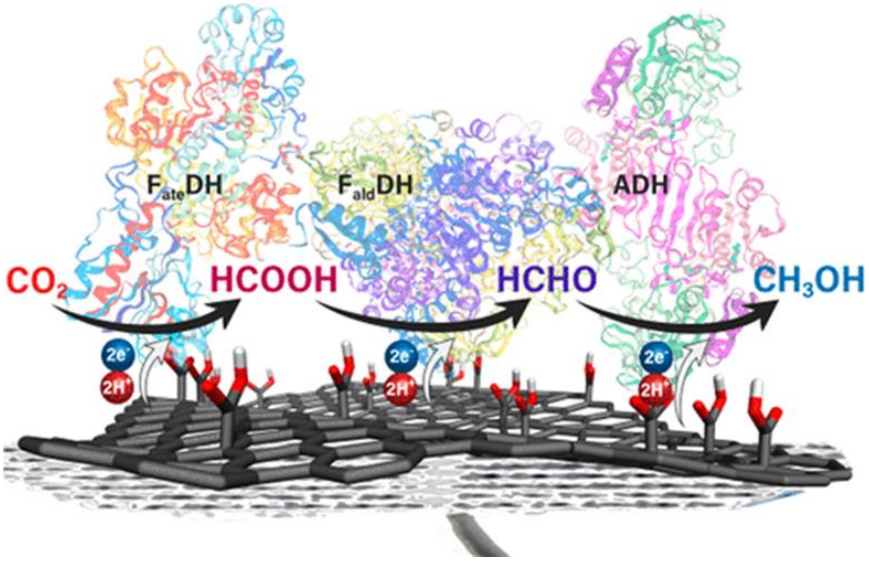

Figure 1.14 Schematic representation of an enzyme catalysed reduction. Reduction of CO_2 to methanol via a direct electron transfer through a functionalised graphene support and without any cofactors. Reproduced with permission from ACS Appl. Mater. Interfaces., 2020, 12, 250-259. Copyright 2020 American Chemical Society. Further permissions related to this material should be directed to the ACS. Link to article: https://pubs.acs.org/doi/10.1021/acsami.9b17777.

A material for enzyme immobilisation that has gained increasing interest is metal-organic frameworks (MOFs). This is a crystalline porous material based on coordination of metal clusters and organic ligands. MOFs display high surface area, large and tuneable pore size, and pore wall accessible for functionalisation which allows for high enzyme loading. Enzymes can either be immobilised through entrapment by being present during the formation of the MOF or in a post-synthetic fashion through enzyme interaction or covalent linkage within a pre-existing MOF (*101*). A common MOF are Zeolitic imidazolate frameworks (ZIFs), composed of imidazole linkers and metal ions. They are easily synthesised at in conditions compatible with the enzyme and allow for the entrapment of them therein. Lyu *et al.* described the immobilisation of cytochrome c embedded in ZIF-8. This resulted in a 10-fold increase of peroxidase activity of the immobilised enzyme compared to its soluble counterpart. Chen *et al.* described the immobilisation of glucose oxidase, horseradish peroxidase and β-galactosidase in ZIF-8 and could achieve a biocatalytic cascade reactor. They reported a 5.3-fold increase of

the catalytic cascades compared with the bulk of the soluble enzymes. Additionally, they immobilised an ADH, lactate dehydrogenase and NAD^+-polymer yielding a coupled enzymatic cascade with cofactor recycling (*102*) (Figure 1.15 A). Several other examples have been reported in the literature (*103-106*) (Figure 1.15 B and C).

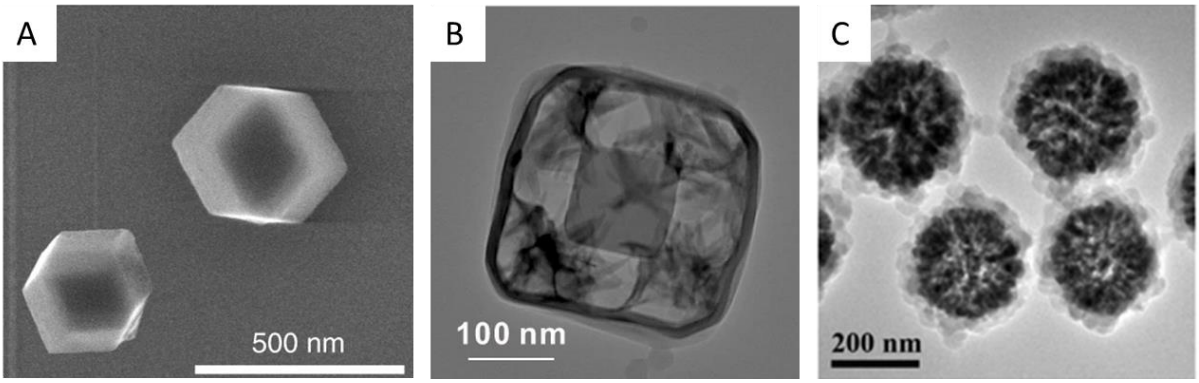

Figure 1.15. Metal-organic-frameworks. A, scanning electron microscope image of two-enzyme–ZIF-8 hybrid NMOFs (Reproduced with permission from Nat. Cal., 2018, 1, 689-695. Copyright 2018 Springer Nature). B, scanning transmission electron microscopy mage of ZIF-8 (Reproduced from Nat. Commun., 2022, 13, 305). C, transmission electron microscopy image of magnetic ZIF-8 (Reproduced with permission from Nanoscale, 2015, 7, 18770-18779. Copyright 2015 Royal Society of Chemistry).

Silica based materials have been extensively used for enzyme immobilisation. Silica possesses several of the crucial features for application within industrial biocatalysis. It is relatively cost-efficient, mechanically, chemically, and thermally stable and its surface is easily functionalised. This is due to the many hydroxyl groups at the surface and the large availability of organosilanes with different functional moieties which can easily be used for functionalisation of the silica surface. Silica offers high available surface area and can easily be produced with a desired morphology or pore structure (*80*).

One of the simplest methods for immobilisation on silica is through adsorption. This has been used for immobilisation of subtilisin and lipase to fumed silica for catalysis in organic solvents (*107, 108*). David *et al.* reported covalent immobilisation of invertase to porous silica with high enzyme loading and activity retention after immobilisation (*109*). The covalent immobilisation of enzymes to silica have previously been heavily utilised in our group. The silica particles used are based on the sol-gel method published by Stöber *et al.* for growth of monodispersed silica spheres (*110*). The enzymes are then covalently immobilised to the surface of the silica particles previously functionalised with amine groups via the crosslinker glutaraldehyde (*76*).

Mesoporous silica nanoparticles (MSNs) are another carrier material with interesting properties for enzyme immobilisation. MSNs are commonly prepared through a sol-gel process, like for ordinary silica material, however here with the addition of surfactants as template for the mesopores. Like ordinary silica they are easy to functionalise, and functionalisation can occur through either post synthesis via grafting, or directly during synthesis. Additionally can their size, morphology and pore size be tuned (*111*)(Figure 1.16 A – F). Due to the large available pore volume inside the MSNs they gained importance as a molecule carrier system. Lai et al. reported the use of MSNs as a carrier for a controlled release system for drug delivery. The drug was loaded into the pores of the MSN and the pore openings were blocked with removable cadmium sulphide nanocrystals (*112*) (Figure 1.16 G). Additionally have examples of enzyme immobilisation on MSNs also been reported (*113, 114*). The enzyme is commonly immobilised through adsorption and is considered to be immobilised within the pores of the MSN. The mesoporous silica should therefor provide a protected environment for the enzyme. However, mesopores of a sufficient diameter, generally >10 nm, are needed for successful immobilisation of the enzymes within the pores (*115*).

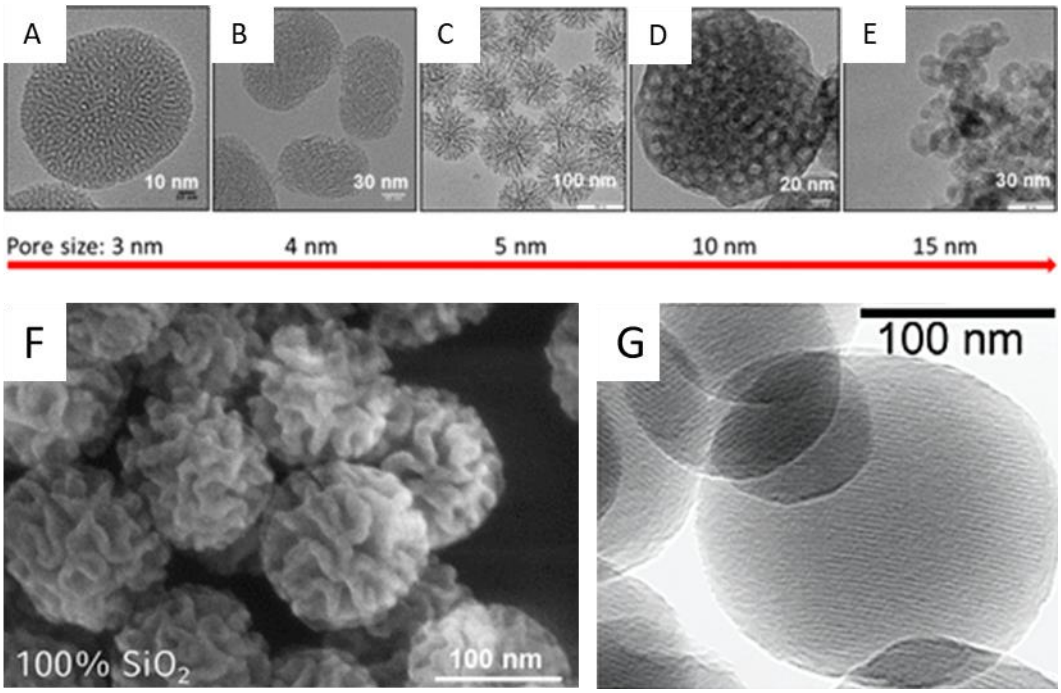

Figure 1.16. Micrographs of MSNs. A, B, C, D, E; transmission electron microscopy micrograph of MSNs with increasing pore size. F; Scanning electron microscopy micrograph of MSN with changed morphology. Reprinted with permission from Chem. Mater., 2017, 29, 1, 371-388. Copyright 2016 American Chemical Society. G; transmission electron microscopy micrograph of MCM-41 MSNs. Reprinted with permission from J. Am. Chem. Soc., 2003, 125, 4451-4459. Copyright 2003 American Chemical Society.

1.3.3.6 Enzyme protection

Previously in this chapter has examples of enzyme entrapment been presented. These methods for immobilisation also serve as a way of protecting the enzyme, since the enzyme is partly shielded against the surrounding environment. However, another method of enzyme protection or stabilisation is by embedding the enzyme in silica or organosilica after immobilisation (*76, 116, 117*). Our group has previously reported multiple examples of such protection strategies. Enzymes have been immobilised at the surface of silica particles followed by shielding of the enzymes with an organosilica layer (*75, 118, 119*). The layer has showed to increase the resistance of the enzyme against physical, chaotropic and biochemical stress (*76*). The effect of the organosilica layer was further investigated and it was reported that enantioselectivity properties could be introduced for an esterase by tuning the composition of the organosilica layer. Moreover was it reported that the layer had increased the esterase resistance against the organic solvent acetonitrile (*120*). Furthermore it was reported that after immobilising an enzyme and adjust the layer thickness, thus partially shielding the enzyme but still stabilising it, large substrates such as proteins could still be processed (*121*).

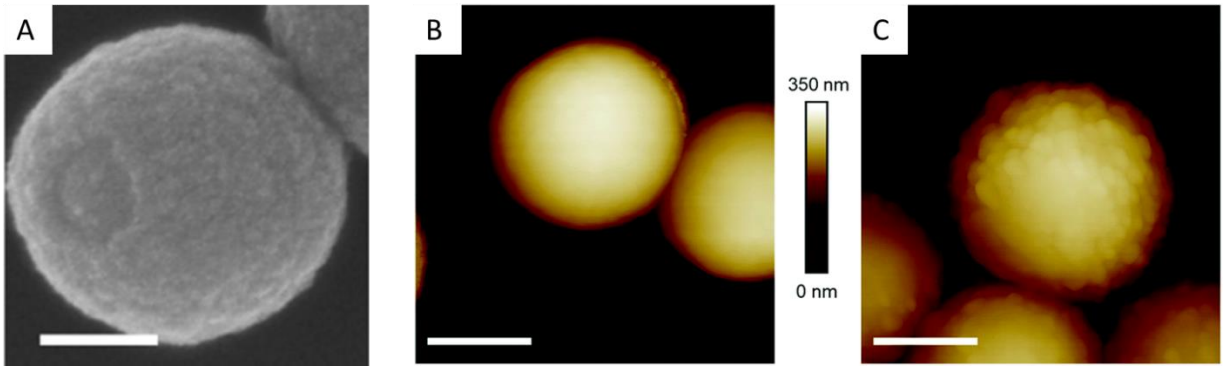

Figure 1.17. Micrographs of silica particles with organosilica layer. A, Scanning electron microscopy micrograph of silica particles after shielding with organosilica layer (Reprinted with permission from Angew. Chem. Int. Ed., 2016, 55, 6285-6289. Copyright 2016 John Wiley and Sons). Atomic force microscopy micrographs of silica particles before (B) and after shielding with organosilica layer (C). (Reprinted with permission from Chem. Commun., 2021, 57, 11960-11963. Copyright 2021 Royal Society of Chemistry).

1.4 Aim and scope

The use of oxidoreductases in neat organic solvents have not been widely reported. The aim of this thesis is to simplify the use of and thus expand the catalytic area in which cofactor dependent oxidoreductases can be used. The focus lies on the design, synthesis, and

characterisation of nanobiocatalysts as a tool for cofactor recycling in neat organic solvents and consequently oxidoreductase catalysis therein.

In Chapter 2 is the focus on the design, synthesis, and characterisation of the nanobiocatalyst. Choice of the nanoparticle carrier is described, and their size and morphology are characterised with field-emission scanning electron microscopy (SEM), transmission electron microscopy (TEM) and cryogenic transmission electron microscopy (cryoEM). Four enzymes catalysing relevant biocatalytic reactions are chosen and produced. They are purified with affinity chromatography and their purity, concentration and activity was determined SDA-PAGE and UV/Vis. Different strategies for enzyme immobilisation was employed and the effect of the immobilisation method in regard to immobilisation yield and remaining activity of the immobilised enzyme was determined with UV/Vis. A protecting organosilica shield is grown at the surface of the particle and the thickness and morphology is investigated with SEM and cryoEM.

In Chapter 3 are the biocatalytic properties of the produced nanobiocatalysts further investigated. The substrate scope is explored, and the catalytic efficiency is determined with GC-FID. The effect of solvents with different hydrophobicity on the catalytic properties of the nanobiocatalysts are also examined with GC-FID. By determining the substrate scope and the hydrophobicity also the cofactor recycling properties can be examined. A multi-step catalytic reaction is performed enhancing the knowledge regarding the cofactor reservoir. The reusability of the nanobiocatalysts is investigated and determined with GC-FID. Finally, are the biocatalytic properties in continuous flow catalysis explored and the efficiency is determined with GC-FID.

Chapter 2

Nanobiocatalyst synthesis and characterisation

2 Nanobiocatalyst synthesis and characterisation

The following chapter describes the synthesis and characterisation of the nanobiocatalysts designed in the frame of this thesis. Different synthetic pathways, immobilisation strategies, and conditions for growth of the protecting organosilica layer are investigated to yield the final system.

2.1 Concept

The research program that serves as a basis for the present thesis focuses on the design, synthesis and characterisation of novel supramolecularly engineered nanobiocatalysts capable of self-sustaining cofactor recycling in neat organic solvents. MSNs were chosen as a carrier for the nanobiocatalysts, due to their high amount of accessible pore volume. Cofactor-dependent enzymes are immobilised on the surface of the nanoparticle (**Figure 2.1**). The porosity of the MSN serves two purposes. First, the porous structure functions as a water reservoir in which the cofactor for the enzymes can be dissolved. Secondly, by acting as a sieve by having a smaller pore size than the total size of the enzyme, thus restricting the immobilisation of the enzyme to the surface of the MSN. At the surface of the MSN, a protecting organosilica layer can then be grown shielding the enzyme against the surrounding environment. Subsequently the catalytic properties of the nanobiocatalyst can then be exploited by dispersing the protected particles in an organic solvent containing a substrate of interest and an additional cosubstrate for the enzyme. The immobilised enzyme can then catalyse the conversion of the substrate, which can diffuse through the layer to the enzyme, while still having access to the cofactor dispersed within the core of the particle. Furthermore, by providing the enzyme with a cosubstrate the enzyme can recycle the cofactor and return it to its original oxidation state by consuming the cosubstrate.

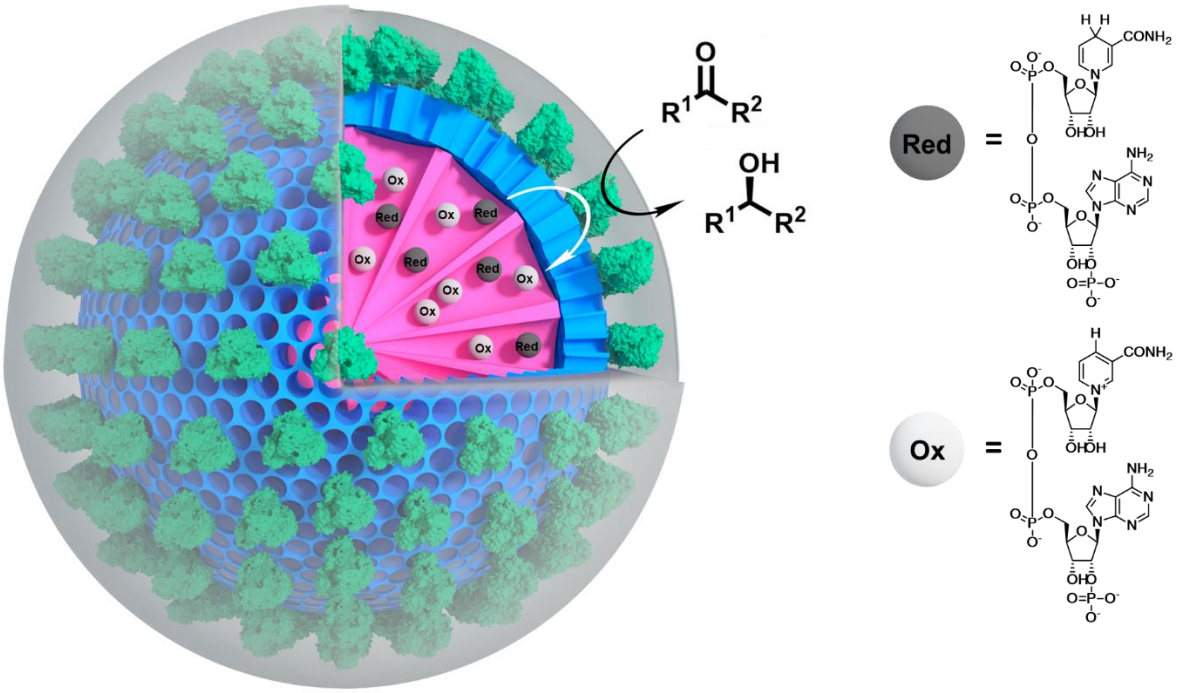

Figure 2.1. Schematic representation of the design of the nanobiocatalyst. In the cross-section in the upper right corner of the image is the two-generational pore structure visible. The first generation of the hierarchical MSN shown in pink, containing the cofactor shown in white and dark grey depending on the oxidation state. The second generation of the hierarchical MSN is shown in blue with the enzyme immobilised on the particle's surface in green. Surrounding the particle, shown in grey, is the organosilica layer. The substrate is dissolved in the surrounding solvent, allowing the enzyme to access both the cofactor and the substrate to perform biotransformations.

2.2 Choice of carrier

2.2.1 MCM-41

The first carrier that was investigated within this work, as possible support for the nanobiocatalysts, was MCM-41 MSNs. These are MSNs that can be straightforwardly produced; they display a high surface area, straightforward synthesis, and a stable mesoporous structure (*112*). The pore size is tuneable, and the particles can therefore be used for a large variety of applications (*122*). The pores, within the nanoparticle, are organized in an hexagonal fashion; they are uniform in size and lack interconnections among one another (*123*). The particles are prepared under basic conditions using cationic surfactants as templates for the mesopores' formation (*124*). The particles, in the current work, were synthesized according to a method previously described using tetraethyl orthosilicate (TEOS) as silica source and cetyltrimethylammonium bromide (CTAB) as a surfactant (*125*). The surfactant was extracted

after the synthesis by calcination yielding mesoporous MSNs. A schematic representation of the synthesis process is provided in **Figure 2.2**.

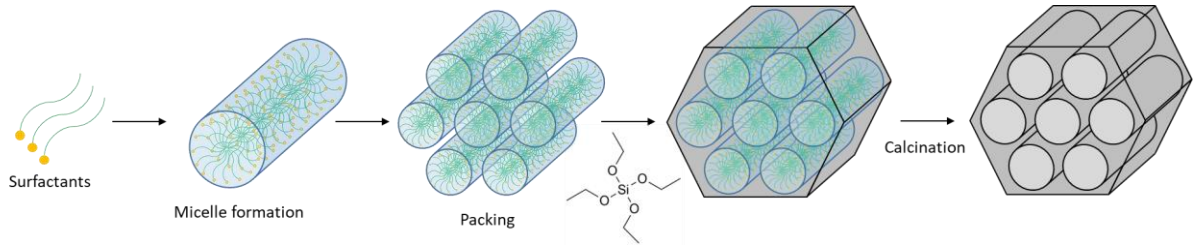

Figure 2.2. Schematic representation of the synthesis of MCM-41 MSNs. By increasing the concentration of surfactant in the solution micelles will be formed. The micelles will then stack together and arrange in a packing formation. The silica can then grow around the surfactants which creates the hexagonal pore structure. After calcination, by which the surfactants are removed from the pores, the MSNs are obtained.

The produced MSNs were characterised by SEM and TEM; representative micrographs are shown in Figure 2.3. The SEM micrographs show nanoparticles with an irregular spherical shape and an average size of 93±15 nm (Figure 2.3 D). This result was obtained by statistical analysis of the acquired SEM micrographs and a size analysis software. Since the particles did not show a completely spherical shape the longest side of each particle was always used when determining the size of the produced particles. In the TEM micrographs the porosity of the final MSNs can be seen (Figure 2.3 B and C). In the TEM close-up micrograph (Figure 2.3 C), the uniform and non-interconnecting pores are visible.

Due to the non-spherical shape of the final particles, the MCM-41 MSNs was determined to be unfavourable as carrier for the nanobiocatalysts. The non-spherical shape would make determination of size increase after further functionalisation of the surface of the particles challenging and not accurate enough.

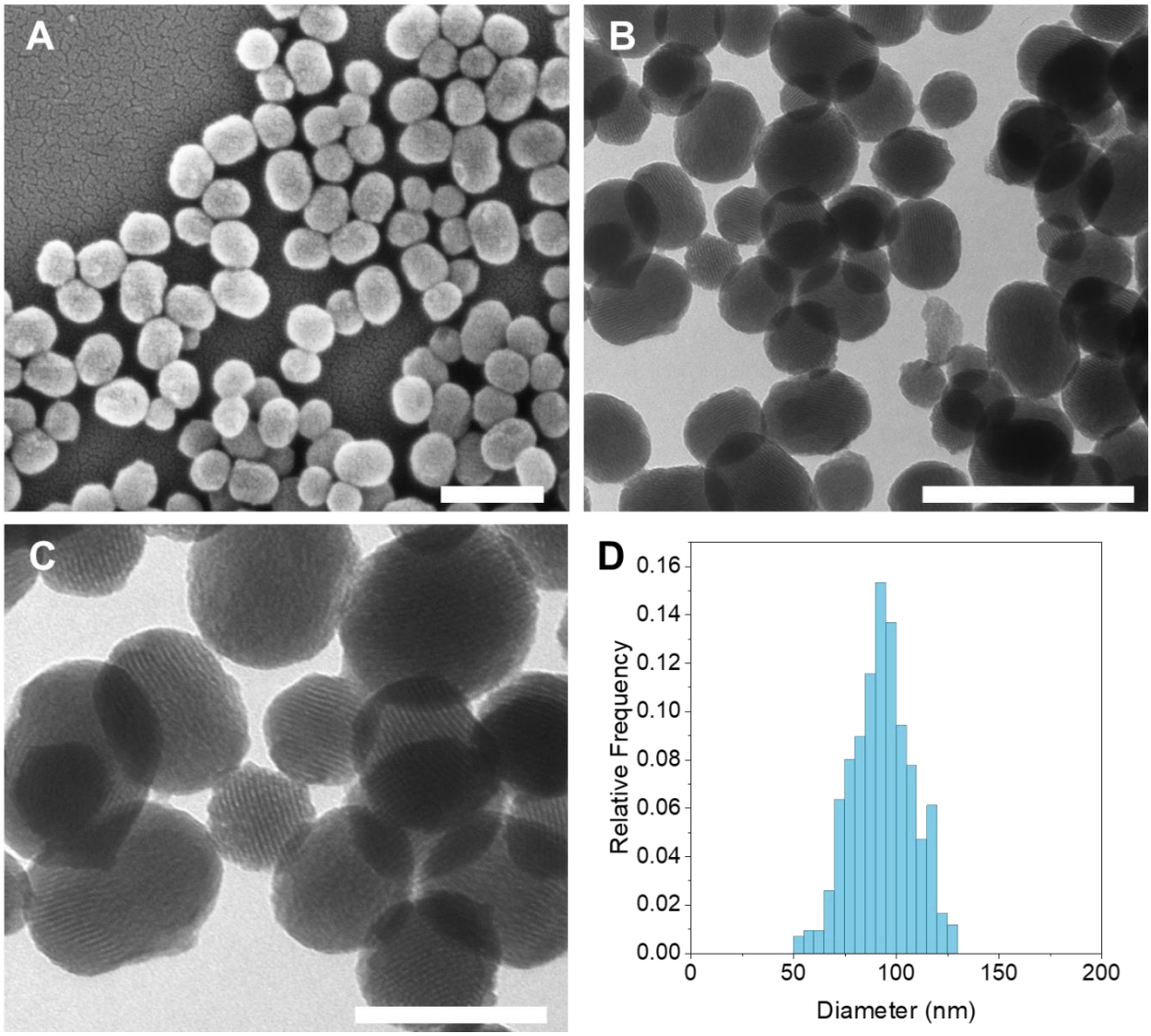

Figure 2.3 Electron micrographs and size distribution of the MCM-41 MSNs. (A) Representative SEM micrographs of the MCM-41 synthetised. (B) Representative TEM micrographs of the MCM-41 synthetised. (C) Close up of TEM micrograph with clearly visible porosity of MCM-4. (D) Distribution histogram of MCM-41. Scale bar represents: (A) 200 nm; (B) 100 nm; (C) 60 nm.

2.2.2 3D-MSN

The second class of carriers investigated within this work was three-dimensional dendritic mesoporous silica nanoparticles (3D-MSNs) (*126*). These are MSNs with a monodisperse as well as tuneable size and a controlled radial mesoporous structure. They are synthesised through a bi-phasic stratification approach and can be grown in multiple generations with each generation having its own individual pore size and thickness. In the synthesis, the lower aqueous phase consists of an organic base as a catalyst for the reaction and the cationic surfactant cetyltrimethylammonium chloride (CTAC) as a template for formation of the mesopores. The upper organic phase consists of TEOS as silica precursor dissolved in a

hydrophobic organic solvent. The two phases allow for the growth of the mesopore wall to occur only at the interfase in a controlled fashion. By varying the TEOS concentration and using various organic solvents with different molecular weight and hydrophobicity values, particles with different mesopore size can be obtained. Figure 2.4 shows a schematic illustration of the synthesis of 3D-MSNs. The obtained particles have a polar surface which will cause the accumulation of the particles in the lower aqueous phase. Since TEOS is dispersed in the organic phase, the mesopore wall can only continue to grow due to a swelling behaviour in the interphase when the particle is in the proximity of the upper organic phase. This is illustrated in the upper part of the scheme in Figure 2.4. Depending on the solvent and the TEOS concentration used, a more or less effective swelling behaviour will occur which will increase or decrease the pore size produced. The lower part of the scheme illustrates the biphasic system, the growth of the first generation of 3D-MSN (shown with a pink particle), the change of the upper organic phase to a different solvent with a changed TEOS concentration causing the growth of the second generation of the particles (illustrated with a blue second-generation particle). This feature of different pore size within individual generations of the particle makes these MSNs an excellent candidate as a carrier for the nanobiocatalysts to be produced in this work.

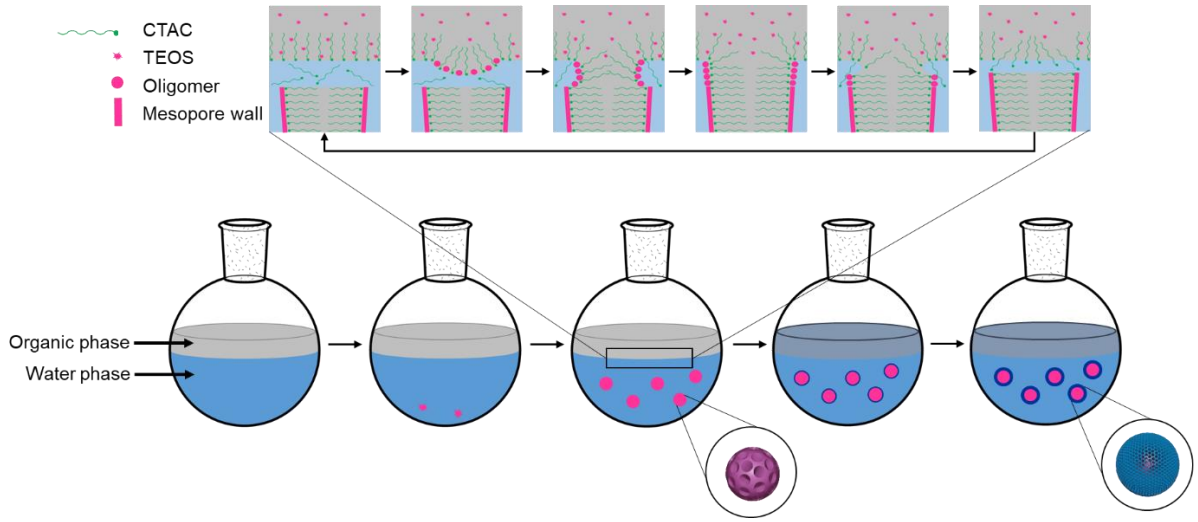

Figure 2.4 Schematic illustration of the synthesis of 3D-MSNs. The upper half of the image illustrates the growth of the mesoporous wall at the interphase between the aqueous and the organic phase. The lower half of the image demonstrates the growth of the first generation of the 3D-MSN. In the fourth flask, the upper organic phase has been replaced, allowing the second generation of the 3D-MSN to grow with a different pore size. Adapted from ref (*126*).

The synthesis parameters of the first generation 3D-MSN were set to obtain particles characterised by large pore size, expected to be 10 nm according to the published procedure (*126*). This allows for a large pore volume and therefore provides space for a higher amount of cofactor loading. For the second generation of the 3D-MSN, the parameters were adjusted to obtain a small pore size, *ca* 2.8 nm according to previously published results (*126*). This will restrict the immobilisation of any enzyme to the outer surface of the MSN, since no enzyme will be able to migrate through the small pores.

The 3D-MSN produced were characterised by means of SEM as well as cryoEM with representative micrographs shown in Figure 2.5 and Figure 2.6. The SEM micrographs display 3D-MSNs with high monodispersity and a spherical shape compared to MCM-41, a slightly uneven surface and an average size of 119 ± 11 nm (Figure 2.5). The size of the particles was determined by statistical analysis of the acquired SEM micrographs and size analysis software.

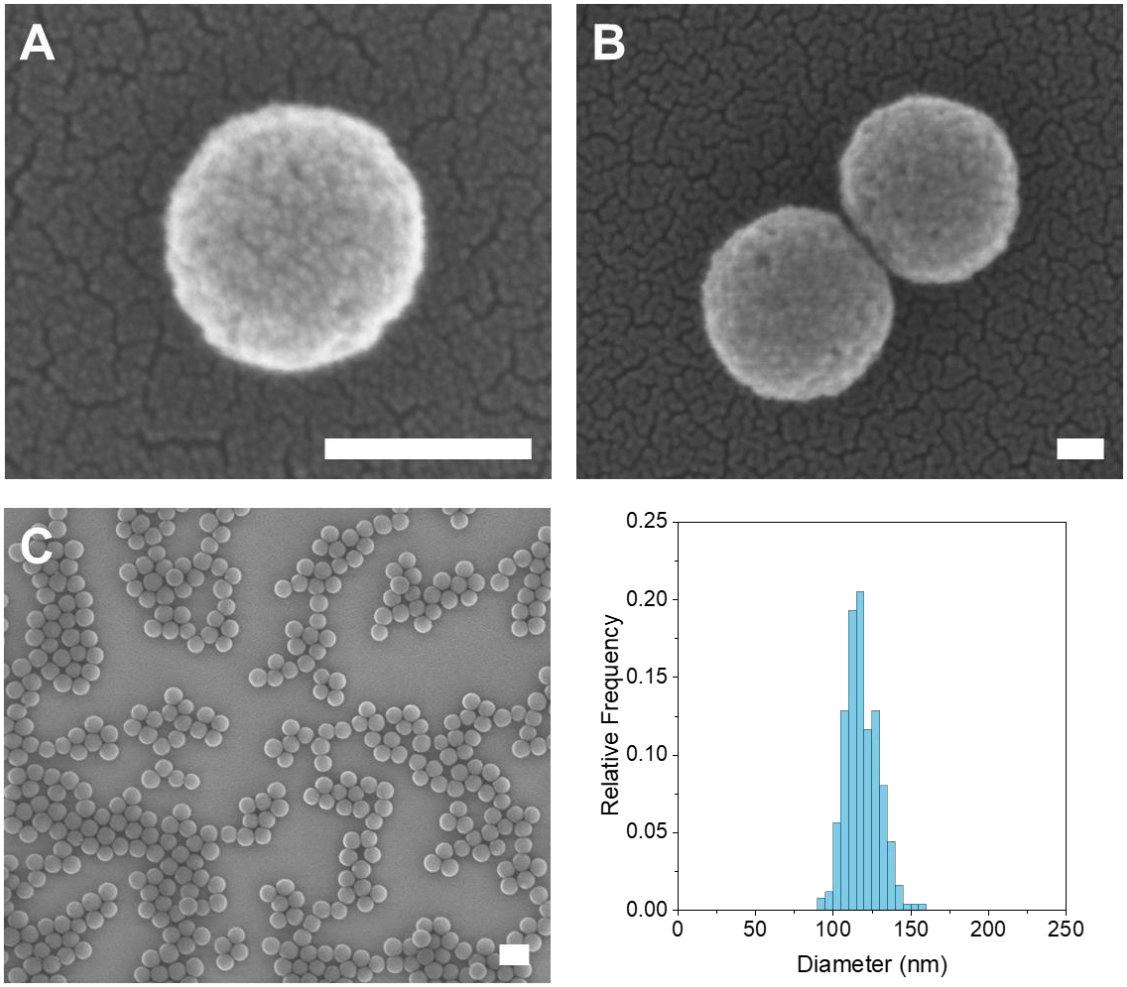

Figure 2.5. SEM micrographs and size distribution of the 3D-MSNs. (A), (B) and (C) Representative SEM micrographs of the 3D-MSN synthesised. Scale bar represents: (A) 100 nm; (B) 30 nm; (C) 200 nm. (D) Histogram of relative frequency of size distribution of 3D-MSN.

In the cryoEM micrographs are the radial mesopore structure of the 3D-MSNs revealed (Figure 2.6). In Figure 2.6 A and B the first generation of the 3D-MSN shown. The radial mesopore structure is clearly visible. In Figure 2.6 C and D are the particles after the growth of the second generation shown. Here the radial pore structure is not as clearly distinguishable, due to the smaller pore size in the second generation of the particles.

The monodisperse nature of the 3D-MSNs in combination with the tuneable pore size makes them a suitable choice as a carrier for the continuous synthesis of the nanobiocatalysts.

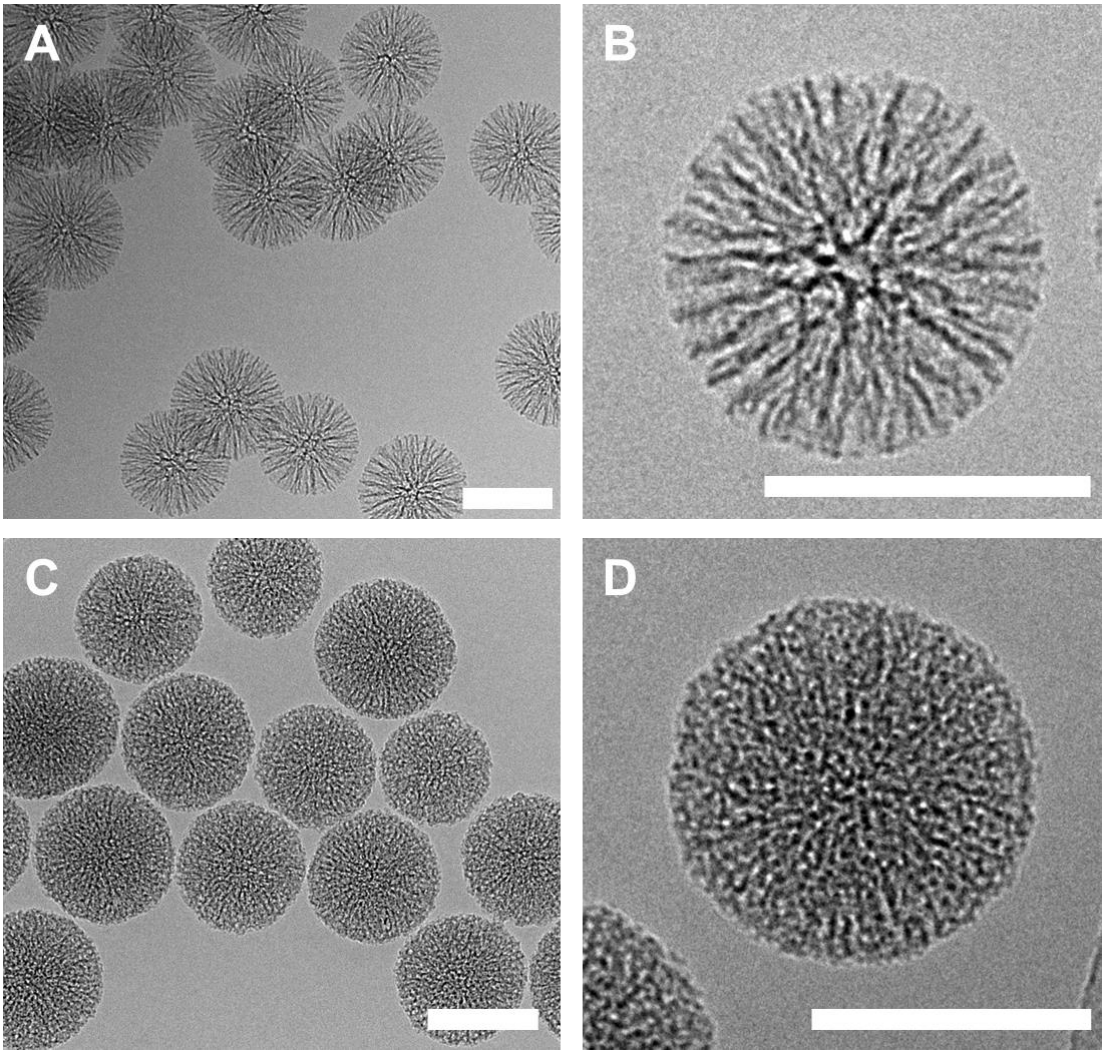

Figure 2.6. CryoEM micrographs of the 3D-MSNs. (A) and (B) Representative cryoEM micrographs of the first generation of the 3D-MSN synthesised. (C) and (D) Representative cryoEM micrographs of the second generation of the 3D-MSN synthesised.Scale bar represents: 100 nm in all micrographs.

2.3 Choice of enzyme

For the synthesis of the nanobiocatalysts four cofactor dependent oxidoreductases were investigated as possible suitable candidates for the final nanobiocatalysts. All four enzymes were expressed and purified within this work. The four enzymes are a secondary alcohol dehydrogenase from *Thermoanaerobacter ethanolicus* (TeSADH), a secondary alcohol dehydrogenase from *Sphingobium yanoikuyae* (SyADH), a reductive aminase from *Aspergillus oryzae* (RedAm) and lastly an ene-reductase of old yellow enzyme type from *"Ferrovum"* sp. JA12 (FOYE).

2.3.1 Enzymes used within this work

All the enzymes used within this work are listed in Table 2.1 together with some characteristics of each enzyme. The molecular weight of each enzyme was calculated from its amino acid sequence. The theoretical pI has been obtained by using the amino acid sequence of each enzyme and the online pI computing tool from Expasy (https://web.expasy.org/compute_pi/) (*127*).

Table 2.1 Enzymes used within this thesis and some characteristics of each.

	RedAm	**TeSADH**	**SyADH**	**FOYE**
Type	Reductive aminase	Alcohol dehydrogenase	Alcohol dehydrogenase	Ene reductase
PDB code	5G6R	7JNQ	4BMV	5OCS (of RmOYE)
MW (kDa)	64	157	58	87
Dimensions (nm)	8.8 x 4.6 x 3.5	8.7 x 8.4 x 8.0	7.7 x 4.2 x 3.6	9.5 x 5.0 x 4.0
pI	5.7	6.38	5.34	6.2
Cofactor	NADPH	NADP(H)	NADP(H)	NADPH
Substrate	Ketone or aldehyde and primary or secondary amines	Secondary alcohol or ketone	Secondary alcohol or ketone	Activated alkene

2.3.1.1 RedAm

RedAm is a reductive aminase from *Aspergillus oryzae* (*42*). The enzyme is an imine reductase homologue that has a high potential for reductive amination; it is also know to possess high substrate promiscuity. The enzyme is a dimer consisting of two identical subunits with a total molecular weight of 62 kDa. The estimated dimension of the enzyme is 8.8 × 4.6 × 3.5, based on structural analysis (PDB code: 5G6R)(*42*).

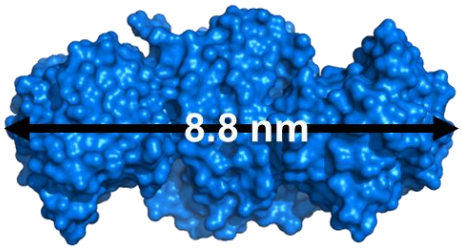

Figure 2.7. RedAm crystal structure displayed in surface mode. Longest dimension measured to 8.8 nm. Protein structure obtained from PDB code: 5G6R (*42*).

2.3.1.2 TeSADH

TeSADH is a secondary alcohol dehydrogenase from the thermophilic, anaerobic bacteria *Thermoanaerobacter ethanolicus*. For this work, a mutated version was selected, namely, TeSADH W110A (*128*, *129*). When compared to the wild-type enzyme, this mutant has been shown to possess a larger catalytic pocket, which allows accommodating larger substrates such as phenol-containing ketones (*74*, *128*). TeSADH W110A is a tetrameric enzyme consisting of identical 40 kDa subunits with an estimated total volume of 8.7 × 8.4 × 8.0 nm, based on protein structural analysis (PDB code: 7JNQ).

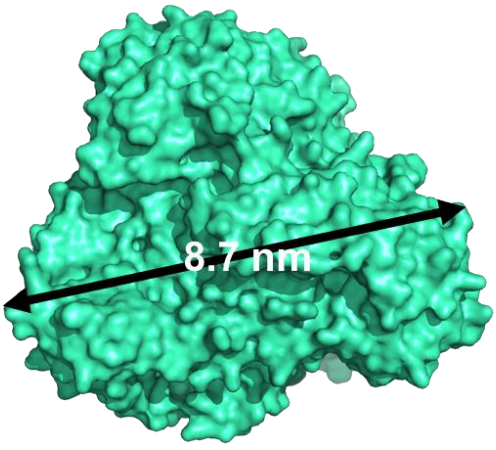

Figure 2.8. TeSADH crystal structure displayed in surface mode. Longest dimension measured to 8.7 nm. Protein structure obtained from PDB code: 7JNQ.

2.3.1.3 SyADH

SyADH is a secondary alcohol dehydrogenase from *Sphingobium yanoikuyae* that has previously shown to be able to accommodate bulky ketones as substrates (*130*, *131*). The enzyme consists of monomers with a molecular weight of 29 kDa which form a dimer. The estimated dimension of the enzyme is 7.7 × 4.2 × 3.6, based on structural analysis (PDB code: 4BMV)(*130*).

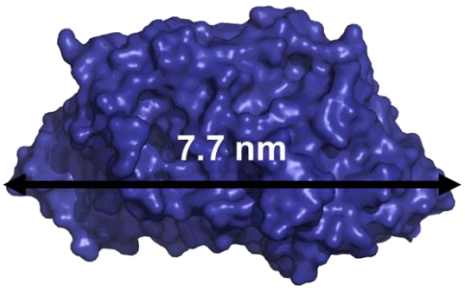

Figure 2.9 SyADH crystal structure displayed in surface mode. Longest dimension measured to 7.7 nm. Protein structure obtained from PDB code: 4BMV (*130*).

2.3.1.4 FOYE

FOYE is an ene-reductase from the acidophilic iron-oxidizing bacteria *"Ferrovum"* sp. JA12 (*40*). It belongs to the family of old yellow enzymes which are flavin-dependent enzymes (*132*). The selection of this enzyme was based on previous reports showing its thermostability and resistance towards several polar organic solvents *(132)*. The enzyme's monomer has a molecular weight of 43.5 kDa. There is currently no protein structure deposited in the PDB database for this enzyme. However, sequence alignment of FOYE with other known ERs has shown that this enzyme possesses the conserved amino acids associated with the thermophilic subclass of ERs (*40*, *133*). Within this group, the enzyme has shown similarity with other described ERs with the highest similarity to a mesophilic reductase, RmOYE from *Ralstonia (Cupriavidus) metallidurans*. Sequence alignment of FOYE displays that it has a 55% identity and 71% similarity with the sequence of RmOYE (*40*). Therefore, the protein structure of the RmOYE has been used for estimating the dimensions of the protein to 9.5 × 5.0 × 4.0 nm (PDB code: 5OCS) (*133*).

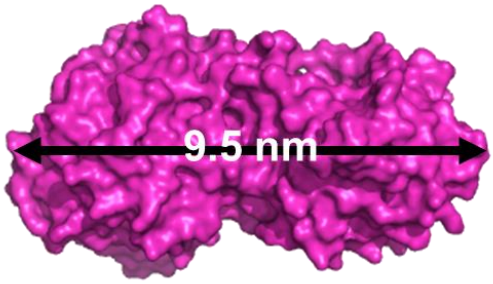

Figure 2.10 RmOYE crystal structure displayed in surface mode. Substitute for FOYE. Longest dimension measured to 9.5 nm. Protein structure obtained from PDB code: 5OCS (*133*).

2.3.2 Enzyme production and purification

All four enzymes produced within this thesis were prepared with *E. coli* as expression system. The sequences for the genes were cloned into the expression plasmid pET28c and the plasmid was transformed into the expression strain *E. coli* BL21 (DE3). TeSADH, SyADH and RedAm were produced using the ZYM-5052 medium for autoinduction (*134*). The incubation time and temperature during induction was optimised for each of the enzymes in regard to enzyme yield. FOYE was expressed in LBNB medium according to previously described literature (*40*, *132*). All four enzymes were expressed with a N-terminal 6xHis-tag, which was utilized for purification of the enzyme through affinity chromatography and in some cases for enzyme immobilisation to the MSNs.

2.3.3 Enzyme characterisation

After expression and purification, the amount of enzyme obtained was determined by means of the protein quantification assay BCA. The biocatalytic activity was measured for each enzyme through assays specific to each enzyme and the purity of the enzyme was controlled with sodium dodecyl sulfate–polyacrylamide gel electrophoresis (SDS-PAGE) (See the conditions for the activity assay in chapter 5.4.4). The enzymes were aliquoted with different concentrations of glycerol, exact concentration for each enzyme is provided in **Table *5.1***, and subsequently stored at -20 °C until further use.

2.4 Enzyme immobilisation

2.4.1 Amino modification

In order to immobilise the enzyme on the surface of MSNs, functionalisation of the surface was needed. The surface of the MSN was therefore chemically modified with (3-aminopropyl)triethoxysilane (APTES) to yield MSN-NH_2. This was done by reacting the

MSNs with APTES in water for 90 minutes at 20 °C. A schematic representation of the process can be seen in Figure 2.11.

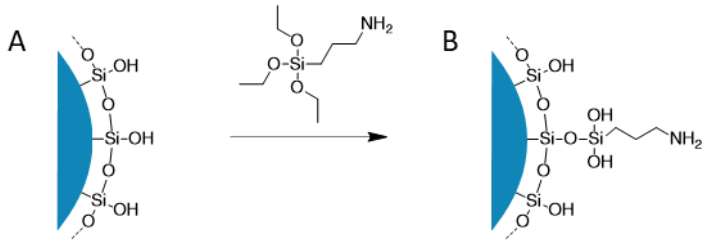

Figure 2.11. Schematic representation of the MSN-NH_2 synthesis. (A) MSN surface before functionalisation. (B) MSN surface after functionalisation with APTES.

By introducing aminopropyl functions at the surface of the MSNs, the surface charge of the particle changes owing to the amine's positive charge, which can effect of the colloidal stability of the particles (*135*). Therefore ζ-potential and dynamic light scattering (DLS) measurements were carried out to assess the change of the surface charge at different pH values after amino-functionalisation (Figure 2.12). This was done by dispersing the MSN and MSN-NH_2 functionalised with different concentration of APTES in water and thereafter titrating the suspension to the targeted pH value. The suspensions ζ-potential was thereafter determined. Additionally, the hydrodynamic size and the polydispersity index (PDI) of the MSN-NH_2 was determined (Figure 2.13, Figure 2.14, respectively). The unfunctionalised MSNs display a negative surface charge from *ca* pH 6 and higher. For the MSN-NH_2 the change from positive to negative surface charge occurs at a higher pH between 7 and 8. The working pH of all enzymes within this thesis are between pH values of 7 to 8. To obtain particles with maximum colloidal stability, a working pH value of 8 or higher would be suitable. This is due to nanoparticles reduced colloidal stability at ζ-potential values between ± 30 mV. Therefore are the compatibility between the pH values required by the enzymes and the ζ-potential values obtained from the MSN-NH_2 not optimal and may generate particle aggregation. The effect of APTES concentration on the colloidal stability of the particles was tested. From Figure 2.13 and Figure 2.14, it can be seen that the PDI and the hydrodynamic size of the MSNs are affected by the change in ζ-potential of the particles. The PDI increases from *ca* 0.15 to 0.3 - 0.5 at pH values between 6 and 8 for all amino functionalised MSN. This occurs with the hydrodynamic size as well, which increases from *ca* 200 nm to up to 1400 nm for the amino functionalised MSNs at pH values between 6 and 8. The results for both measurements suggest that the PDI and the hydrodynamic size increase when the ζ-potential goes to more neutral values. An increase in the hydrodynamic size of the particles in combination with more neutral zeta

potential values should however not be interpreted as an increased particle size. In this case it is rather a sign of aggregation, which can also be followed in the graph of PDI values. The particles aggregate together due to colloidal instability and are therefore detected as larger. Moreover, since the PDI is also significantly increasing, it is a further proof of aggregation of the particles, since the aggregation does not occur evenly.

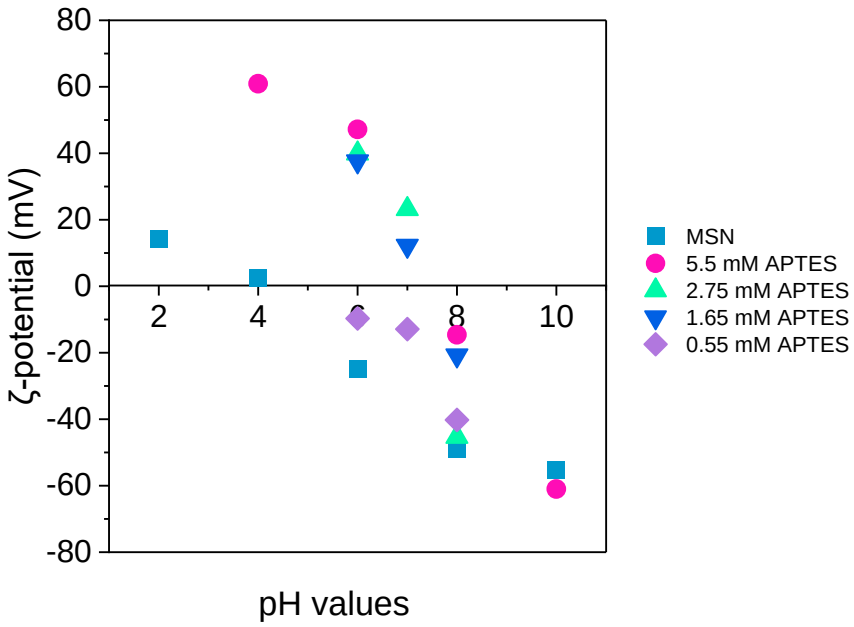

Figure 2.12. ζ-potential measurements of amino functionalised 3D-MSNs. Decreasing ζ-potential is observed at increased pH values. The unfunctionalised MSNs display a neutral surface charge at a pH value of *ca* 4. This is the lowest values of all particles. Amino functionalised MSNs display a neutral surface charge at pH values of *ca* 6 – 8. This can cause colloidal instability of MSN-NH_2 at pH values of 6 – 8.

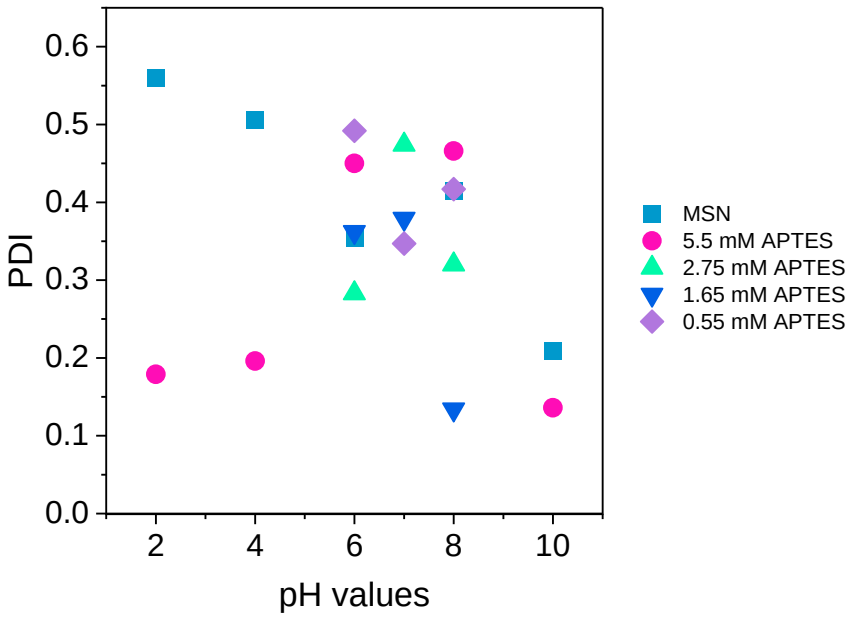

Figure 2.13. PDI measurements of amino functionalised 3D-MSNs. Increasing PDI is observed at decreasing pH values for unfunctionalised 3D-MSNs. Amino functionalised MSNs show an increase in PDI at pH values of *ca* 6 – 8. This indicates colloidal instability of MSN-NH_2 at pH values of 6 – 8.

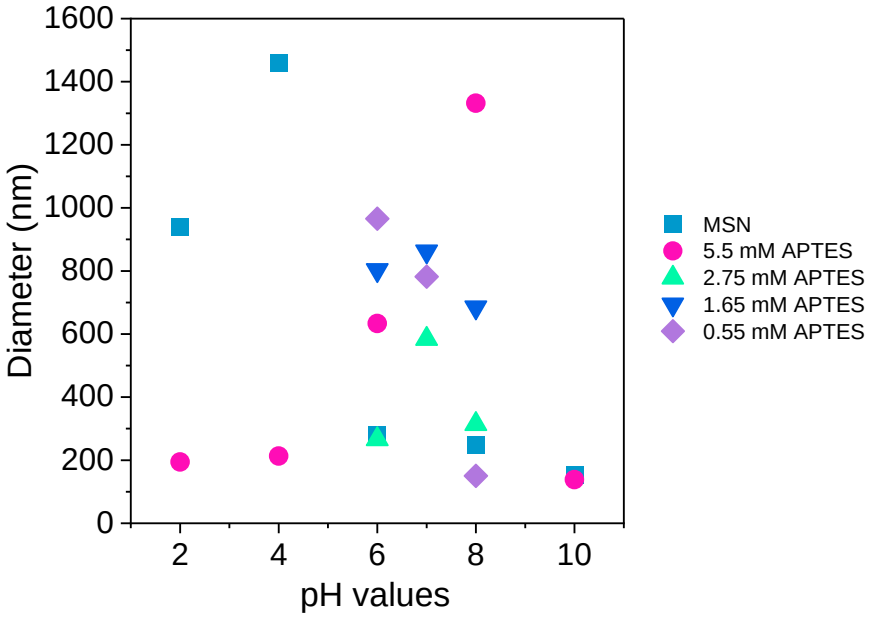

Figure 2.14. Hydrodynamic size of the 3D-MSNs. Increasing hydrodynamic size is observed at decreasing pH values for unfunctionalised 3D-MSNs. Amino functionalised MSNs show an increase in hydrodynamic size at pH values of *ca* 6 – 8. This indicates colloidal instability of MSN-NH_2 at pH values of 6 – 8.

2.4.2 Immobilisation strategies

Three major immobilisation strategies were tested within this thesis. Three were covalent immobilisation via the homobifunctional cross-linkers glutaraldehyde or ethylene glycol bis(succinimidyl succinate) (EGS) or immobilisation by affinity between the His-tag of the enzymes and Ni^{2+}:organic ligand functionalised MSNs.

2.4.2.1 Covalent immobilisation

In previous publications from our group, covalent enzyme immobilisation was performed with glutaraldehyde (*76*, *119*) and this immobilisation method was therefore carried out also in this work. Immobilisation using glutaraldehyde as crosslinker occurs through the reaction of the surface available lysine residues of the enzyme and the amine groups on the surface of the MSN-NH_2 with the aldehyde functions of glutaraldehyde by forming imines. A schematic representation of the immobilisation using glutaraldehyde is shown in Figure 2.15. This functionalisation is carried out by incubating MSN-NH_2 in buffer with 10.6 mM of glutaraldehyde at 20 °C for 20 minutes. The particles are thereafter collected, washed, and then incubated with one of the enzymes at 20 °C for 30 minutes followed by a final washing to remove the unbound enzyme; this yields $MSN_{G\text{-}Enz}$. The amount of immobilised enzyme was determined by analysing the soluble fraction of the enzyme immobilisation reaction mixture, collected by centrifugation, by means of a BCA assay.

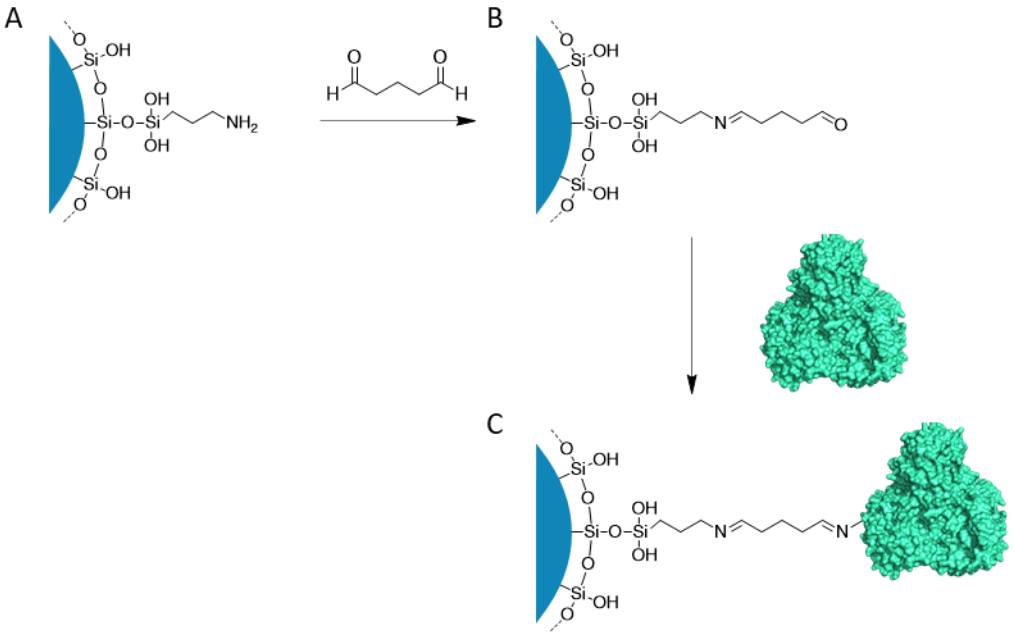

Figure 2.15. Schematic representation of immobilisation with glutaraldehyde. (A) MSN-NH_2 surface before functionalisation with glutaraldehyde. (B) MSN-NH_2 surface after functionalisation with glutaraldehyde. (C) Enzyme immobilised on MSN surface through imine formation between glutaraldehyde and surface available lysine on enzyme.

When this immobilisation was carried out with RedAm, the enzyme concentration used for immobilisation was 0.2 mg/mL. This yielded in an enzyme immobilisation rate of 91 % corresponding to 60 µg of enzyme per mg of MSN. Afterwards, the activity of the immobilised enzyme was tested, and could be determined to be 0.0017 U/mg of immobilised enzyme. This activity corresponds to 1.8 % of the activity of the soluble enzyme. Due to the low remaining activity after immobilisation, the $MSN_{G\text{-}RedAm}$ was deemed not to be a viable option for the final nanobiocatalysts, and an alternative crosslinking strategy was therefore required.

Consequently, an alternative homobifunctional crosslinkers i.e., EGS and PEGylated bis(sulfosuccinimidyl)suberate (BS(PEG)5) were tested. Similarly, to glutaraldehyde, both of these crosslinkers react with the surface available lysines of the enzyme and the amines of the MSN-NH_2. A schematic representation of the immobilisation with EGS is shown in Figure 2.16. The reactive groups of BS(PEG)5 are the same as for EGS and a schematic is therefore not shown, as the difference is only the length and substituents of the spacer arm.

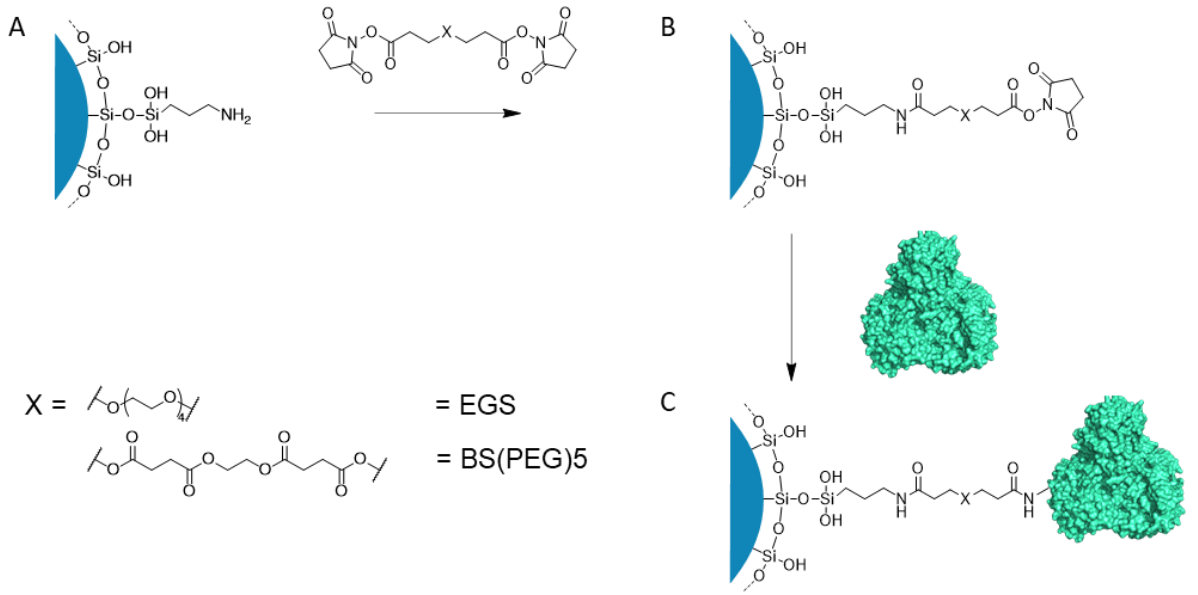

Figure 2.16. Schematic representation of immobilisation with EGS. (A) MSN-NH_2 surface before functionalisation with EGS or BS(PEG)5. (B) MSN-NH_2 surface after functionalisation with EGS or BS(PEG)5. (C) Enzyme immobilised on MSN surface through amide bond formation between EGS or BS(PEG)5 and surface available lysine on enzyme.

The immobilisation of RedAm on the surface of the MSN-NH_2 was caried out in the same way as with glutaraldehyde and the synthesis yielded $MSN_{EGS\text{-}RedAm}$ and $MSN_{BS(PEG)5\text{-}RedAm}$. The immobilisation rate for $MSN_{EGS\text{-}RedAm}$ and $MSN_{BS(PEG)5\text{-}RedAm}$ was determined to 84 % and 74 %, which corresponds to 55 µg and 49 µg of enzyme per mg of MSN, respectively. The activity was determined to be 0.021 U/mg and 0.018 U/mg of immobilised enzyme. This corresponds to 22 % and 19 %, respectively compared to the activity of the soluble enzyme (Figure 2.17). The reason for this increase in remaining activity when changing crosslinker even though the same amino acids of the enzyme is used could be attributed to the length of the spacer arm. The spacer arm of EGS is 7 atoms longer, while BS(PEG)5 is 14 atoms longer than the spacer arm of glutaraldehyde. Previously, earlier literature has established that the length of the spacer arm has an impact on the rigidification of the enzyme after immobilisation (*79*, *81*). One argument is that a shorter spacer arm will only give a low number of anchoring points from the enzyme to the carrier, since the length of the spacer restricts the access to larger amounts of anchoring points. However, due to the spacer's short length, the mobility of the amino acids involved in the anchoring is more restricted. This can cause a high rigidification of the enzyme by each anchoring point. Therefore, a more extended spacer arm would give less rigidification of the enzyme, and a higher probability of multiple anchoring points. Depending on the enzyme, these two different cases could have divergent effects. However, it seems that

the extended spacer of EGS and BS(PEG)5 does not have any positive effect on the efficiency of the immobilisation, which is reasonable since the same amino acids are used and the availability of these amino acids does not change when changing the crosslinker. However, it does not seem that the greater length of the crosslinker could enhance the immobilisation efficiency by reaching to multiple anchoring points. The vast difference between the samples is the increased retention of activity compared to the soluble enzyme. The reduced rigidification caused by the enhanced length of a spacer most likely therefore allows for a higher conformational mobility of the enzyme. As a consequence, the enzyme could easier accommodate the cofactor and the substrate in its active site. Due to the slightly higher immobilisation efficiency and remaining activity after immobilisation for the enzyme when immobilised with EGS compared to BS(PEG)5, EGS was deemed to be the better candidate in the quest for synthetising the nanobiocatalysts. Therefore, in further experiments only EGS was utilized.

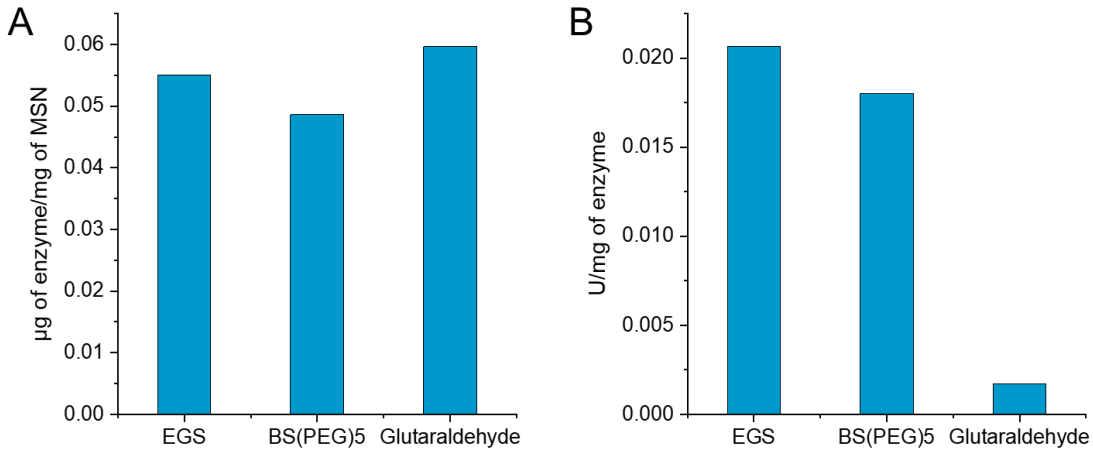

Figure 2.17. RedAm immobilisation and activity with different crosslinkers. Comparison of results obtained from three crosslinkers, EGS, BS(PEG)5 and glutaraldehyde (A) Amount of immobilised enzyme per mg of MSN. Similar immobilisation with all crosslinkers. (B) Activity per mg of immobilised enzyme. Significant increase in remaining activity when using EGS or BS(PEG)5 compared to glutaraldehyde for immobilisation.

The other preselected enzymes, SyADH, TeSADH W110A and FOYE were immobilised with the strategy described above. The immobilisation amount, immobilisation rate, activity per mg of immobilised enzyme and the remaining activity are listed in **Table 2.2**. This set of data shows a reasonably good immobilisation level for all enzymes within this work. However, it can be concluded that not only RedAm suffers from a high loss of activity after immobilisation

compared to the soluble enzyme. The only enzyme with a high remaining activity after immobilisation is TeSADH.

Table 2.2. Results of immobilisation with EGS and determined activity.

$MSN_{EGS-Enz}$	RedAm	FOYE	TeSADH	SyADH
Immobilised enzyme (µg/mg)	55	52	30	65
Immobilisation rate (%)	84	98	53	75
Activity of immobilised enzyme (U/mg of enzyme)	0.021	4.7	77	0.33
Remaining activity (%)	22	19	70	13

2.4.2.2 Immobilisation through affinity

After immobilisation of all the enzymes it was discovered that also FOYE and SyADH lost a large part of their activity even when using EGS as a crosslinker. It is important to consider that although the remaining activity for RedAm after immobilisation was significantly better when immobilised with EGS rather than glutaraldehyde, it was still far from the activity of the soluble enzyme. One possible explanation for the reduced activity after immobilisation could be an unfavourable orientation of the enzyme after immobilisation. EGS is targeting the surface available lysine residues of the enzyme for immobilisation, which are present at multiple points on the enzyme surface (Figure 2.18). Therefore, the orientation of the enzyme after immobilisation is not controlled and the immobilisation attachment point could for example occur close to the active sit of the enzyme which creates a steric hindrance for efficient cofactor and substrate access (*136*).

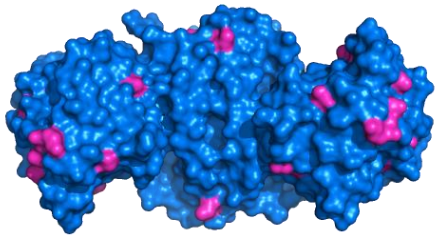

Figure 2.18 Surface of RedAm with surface available lysine marked in pink.

Alternative cross-linkers for an orientation-controlled immobilisation were therefore investigated. All the enzymes in this work have been purified via affinity chromatography by using a His-tag that was engineered to the sequence of the protein. A viable strategy would be to also exploit this tag for an orientation-controlled immobilisation (*137*). For this purpose, the MSN-NH_2 were modified to yield a nitrilotriacetic acid (NTA) functionalised surface to chelate Ni^{2+} and thereafter allow for immobilisation of the enzyme through affinity between the His-tag and the Ni^{2+}.

The functionalisation was done by incubating MSN-NH_2 in buffer with 21.2 mM of glutaraldehyde at 20 °C for 20 minutes. The particles were thereafter collected, washed, and then incubated with 25 mM of Nα,Nα-Bis(carboxymethyl)-L-lysine (LysNTA) for 30 minutes. The imines formed were reduced with $NaBH_4$ and the particles were washed. Subsequently, the particles were incubated with 100 mM of $NiSO_4$ to load the LysNTA with Ni^{2+}. The particles were washed and then incubated together with 0.2 mg/mL of enzyme at 20 °C for 30 minutes followed by a final wash to remove the unbound enzyme. This yields $MSN_{NTA\text{-}Enz}$ and the amount of immobilised enzyme was determined by analysing the supernatant from the enzyme immobilisation reaction with BCA assay. A schematic of the immobilisation strategy through His-tag affinity is shown in Figure 2.19.

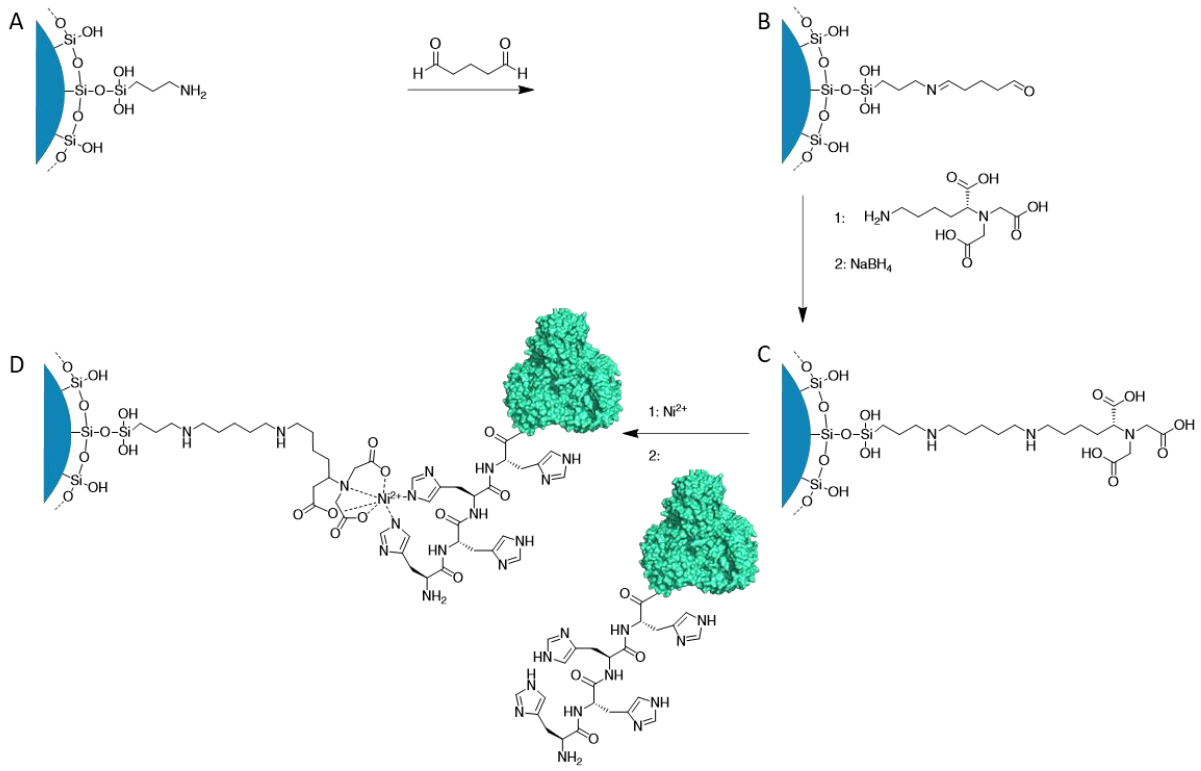

Figure 2.19. Schematic representation of enzyme immobilisation by His-tag affinity. (A) MSN-NH_2 surface before functionalisation with glutaraldehyde. (B) MSN-NH_2 surface after functionalisation with glutaraldehyde. (C) MSN-LysNTA surface after functionalisation with LysNTA through imine formation and subsequent reduction to amines. (D) Chelation of Ni^{2+} to MSN-LysNTA and then enzyme immobilisation through affinity between enzyme's His-tag and NTA:Ni^{2+}.

The affinity immobilisation strategy was tested for all four enzymes and the results are summarised in Table 2.3. From this set of data it is possible to conclude that the orientation-controlled affinity immobilisation is favourable for all the enzymes within this work but in particular for RedAm, FOYE and SyADH. The study of immobilisation efficiency does not reveal any major differences compared to the immobilisation achieved with glutaraldehyde, but a relevant difference can be observed in the remaining activity after immobilisation. For example, for RedAm the remaining activity has increased by a factor of three, from 22 % to 78 % and for FOYE it has increased close to a factor of four, from 19 % to 94 %. The increase in activity is most likely a combination of several aspects. One aspect is that the enzyme may benefit by a reduced conformational rigidity previously caused by the covalent attachment from EGS. Additionally, the longer linker gives the enzyme more freedom for movement when binding in the cofactor and the substrate. Lastly, with immobilisation through the His-tag each enzyme will only have one anchoring point (per monomer) to the particle and the enzyme will always have the same orientation. For neither of these enzymes the N-terminal His-tag is

located close to the active site of the enzyme. With only one anchoring point the enzyme can also experience less strain that previously could have been applied by multiple anchoring points to the same enzyme.

Table 2.3. Results of enzyme immobilisation through affinity and determined activity.

$MSN_{NTA-Enz}$	RedAm	FOYE	TeSADH	SyADH
Immobilised enzyme (µg/mg)	72	52	52	56
Immobilisation rate (%)	74	100	77	76
Activity of immobilised enzyme (U/mg of enzyme)	0.24	23	51	1.36
Remaining activity (%)	78	94	79	47

Additionally, to the produced particles listed in Table 2.3, particles with co-immobilised TeSADH and FOYE were prepared as well to use for a catalytic cascade reaction. The co-immobilised particles were prepared as the $MSN_{NTA-Enz}$ except for the enzyme immobilisation step. After having yielded MSN_{NTA} the particles were incubated with a reduced concentration of TeSADH (0.1 mg/mL). This was done in order to reach sub maximal immobilisation yield on the surface of the MSN_{NTA}. After incubation with TeSADH the particles were washed and the immobilisation of FOYE was carried out as described previously. This yielded $MSN_{Co-TeSADH/FOYE}$. The amount of immobilised enzyme was determined by analysing the supernatant from both enzyme immobilisation reaction reactions with BCA assay. The immobilisation rate for TeSADH and FOYE was determined to be 96 % and 69 % which corresponds to 26 µg and 52 µg of enzyme per mg of MSN respectively. The activity for each enzyme was determined to 36 U/mg and 18 U/mg of immobilised enzyme. This corresponds to 92 % and 107 %, respectively, compared to the activity of the soluble enzyme. Decreased immobilisation rate of FOYE compared to the single immobilisation rate was expected, as part of the surface is already occupied by TeSADH. That the total activity of TeSADH have decreased in this experiment from the data from single immobilised TeSADH is because two different batches of expressed protein was used for these experiments.

2.5 Enzyme shielding in organosilica layer

To shield the enzymes immobilised on the surface of the particles, a soft organosilica layer was grown at the surface of the particles. The organosilica layer was grown to protect the enzyme

and to ensure higher structural stability against destructive effects owing to solvent exposure that the particles later will be dispersed in. This layer growth process has previously been described for SNPs by our group (*76, 119*). The dimensions of each enzyme were presented earlier in this chapter (Table 2.1). The goal during the layer growth step was to completely shield the enzyme. Consequently, the targeted layer thickness was greater than the longest dimension of each enzyme structure. However, when using the same conditions as previously described but with MSN_{Enz} as a carrier, it yielded particles with a layer thickness of only 5 nm after 20h of incubation. This thickness does not completely shield any of the enzymes used and the parameters therefore needed optimization. A schematic representation of the layer growth process is shown in Figure 2.1

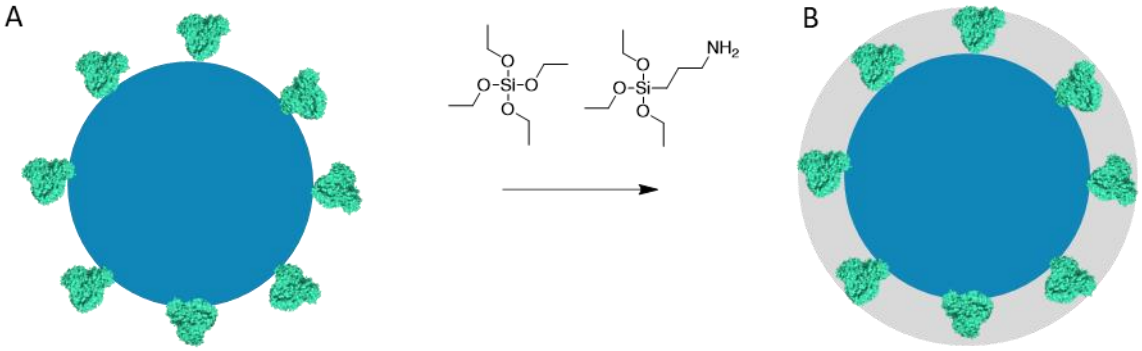

Figure 2.20. Schematic representation of the growth of shielding organosilica layer. (A) MSN_{Enz} are incubated with TEOS and APTES for growth of organosilica layer. (B) $MSN_{Enz\text{-}OrgS}$ with organosilica layer completely shielding the immobilised enzymes.

All enzymes within this work are cofactor-dependent oxidoreductases. When the final nanobiocatalysts are produced and used for biotransformation in organic solvents the mesoporous reservoir needs to be pre-loaded with cofactor. If the reservoir is not pre-loaded with cofactor the enzyme will not have any other access to cofactor and no catalysis can take place. The MSN_{Enz} were, prior to layer growth, dispersed in 1.5 mM $NADP^+$ in order to passively load the mesoporous reservoir by diffusion. The layer growth was then carried out by incubating the MSN_{Enz} with TEOS and APTES to produce the organosilica layer. The incubation time and temperature varied depending on which nanobiocatalysts that were produced.

2.5.1 Layer growth for enzymes immobilised with EGS

In order to grow the shielding layer, $MSN_{EGS\text{-}TeSADH}$ were reacted with 50 mM of TEOS and 9.4 mM of APTES for 20 h at 20 °C which yielded $MSN_{EGS\text{-}TeSADH\text{-}OrgS}$. The particles were characterised by SEM (Figure 2.22) and cryoEM (Figure 2.23). The size of the particles after layer growth was determined by statistical analysis of the acquired SEM micrographs and size analysis software. The layer thickness was then calculated by subtracting the size of the unshielded particle from the shielded particle and then divided by two to obtain the layer thickness increase from the surface. The particle size after shielding was determined to 141 ± 11 nm which yielded a layer thickness of 11 nm and therefore completely shields the immobilised TeSADH (longest dimension of 8.7 nm). A histogram of the particles size before and after shielding is presented in Figure 2.21. A noteworthy finding is a constant polydispersity of the particle size before and after shielding, confirming a homogenous layer growth.

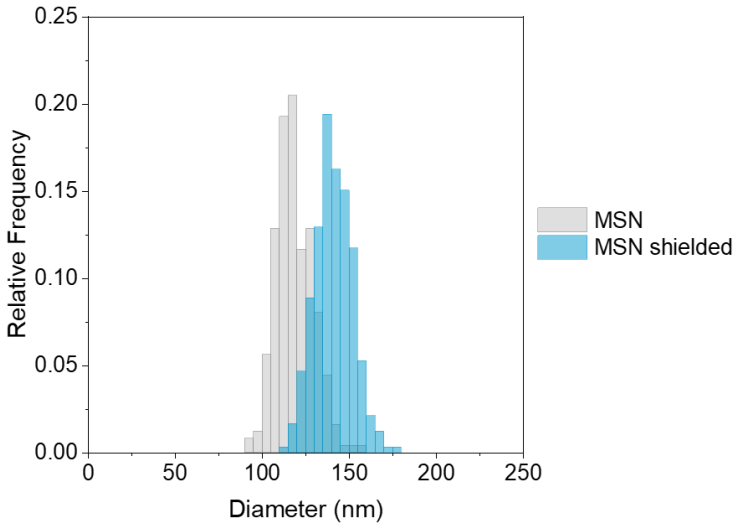

Figure 2.21. Histogram of the MSN particle size before and after shielding. Relative frequency of size distribution of unshielded MSN, in grey, and shielded $MSN_{EGS\text{-}TeSADH\text{-}OrgS}$ in turquoise. At least 240 particles were measured of each type.

The morphology of the shielded particles has changed compared to the bare MSN. This is particularly visible in Figure 2.22 C and D where some structure can be seen on the surface of the particles. In Figure 2.22 A a crack in the organosilica layer can be seen with the inner mesoporous reservoir still intact, which is a further proof of the change in morphology as well as rigidity between the two materials.

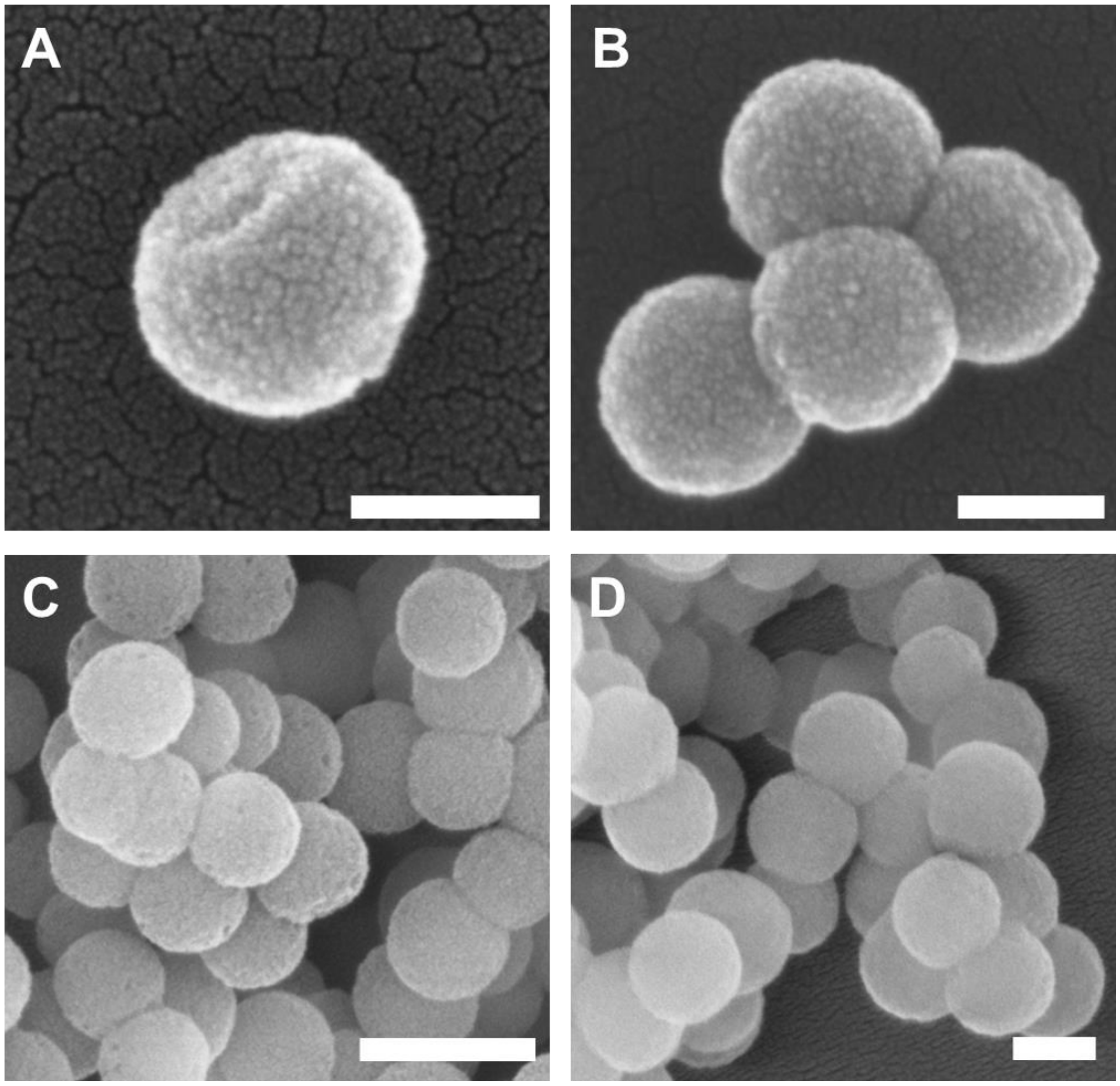

Figure 2.22. SEM micrographs of the shielded MSNs. All micrographs display shielded $MSN_{EGS\text{-}TeSADH\text{-}OrgS}$. (A) A crack in the organosilica layer is visible with the mesoporous core still intact, visible through the hole. (B), (C), (D) Morphology of the organosilica layer is visible. Scalebar represents 100 nm for (A), (B) and (D) while it represents 200 nm for (C).

The property differences between the organosilica layer and the core MSN is also visible in the cryoEM micrographs (Figure 2.23). The porosity of the mesoporous core is still clearly evident in all the particles. Additionally, there is a degree of transparency present when multiple particles are stacked on top of each other, indicating a lower material density which is further proof of porosity maintained within the core particle. This indicates that the organosilica layer has grown on the surface of the particles and did not fill the mesopores within the core. The organosilica layer on the other hand appears smooth in the cryoEM micrographs with no visible mesopores. A clear border between the two materials is indicated with white arrows in Figure 2.23 C. Like in the SEM micrographs in Figure 2.23 B, there is another crack in the organosilica

layer, indicated with a white arrow, with the core particle still intact and sticking out. These cracks, in the layer are most likely caused by two particles having been close together during the layer growth. When they later separated the core got exposed. The presence of these cracks indicates the softness and formability of the organosilica layer, which can provide comfortable support for the immobilised enzyme.

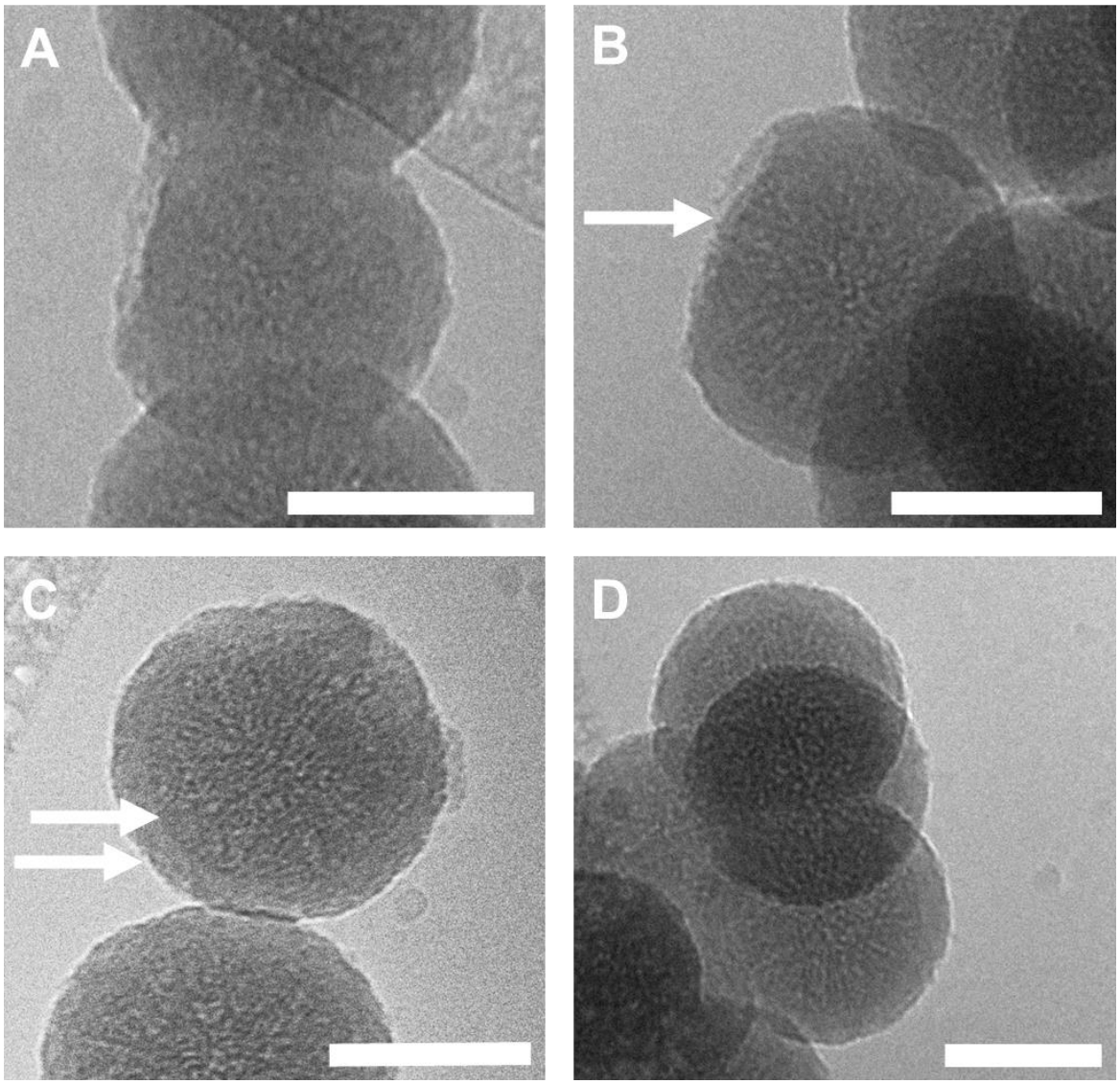

Figure 2.23. CryoEM micrographs of the shielded MSNs. Representative cryoEM micrographs of the shielded $MSN_{EGS\text{-}TeSADH\text{-}OrgS}$. (A) Shielded MSN with crack in layer. (B) White arrow points out crack in organosilica layer exposing the still intact MSN core. (C) White arrows point out structural difference between MSN core and the surrounding organosilica layer. (D) Overlapping $MSN_{EGS\text{-}TeSADH\text{-}OrgS}$ with pore structure still visible. Scalebar represents 100 nm for all micrographs.

The layer growth was also carried out for the other enzymes immobilised with EGS. The final layer thickness, the specific activity and the remaining activity compared to the soluble enzyme

for each enzyme is presented in Table 2.4 It can be deducted from the observed values that the activity has dropped for all samples after shielding. Especially for RedAm, FOYE and SyADH the activity appears particularly low. It was also for these enzymes that a substantial amount of the activity was reduced after immobilisation with EGS. A cause for this loss could be additional rigidity applied to the enzymes with the layer in addition to the rigidity caused by the crosslinker. These results with almost non existing activity after shielding were a contributing factor to that the affinity immobilisation strategy was investigated. Results of shielding effect on affinity-immobilised particles are presented later in chapter 2.5.2. For TeSADH there was a loss of activity after shielding, however 28 % of the activity is still remaining. Therefore, these particles were deemed to be suitable for application in biotransformation reactions and continuous flow catalysis presented in chapter 3.

Table 2.4. Layer thickness of $MSN_{EGS\text{-}Enz}$. and determined activity.

$MSN_{EGS\text{-}Enz\text{-}OrgS}$	RedAm	FOYE	TeSADH	SyADH
Layer thickness (nm)	8	9	11	11
Activity of shielded enzyme (U/mg of enzyme)	0.002	0.1	31	0.076
Remaining activity (%)	0.2	0.4	28	4

2.5.2 Layer growth for enzymes immobilised through affinity

A shielding layer was grown also on the $MSN_{NTA\text{-}Enz}$ particles. Interestingly the layer growth speed increased significantly for these particles compared to the $MSN_{EGS\text{-}Enz}$ when grown in the same conditions (Figure 2.24 A). Additionally, the morphology of the surface of the particles after shielding changed and appeared as if the layer had grown almost uncontrolled due to its rough and un-homogeneous appearance (Figure 2.24 B).

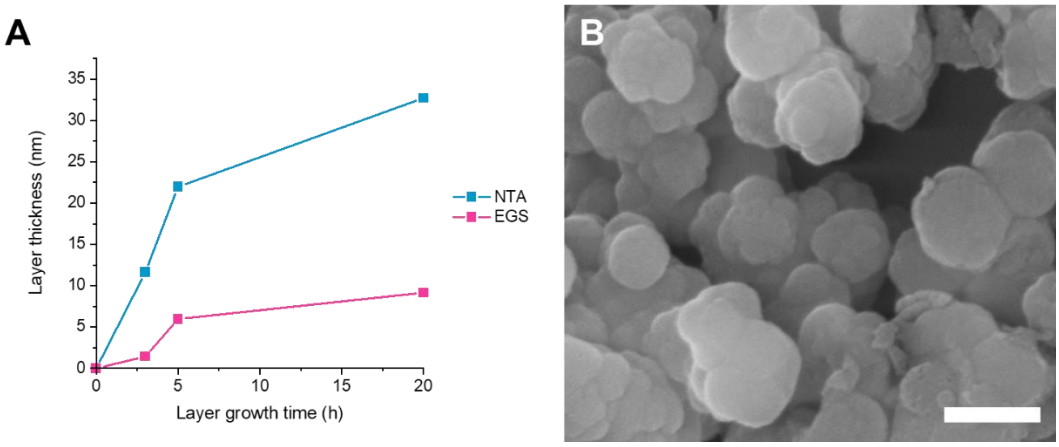

Figure 2.24. Layer growth kinetics and SEM micrograph. (A) Comparison of layer growth kinetic for layer growth on $MSN_{EGS\text{-}FOYE}$ compared to $MSN_{NTA\text{-}Enz}$ with layer growth conditions for MSN_{EGS} or MSN_{G}. (B) Representative SEM micrograph of $MSN_{NTA\text{-}Enz}$ after 20 h of layer growth. Inhomogeneous organosilica layer that has grown with poor control can be observed. The scalebar represents 200 nm.

Due to the observed increase in layer thickness and layer growth speed, the conditions for the layer growth on $MSN_{NTA\text{-}Enz}$ needed to be adjusted and optimized. Several trials were made and the conditions that turned out to be the most successful included the reduction of TEOS and APTES concentration to 26.6 mM and 5 mM respectively in combination with an incubation temperature of 10 °C for the layer growth. This combination seemed to slow down the layer growth sufficiently and a layer thickness of between 7.8 to 11.5 nm was obtained after 5 hours of incubation (Table 2.5). In Figure 2.21 SEM micrographs of the particles produced using these conditions are shown. The morphology of the surface is still not similar to the morphology of the $MSN_{EGS\text{-}Enz\text{-}OrgS}$ but the layer has grown in a more controlled fashion. This has left particles with rough surface structure.

Table 2.5. Layer thickness of $MSN_{NTA\text{-}Enz}$ and determined activity.

$MSN_{NTA\text{-}Enz\text{-}OrgS}$	RedAm	FOYE	TeSADH	SyADH
Layer thickness (nm)	8.2	11.5	7.8	8.6
Activity of shielded enzyme (U/mg of enzyme)	0	6.5	32	0.84
Remaining activity (%)	0	39	51	29

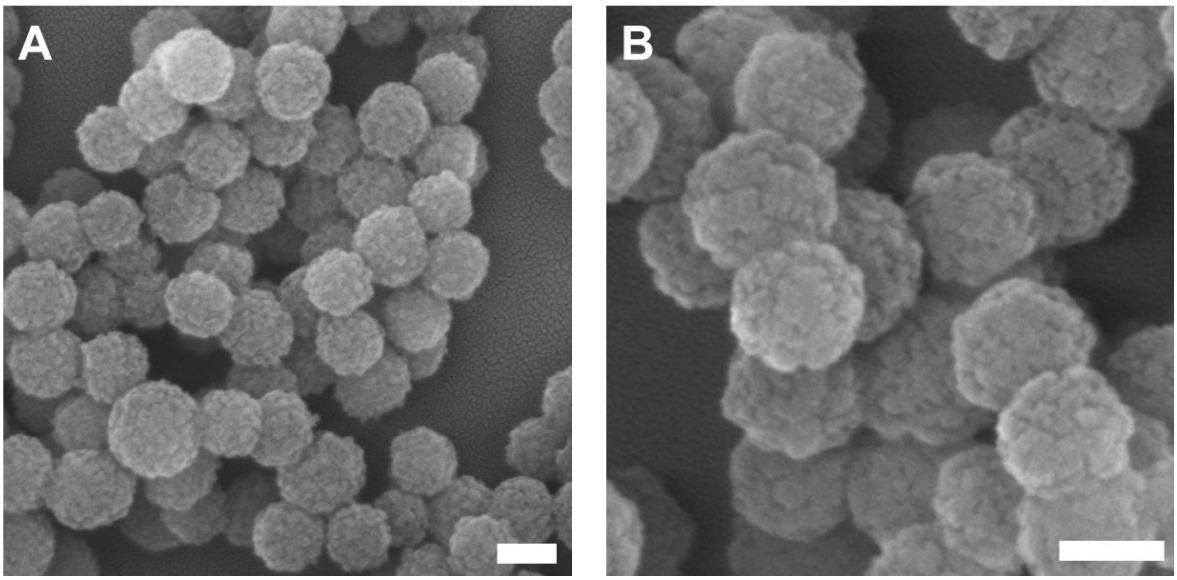

Figure 2.25. SEM micrographs of shielded MSNs. All micrographs display $MSN_{NTA\text{-}Enz\text{-}OrgS}$ Representative SEM micrographs are shown. Structured organosilica surface of $MSN_{NTA\text{-}Enz\text{-}OrgS}$ after 5 h of layer growth at 10°C with reduced TEOS and APTES concentration. Scale bars represent 100 nm

The shorter layer growth time, in combination with the more orientation-controlled immobilisation through affinity binding has a positive impact on the enzymatic activity after layer growth for three of the four enzymes. For RedAm no activity could be detected even with these conditions. Therefore, it seems that the conditions for achieving layer growth are too harsh for this enzyme.

Furthermore, the soluble RedAm loses a major part of its activity if incubated with stirring in a similar fashion as MSN_{Enz} during the immobilisation and the layer growth. The shielding organosilica layer is not able to stabilise the enzyme to be able to recover any of the activity of the immobilised enzyme. However, the loss of activity of the soluble enzyme suggests additional stability issues with this enzyme. Further studies would be needed to determine the cause of this loss of activity after layer growth. For example, could differential scanning fluorimetry be done to evaluate how much folded protein is present after layer growth. This could rule out a loss of activity owing to poor diffusion of the substrates to the active site of the enzyme and not denaturation of the enzyme structure.

Moreover, at this stage of work, also SyADH was ruled, not because of poor remaining activity but simply due to TeSADH displayed higher catalytic efficiency.

Lastly, in this part of the work, growth of an organosilica layer on the $MSN_{Co\text{-}TeSADH/FOYE}$ was carried out. These where particles were the immobilisation was carried out through affinity as

well. The same conditions for the layer growth on $MSN_{NTA\text{-}Enz}$ that was previously described in this chapter for $MSN_{NTA\text{-}Enz}$ were tried also for these particles. The obtained layer thickness was 9.2 nm and the activity was determined to 8.4 U/mg and 30 U/mg for FOYE and TeSADH respectively. This corresponded to 50% and 55% or remining activity compared to the soluble enzyme. The co-immobilisation of enzymes and subsequently shielding was deemed to create viable nanobiocatalysts.

Chapter 3

Application of nanobiocatalysts in biotransformations

3 Application of nanobiocatalysts in biotransformations

The following chapter describes the investigation of the biocatalytic and cofactor recyclability properties in organic solvents of the nanobiocatalysts produced in chapter 2. The nanobiocatalysts were tested in two main ways, batch mode and continuous flow mode. The $MSN_{EGS\text{-}TeSADH\text{-}OrgS}$ and $MSN_{Co\text{-}TeSADH/FOYE}$ were used for the experiments.

3.1 Biotransformations in batch mode

3.1.1 Biotransformations with TeSADH W110A in batch mode

To assess the biocatalytic properties and cofactor recycling ability of the produced $MSN_{EGS\text{-}TeSADH\text{-}OrgS}$ described in chapter 2, a series of relevant ketones were selected as substrates for TeSADH W110A. The substrates were benzylacetone (**1**), phenylacetone (**2**), cyclohexanone (**3**), 6-methyl-5-hepten-2-one (**4**), 4-phenyl-3-buten-2-one (**5**), phenoxy-2-propanone (**6**), 4-(4-methoxyphenyl)-2-butanone (**7**) and β-tetralone (**8**) (*128*). Additionally, four different solvents with increasing hydrophobicity were selected: ethyl acetate (EtOAc), methyl *tert*-butyl ether (MTBE), toluene and heptane. The different solvents were selected to investigate the impact of hydrophobicity on the catalytic potential of the nanobiocatalyst.

The biotransformations were carried out by removing the buffer the $MSN_{EGS\text{-}TeSADH\text{-}OrgS}$ were stored in, and then dispersing the nanobiocatalysts in the reaction solution. For each reaction, 1.92 mg of particles was used, which represents 0.058 mg of TeSADH W110A. The reaction solution consists of 30 mM of one of the ketones and 2 M of isopropanol (*i*-PrOH) as cosubstrate acting as a hydride source for the cofactor recycling. These two chemicals were then dissolved in one of the four solvents. The large excess of *i*-PrOH compared to the ketone was used to maximise the reduction of the ketone. As previously mentioned in chapter 2, the nanobiocatalysts were loaded with $NADP^+$ through diffusion before the growth of the organosilica layer and were afterwards kept in buffers supplemented with $NADP^+$ to keep the mesoporous reservoir loaded. However, no additional $NADP^+$ (or NADPH) was added to the system during the duration of these experiments. The reaction mixtures were incubated for 18 hours at 45 °C under stirring. After incubation the particles were removed and the conversion to the corresponding alcohol was determined with gas chromatography equipped with flame ionisation detection (GC-FID), using calibration curves established with the substrates and products. The catalysed reaction and the conversion of each ketone in the four solvents are presented in **Table 3.1**.

Table 3.1. Biotransformation reduction of ketones in organic solvents On top of the table the reaction catalysed by the enzyme is shown. The cosubstrate *i*-PrOH is oxidized to acetone by the enzyme while simultaneously reducing $NADP^+$ present in the mesopores. This then allows the enzyme to reduce the ketone to its corresponding alcohol and consequently oxidize the cofactor and therefore completing on recycling cycle.

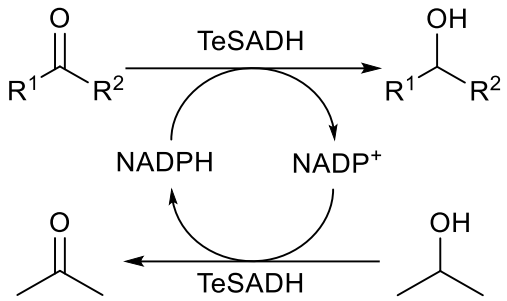

n	Ketone	Conversion (%)			
		MTBE	EtOAc	Toluene	Heptane
1	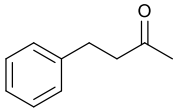	90	20	74	98
2	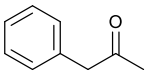	>99	45	92	>99
3	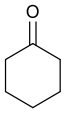	>99	>99	>99	>99
4	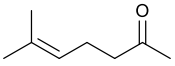	87	46	89	87
5	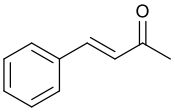	8	0.3	6	43
6	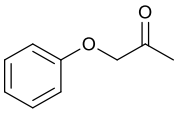	>99	45	97	>99
7	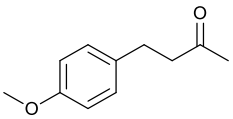	65	11	37	98
8	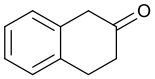	>99	76	>99	>99

One can conclude from the data in **Table 3.1** that the $MSN_{EGS\text{-}TeSADH\text{-}OrgS}$ transformed all substrates with the cofactor from the mesoporous core of the MSN. Since the loading of the pore of the MSN took place through diffusion and the pore volume of the MSN is 0.527 cm^3 per g of MSN, the amount of $NADP^+$ present for each reaction is estimated to be *ca* 1.5 nmol. This value is drastically lower than the amount of available substrate i.e. 6 µmol. Additionally,

the conversion of the substrate requires the reduced form of the cofactor, only available to the enzyme when one oxidation of the cosubstrate has already taken place. The successful conversion therefore confirms that the mesoporous reservoir allows the cofactor to reach the active site of the enzyme to first be reduced while simultaneously oxidise the cosubstrate *i*-PrOH coming from the surrounding solvent. Thereafter, the now reduced cofactor NADPH can be oxidised by the enzyme and consequently reduce the ketone to its corresponding alcohol thus completing the cycle of the cofactor and bringing it back to its original oxidation state.

The reaction efficiency was as high as 98 % for six of the eight substrates tested (1, 2, 3, 6, 7 and 8). The highest conversion overall was achieved with **3**, with which a value greater than 99 % conversion was obtained with all solvents tested. For **8**, equally high conversion was achieved in three of the solvents, MTBE, toluene and heptane, while for **2** and **6** it was obtained in MTBE and heptane. For **1**, the highest conversion achieved was 98 % in heptane and **4** reached the highest conversion of 89 % in toluene. On the contrary, the substrate with the lowest conversion were **5** which reached the highest conversion of 43 % in heptane but did not exceed 8 % with the other solvents. However, this lower level of conversion of substrate **6** by TeSADH W110A is in agreement with earlier literature of the same substrate and enzyme combination in water:*i*-ProOH mixtures (*128*).

The results discussed above shows that overall, the catalytic properties of the enzyme have been preserved and this further suggests that the conformation of the enzyme has been maintained within the organosilica layer. The conformation of the enzymes active site for both the cofactor and the substrate have consequently not been altered by the shielding layer. In a previous work, we demonstrated that the organosilica shielding layer had altered the promiscuity of the enzyme due to a changed substrate scope of the shielded enzyme compared to the soluble enzyme (*120*). This phenomenon was not observed in this work since the promiscuity of the enzyme appeared unchanged, with the tested substrate, before and after shielding (*128*).

The ee of the reduction of **1** by $MSN_{EGS\text{-}TeSADH\text{-}OrgS}$ were also determined in all four solvents. The ee were determined by chiral GC-FID and this experiment showed a >98 % ee of (S)-4-phenyl-2-butanol for all the four solvents in this work. This result indicates that the enantioselectivity of the TeSADH was not affected by the solvent. It can therefore be concluded that the shielding organosilica layer have not hampered the enantioselectivity of the enzyme. This is also further proof that the conformation of the enzyme and the active site have not been

affected by the shielding organosilica layer. The shielding has rather helped to maintain the enantioselectivity of the enzyme. This is something that was not observed in an earlier study of this enzyme's enantioselectivity in organic solvents (*74*).

The results from Table 3.1 suggest that there is a connection between the hydrophobicity of the solvent and the catalytic efficiency of the nanobiocatalyst with higher achieved conversion with increased hydrophobicity of the solvent. An example of this has been plotted in a Figure 3.1 with the conversion of **1** and **2** versus the hydrophobicity (using the octanol-water partition coefficient log*P*) of the solvents used. This behaviour can be explained by the lower capability of a solvent with higher hydrophobicity to strip the enzyme of structurally needed water molecules (*27*). However, there is an exception to this trend where the conversion for most substrates is slightly higher in MTBE compared to conversion observed in toluene. This may be attributed to a competitive inhibition by toluene with the substrates tested (*74*). Indeed, the active site of the enzyme is known to accommodate aromatic moieties well in its hydrophobic pocket (Ala85, Ala110 and Tyr267) (*46*).

These results also point out the importance of the solvent for the reaction efficiency. It was initially expected that the enzyme could catalyse the reaction in the highly hydrophobic solvent heptane, as reported in previous studies (*74*). However, the results revealed high conversion in solvents with lower hydrophobicity as well. These solvents were thought to be of greater challenge to the enzyme by more efficiently removing structural water molecules. The remaining catalytic stability of the enzyme is most likely due to a combined effect of the water reservoir in the core of the particle and the shielding organosilica layer, where the former is in close vicinity of the enzyme and the latter have the ability to establish interactions with the surface of the enzyme (*76*).

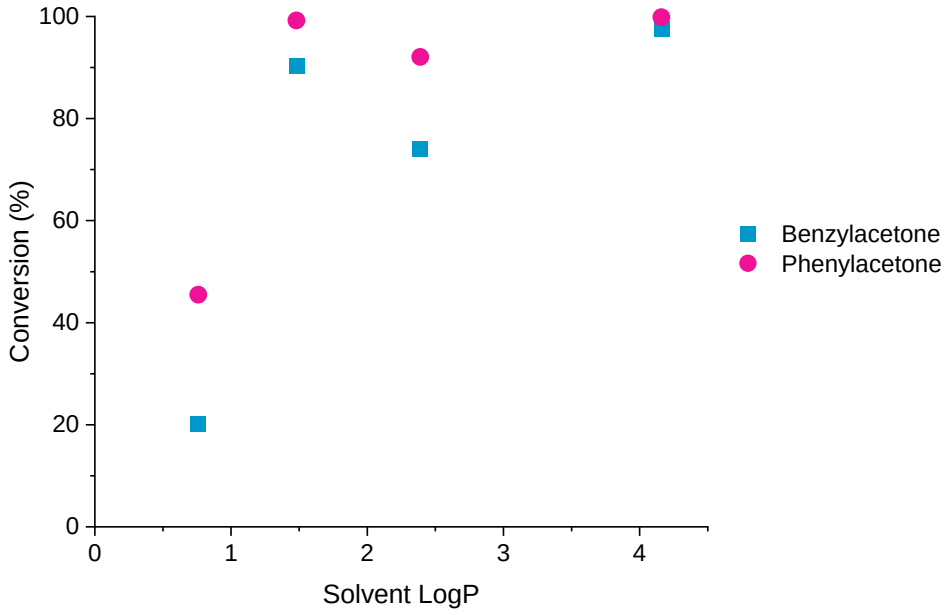

Figure 3.1. Ketone reduction as a function of the solvent hydrophobicity. Reduction of benzylacetone (turquoise) or phenylacetone (pink) (in % of starting amount) to their corresponding alcohols. Log*P* values of the solvents used: EtOAc (0.76), MTBE (1.48), toluene (2.39) and heptane (4.16).

In order to assess the recyclability and the long-term stability of the $MSN_{EGS\text{-}TeSADH\text{-}OrgS}$ in organic solvents a recycling experiment was set up. The experiment was performed in a similar fashion as the previously described biotransformations. Either ketone **1** or **2** were used as substrate and to assess the recyclability the biotransformation was performed up to 9 cycles with the same particles. The recyclability was tested in two ways, with or without re-equilibration of the $MSN_{EGS\text{-}TeSADH\text{-}OrgS}$ in buffer supplemented with $NADP^+$ between each repetition cycle. The incubation step in the buffered $NADP^+$ solution was done by resuspending the particles in the buffer after collecting the supernatant for GC analysis. The particles were then collected again by centrifugation to remove any remaining MTBE, substrate or product and again resuspended in the buffered $NADP^+$ solution. The $MSN_{EGS\text{-}TeSADH\text{-}OrgS}$ were then incubated for 15 minutes to allow the aqueous phase contained in the mesoporous core to re-equilibrate with the buffered environment. Finally, the $MSN_{EGS\text{-}TeSADH\text{-}OrgS}$ were once again collected by centrifugation, the buffered $NADP^+$ solution was removed, and the $MSN_{EGS\text{-}TeSADH\text{-}OrgS}$ were resuspended in the fresh reaction solution for the next cycle. For the $MSN_{EGS\text{-}TeSADH\text{-}OrgS}$ without incubation the particles were instead washed with the reaction solution, without substrate, between each cycle in order to remove any unreacted substrate or remaining

product before the next cycle. The results from the recycling experiment are presented in **Figure 3.2**.

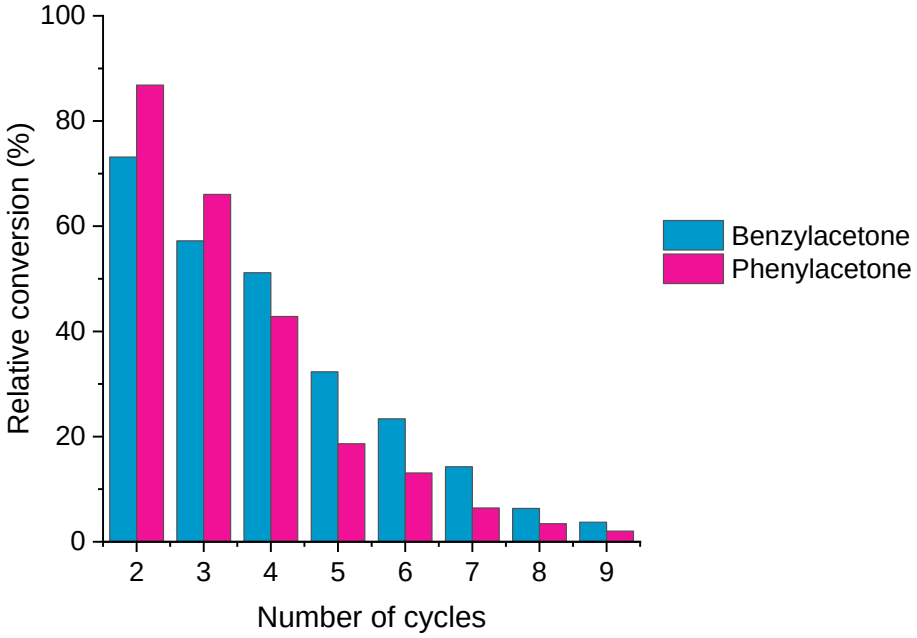

Figure 3.2. Recyclability study of the nanobiocatalysts. Reduction of benzylacetone (turquoise) or phenylacetone (pink) to their corresponding alcohols. Relative conversion (%) obtained after repeated biotransformations reusing the same nanobiocatalysts. Nanobiocatalysts are re-equilibrated with buffered $NADP^+$ solution in between each cycle.

For the recycling of the $MSN_{EGS\text{-}TeSADH\text{-}OrgS}$ without incubation in buffer/$NADP^+$ between the cycles, the recycling is ineffective. Only 7 % (for **1**) and 13 % (for **2**) is remaining of the initial conversion after the second cycle and by the third cycle no conversion can be measured. This is most likely due to a slight yet relevant leaking of water from the porous core of the particles into the surrounding solvent caused by the thorough washing with MTBE. This can then increase the enzymes exposure to the surrounding solvent and the enzyme has therefore a restricted access to the polar cofactor. From Figure 3.2 it can be seen that for the $MSN_{EGS\text{-}TeSADH\text{-}OrgS}$ with incubation step the recyclability has improved significantly with 73 % (for **1**) and 87 % (for **2**) remaining of the initial conversion after the second cycle (first recycling) and conversion can be detected for up to 9 cycles, which represents 9 days of incubation in MTBE. The fact that the conversion rate is decaying at similar levels for both substrates tested suggests that the tertiary and quaternary structure of the enzyme and its active site is retained. By adding the step of incubation/re-equilibration in buffered $NADP^+$ solution it allows the conditions for

the enzyme to be kept constant. The access for the enzyme to $NADP^+$ is not restricted and additionally the enzymes structural water can be maintained.

3.1.2 Biotransformation cascade with TeSADH and FOYE

To further investigate the cofactor recyclability properties of the nanobiocatalyst another biotransformation experiment was performed. In this experiment were $MSN_{Co\text{-}TeSADH/FOYE\text{-}OrgS}$ utilized. These particles were prepared using the affinity immobilisation technique and have both FOYE and TeSADH W110A immobilised on them. However, when up-scaling the synthesis of the nanobiocatalysts the growth of the organosilica layer did not reach the expected thickness and the enzymes are therefore for not completely shielded by the layer. The particles were nevertheless used for this experiment to proof the functionality of the cofactor recycling from the reservoir. This experiment was carried out in a similar fashion as the previously described biotransformations. However, FOYE being an ER, the starting substrate for the reaction was changed. As substrate was 2-cyclohexen-1-one used and *i*-PrOH were used as hydride source for TeSADH to reduce $NADP^+$ to NADPH. This then allows FOYE to reduce 2-cyclohexen-1-one to cyclohexanone while oxidizing NADPH to $NADP^+$ and completing the cycle of the cofactor. The reaction is shown in Figure 3.3.

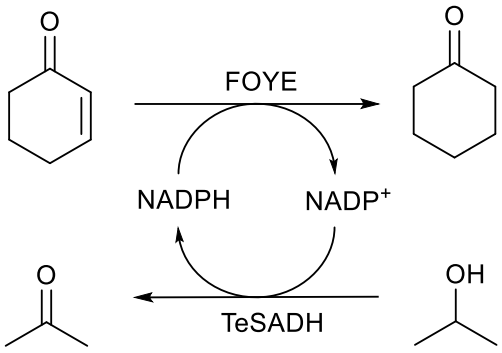

Figure 3.3. The reaction catalysed by FOYE with cofactor recycling. $NADP^+$ were dissolved within the mesoporous core of the nanobiocatalysts. 2-cyclohexen-1-one and *i*-PrOH are dissolved in the organic solvents the nanobiocatalysts are dispersed in. *i*-PrOH functions as a hydride source for the cofactor recycling by TeSADH W110A. Conversion is determined by GC-FID analysis of the concentration of 2-cyclohexen-1-one and its reduced product.

2-cyclohexen-1-one as well as cyclohexanone are possible substrates for TeSADH, whereas the latter was used for the biotransformations earlier in this chapter. Therefore, there are two alternative products that can be formed during this reaction, cyclohexanol and 2-cyclohexen-1-ol, shown in Figure 3.4. Note that in the case of the formation of 2-cyclohexen-1-ol no further

reduction to cyclohexanol occurs. This is due to the need for activated alkenes for FOYE to catalyse the reduction.

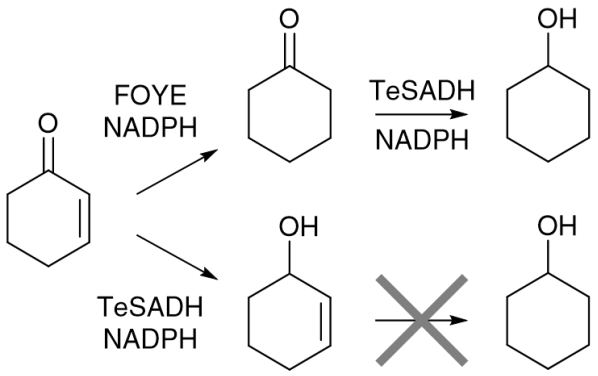

Figure 3.4. Possible side products from 2-cyclohexen-1-one. 2-cyclohexen-1-one can be reduced by either FOYE to cyclohexanone or by TeSADH W110A to 2-cyclohexen-1-ol. 2-cyclohexen-1-ol is not a possible substrate of FOYE and no further reduction can occur from this compound. However, cyclohexanone can be further reduced by TeSADH to cyclohexanol. Which products that are obtained can be determined with GC-FID.

The reaction solution containing 100 mM cyclohexen-1-one and 500 mM of *i*-PrOH in MTBE was prepared. As for the experiments carried out with $MSN_{EGS\text{-}TeSADH\text{-}OrgS}$ were the nanobiocatalysts already loaded with $NADP^+$ and no additional $NADP^+$ was added for the reaction. The amount of MSN used for the reaction was 1.28 mg and they were dispersed into the reaction solution. The reaction mixtures were incubated for 18 hours at 30 °C with 400 rpm stirring. After incubation the particles were removed and the conversion to the possible products was determined with GC-FID. A graph plotting the formation of products at three timepoints during the reaction is shown in Figure 3.5.

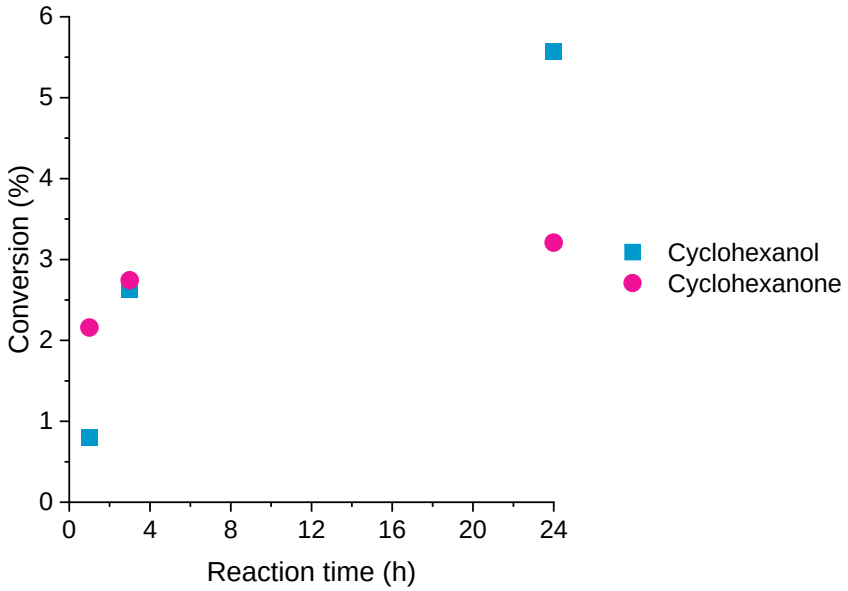

Figure 3.5. Biotransformation results obtained with $MSN_{Co\text{-}TeSADH/FOYE\text{-}OrgS}$. The reduction of 2-cyclohexen-1-one was catalysed by $MSN_{Co\text{-}TeSADH/FOYE\text{-}OrgS}$. Samples were collected after 1 h, 3 h and 20 h and conversion (%) was determined with GC-FID. Accumulation of cyclohexanone was initially high but reached a plateau after 3 hours. The double reduction to cyclohexanol were low at first but increased past the conversion obtained with cyclohexanone after 24 hours of incubation.

As seen in the Figure 3.5 the reaction starts with a faster accumulation of cyclohexanone than cyclohexanone, 2 % compared to 0.8 %. After three hours of incubation, the concentration of cyclohexanol and cyclohexanone are close to equal at 2.7 % and 2.6 % respectively. After 24 hours of incubation the concentration of cyclohexanone has not significantly increased while the concentration of cyclohexanol has increased to 5.6 %. The reaction was incubated for another 24 hours however, no further conversion was obtained (not shown). No formation of 2-cyclohexen-1-ol could be observed. This could be why compound **5** (4-phenyl-3-buten-2-one) also showed poor conversion in the previous experiment. Most likely the rigidity of the alkene causes a poor substrate fit in the active site of the TeSADH W110A and therefore the conversion of these substrates is low. The initial high conversion of cyclohexanone could be explained by the excess of *i*-PrOH making it more likely for the TeSADH W110A to catalyse the oxidation to acetone. Additionally, without the initial oxidation of *i*-PrOH there would be no NADPH available for the reductions of 2-cyclohexen-1-one or cyclohexanone. Moreover, the observation of the conversion of cyclohexanone saturating after three hours might not mean that FOYE is not catalysing the reaction further. It could instead be due to further formation of cyclohexanol. That not all cyclohexanone is further converted to cyclohexanol is however

surprising considering the excellent cyclohexanone conversion in **Table 3.1**. Possible reasons for the low final conversion could be that the incubation temperature for this experiment were lower than in the previous experiment. This was done because FOYE is a less thermostable enzyme than TeSADH W110A. Another reason could be the decreased concentration of *i*-PrOH (500 mM compared to 2 M). The concentration was decreased because of uncertainty of how high concentrations of the polar solvent *i*-PrOH would affect the stability of FOYE. Additionally, to reach the final product of cyclohexanol two NADPH are required, increasing the need of *i*-PrOH which can affect the final outcome of the reaction. Most likely is a combination of these effect the cause to the not satisfactory final conversion.

Within the pores of the MSN were *ca* 1 nmol of $NADP^+$ available in the experiment. The amount of converted 2-cyclohexen-1-one were 3.5 µmol and 2.2 µmol of that were further converted to cyclohexanol. This is even with the poor final conversion obtained a large quantity of cofactor cycles performed. In this experiment was the recycling of cofactor no longer handled by the same enzyme, therefore the cofactor needed to migrate between two enzymes for the continued conversion of the products. This experiment has therefore provided further support for an effective recycling of the cofactor within the particle and a successful utilization of the mesopores within the nanobiocatalyst.

As a final remark it should be mentioned that this experiment was only an initial trial and that the parameters for the experiments were not optimised. With further optimisation of for example cosubstrate concentration, substrate concentration, incubation temperature and also the ratio between the two enzymes a more efficient system could be developed. This would also allow for further investigations of the effect of different organic solvents as well as other possible multi-step reactions.

3.2 Biotransformation in a continuous flow

The possibility to use the produced nanobiocatalysts for continuous flow catalysis was also investigated. To test this the $MSN_{EGS\text{-}TeSADH/FOYE\text{-}OrgS}$ previously described in chapter 2 and used for biotransformations in batch mode earlier in this chapter were used. The reaction studied is presented in Figure 3.6.

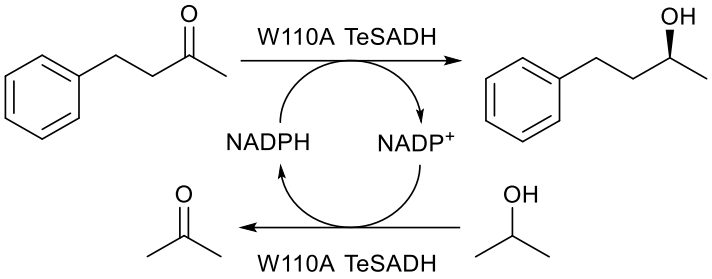

Figure 3.6. Reaction studied in continuous flow experiment. $NADP^+$ were loaded within the mesoporous of the nanobiocatalysts. Benzylacetone and *i*-PrOH are dissolved in the organic solvents that is pumped through the packed-bed reactor. The function of *i*-PrOH is as a hydride source for the cofactor recycling. Conversion is determined by GC-FID analysis of the concentration of benzylacetone and its corresponding alcohol.

As proof-of concept, the $MSN_{EGS\text{-}TeSADH/FOYE\text{-}OrgS}$ were packed into a column to yield a packed-bed reactor column. The column had a volume of 831 µL and a quantity of 140 mg of $MSN_{EGS\text{-}TeSADH/FOYE\text{-}OrgS}$ was used to fill the column. The column was then flushed with a 1.5 mM $NADP^+$ buffered solution to ensure that the mesoporous core of the particles were equilibrated with $NADP^+$. The column was then flushed with a reaction solution of 30 mM benzylacetone and 3 M isopropanol dissolved in MTBE. The flow rate was at first higher to flush out the remaining water. The flow was then decreased and the flow through was collected at different flow rates and samples were taken to determine the conversion of benzylacetone to 4-phenyl-2-butanol with GC-FID. A schematic of the experimental set up is shown in Figure 3.7.

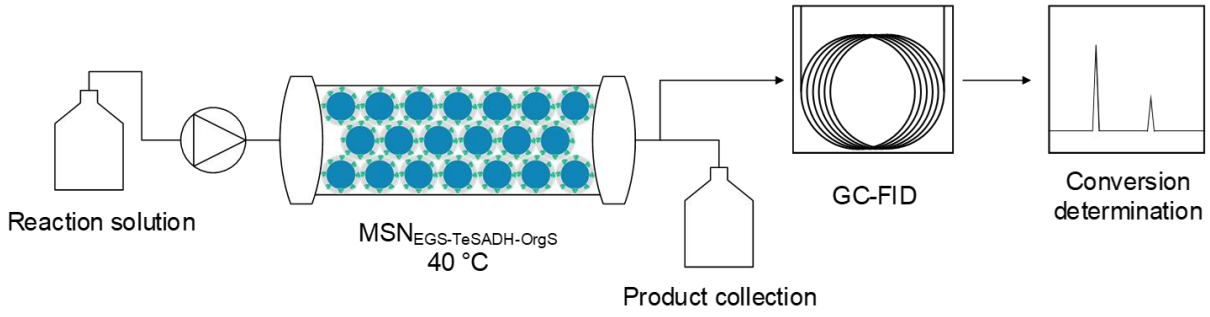

Figure 3.7. Schematic of the experimental setup for the continuous flow experiments. A reaction solution consisting of benzylacetone and *i*-PrOH in MTBE is pumped through the packed-bed reactor, filled with $MSN_{EGS\text{-}TeSADH\text{-}OrgS}$. The reactor is heated to 40 °C for the reaction to increase the catalytic efficiency of TeSADH W110A. $NADP^+$ were pre-loaded within the mesoporous of the nanobiocatalysts. The reaction solution is collected after the reactor and samples are collected during the run to determine conversion at different flow rates with GC-FID.

The conversions obtained from the continuous flow experiment are presented in **Table 3.2**.

Table 3.2. Conversion of benzylacetone during continuous flow catalysis experiment.

Flow (µL/min)	Conversion (%)
50	13
20	41
10	95

As in the previous batch experiments it was also possible for the nanobiocatalysts to catalyse the reaction in this continuous flow system. This is additional evidence of that the cofactor is retained and recycled within the mesoporous core of the particle. If the cofactor was not retained within the core of the particle, it would have been flushed out with the excess buffer at the start of the experiment and the immobilised enzyme would not have been able to catalyse any conversion of the substrate to the product.

The efficiency of the $MSN_{EGS\text{-}TeSADH/FOYE\text{-}OrgS}$ to convert the substrate varied with the flow rate, with higher conversion being achieved at lower flow rates. The highest conversion was determined to 95 % being achieved at a flow rate of 10 µL/min. The reduced conversion obtained at increased flow rates could be allocated to a brief residence time of the substrate within the column. By further developing this system and use a column with a larger volume this issue could be avoided.

Chapter 4

Summary and outlook

4 Summary and outlook

The availability of cofactor recycling systems for oxidoreductases is crucial for their utilisation as biocatalysts for synthesis in organic solvents. This doctoral thesis focuses on the design, synthesis, and characterisation of nanobiocatalysts and their application as a cofactor recycling tool for oxidoreductase catalysis in organic solvents.

First the synthesis and characterisation of the nanobiocatalyst carrier is discussed. SEM experiments revealed that the monodisperse shape of the 3D-MSN obtained from a biphasic approach synthesis was suitable as carrier for the nanobiocatalyst. The hierarchical pore structure of the MSN was characterized with cryoEM. The effect on colloidal stability of nanoparticles after amino modification was investigated with DLS and ζ-potential measurements. However, the parameters needed for later experiments did not allow for changing the functionalisation conditions to improve the colloidal stability.

The four enzymes chosen for this research, RedAm, TeSADH, SyADH and FOYE, were successfully produced and purified in sufficient quantities to carry out the experiments. For all enzymes the culture conditions were optimised in regard to enzyme yield. The purity, concentration and activity of the produced enzymes were determined with SDS-PAGE and UV/Vis.

Four different immobilisation strategies were investigated. The amount of immobilised enzyme and the remaining activity after immobilisation was determined with UV/Vis. It could be concluded that the remaining activity after immobilisation largely dependent on the type of linker used for immobilisation but also on the enzyme in question. The shortest crosslinker, glutaraldehyde, yielded low remaining activity for the immobilised enzyme. Therefore, two other crosslinkers, EGS and BS(PEG)5, were tested. After experiments with EGS and BS(PEG)5 it could be concluded that they did yield higher remaining activity after immobilisation compared to the remaining activity obtained through glutaraldehyde immobilisation. Due to the similar results, with EGS and BS(PEG)5, with regards to remaining activity and immobilisation yield, EGS was chosen over BS(PEG)5 for further experiments. The reason for increased remaining activity could be because of less rigidification of the enzyme due to the longer spacer arm for EGS and BS(PEG)5 compared to glutaraldehyde. Even though the remaining activity was increased when using EGS it was still far from the activity of the soluble enzyme for FOYE, SyADH and RedAm. Therefore, a fourth crosslinker based on non-covalent immobilisation through affinity with the enzymes His-tag was tested.

This allows for an orientation-controlled immobilisation which can improve the orientation of the enzyme and reduce the rigidity the enzyme experiences. The remaining activity after immobilisation increased for RedAm, SyADH and FOYE.

A protecting organosilica layer was grown at the surface of the nanobiocatalyst. The conditions for the layer growth were adjusted to yield a layer that completely covers the enzyme. The organosilica layer was characterized with SEM and cryoEM to determine the layer thickness and for visualization of the layer in contrast to the core particle. The morphology of the layer grown on particles with affinity immobilisation were different compared to the layer grown on other particles. The layer growth conditions therefore needed to be adjusted to yield appropriate nanobiocatalysts. TeSADH gave suitable nanobiocatalysts with both immobilisation strategies in regard to remaining activity after shielding. SyADH and FOYE generated significantly better final nanobiocatalysts after shielding when immobilised with the affinity strategy. RedAm did not yield suitable nanobiocatalysts after shielding and it was deemed to be due to poor stability of the enzyme.

The biocatalytic properties of the produced nanobiocatalysts were further investigated. $MSN_{EGS\text{-}TeSADH\text{-}OrgS}$ pre-loaded with cofactor were used for biotransformation reactions in different organic solvents, heptane, toluene, MTBE and EtOAc with eight different substrates. The conversions were determined with GC-FID. The nanobiocatalysts could convert the substrates in all cases, which indicates the functionality of the internal cofactor recycling. It could also be concluded that the hydrophobicity of the solvent had an effect on the conversion efficiency with lower conversions obtained in solvents having lower hydrophobicity. Since the substrate scope of the shielded enzymes were unchanged compared to that of the soluble enzyme it was concluded that the layer had not hampered the selectivity of the enzymes. The enantioselectivity of the nanobiocatalysts were similar in all solvents, giving further confirmation of a non-restricted enzyme after shielding. The particles were reusable if a re-equilibration in buffered cofactor solution was included. Nanobiocatalysts with co-immobilised FOYE and TeSADH were successfully used for a cascade reaction. This was a further proof of successful cofactor recycling with the help of the reservoir within the core of the particles. Lastly as a proof-of-concept were the $MSN_{EGS\text{-}TeSADH\text{-}OrgS}$ packed in a column for continuous flow catalysis. The successful conversion of the substrate gives additional evidence of the cofactor recycling withing the reservoir.

In summary, the presented research presents a new method for employing oxidoreductases as biocatalysts in organic solvents. This work shows a way to overcome the limitation this class of enzyme currently experiences when it comes to catalysis of hydrophobic substrates, not soluble in water. The system developed is expected to simplify and broaden the catalytic opportunities for oxidoreductases in neat organic solvents.

Chapter 5

Experimental

5 Experimental

5.1 Materials

Unless otherwise stated, all chemicals were purchased from commercial suppliers (Sigma Aldrich, ThermoFisher Scientific, Roth, TCI, Toronto, Thermoscientific – Acros) and used without further purification. Milli-Q water (resistivity 18 MΩ.cm) was obtained using a Synergy water purification system (Millipore Merck).

5.2 Electron microscopy

5.2.1 Scanning electron microscopy and particle size measurements

An aliquot (2 µL) of appropriately diluted particle suspension was spread on a silicon wafer (Agar scientific). The sample was dried under ambient conditions and then sputter-coated with a gold-platinum alloy for 15 sec at 20 mA. Micrographs were acquired using a Zeiss SUPRA® 40VP SEM, with InLens mode and an accelerating voltage of 10 kV. Particle sizes were measured on micrographs acquired at a magnification of 200'000 X using the Olympus Analysis software package. At least 100 measurements were made per sample.

5.2.2 Transmission electron microscopy

An aliquot (2 µL) of appropriately diluted particle suspension was adsorbed onto formvar coated grid (EMS). The sample was dried under ambient conditions. Micrographs were acquired using a Zeiss EM 900 TEM.

5.2.3 Cryo-electron microscopy

CryoEM measurements were carried out by Dr. Mohamed Chami and Carola Alampi at the BioEM lab, University of Basel.

An aliquot (4 µL) of sample was adsorbed onto holey carbon-coated grid (Lacey), blotted (3 s) with filter paper and plunge-frozen into liquid ethane (-180°C) using a vitrobot (FEI). Frozen grids were transferred onto a CM200 FEG microscope (Philips) using a Gatan 626 cryo-holder (Gatan). Electron micrographs were recorded at an accelerating voltage of 200 KV using low-dose system (20 to 30 e-/Å2, -175 °C). Defocus values were -4 µm. Micrographs were recorded on 4K x 4K TemCam-F416 CMOS based camera (TVIPS).

5.3 MSN synthesis

5.3.1 MCM-41 synthesis

The MCM-41 were prepared by a procedure previously described by Radu *et al.* (*125*). In brief the particles were synthesized as follows, 0.5 g of CTAB was dissolved in 240 mL of Milli-Q water. 1.75 mL of 2 M NaOH was added, and the solution was incubated at 80 °C until equilibrated. 2.5 mL of TEOS was added dropwise to the solution under constant stirring, 600 rpm, and the solution were thereafter incubated for 2 hours at 80 °C with constant stirring, 600 rpm. A white precipitation appeared after the incubation time. The reaction was stopped by filtration of the reaction suspension. The filtrate was extensively washed with Milli-Q water and thereafter methanol. The filtrate was scraped off the filter paper and was dried overnight at room temperature. The filtrate was then calcinated at 600 °C for 4 hours to remove the remaining surfactant from the pores of the particles. The obtained MCM-41 MSNs were transferred to a glass yar and stored at room temperature.

5.3.2 3D-MSN synthesis

The 3D-MSNs were prepared by an adapted procedure described by Shen *et al.* (*126*). The particles are synthesized as followed, 60 mL of CTAC (25 wt %), 620 µL of triethylamine and 90 mL of water was added into a 250 mL round bottom flask. The solution was equilibrated at 60 °C with 150 rpm stirring for 1 hour. 50 mL of 10 % (v/v) TEOS in cyclohexane was added slowly to the solution and the reaction was incubated for 14 hours. The lower phase was transferred to a new 250 mL round bottom flask and 50 mL of 20 % (v/v) TEOS in 1-octadecene was added to the solution. The reaction was incubated for 6 hours at 60 °C with 150 rpm stirring. The lower phase was collected and centrifuged at 20’000 g for 20 min and the pellet was resuspended in 150 mL ethanol. This procedure, called the washing step, was repeated thrice. For the last resuspension the pellet was resuspended in 150 mL of 0.6 wt% NH_4NO_3 in ethanol. The MSN was then incubated at 60 °C with 150 rpm stirring for 6 h to extract the surfactant template. After incubation the suspension was centrifuged at 20’000 g for 20 min and resuspended once again in 150 mL of 0.6 wt% NH_4NO_3 in ethanol. The extraction procedure was then repeated two more times. After the last extraction the washing step was done four more time, twice by resuspending the particles in ethanol and twice with water. After the final washing step were the particles concentrated to approximately 20 mL and stored at 4 °C until further use.

5.4 Protein expression, purification and analysis

5.4.1 Composition of culture media for bacterial expression cultures

Luria-Bertani Medium (Miller) (LB)

Composition for 1 L final volume

5 g yeast extract

10 g tryptone

10 g NaCl

LB Agar

Composition for 1 L final volume

5 g yeast extract

10 g tryptone

10 g NaCl

20 g agar

ZYM-5052 for auto induction

Composition for 1 L final volume

5 g yeast extract

10 g tryptone

20 mL 50 x M

20 mL 50 x 5052

2 mL 1 M $MgSO_4$

0.2 mL trace elements

50 x M

1.25 M Na_2HPO_4

1.25 M KH_2PO_4

2.5 M NH_4Cl

0.25 M Na_2SO_4

50 x 5052 for 1 L

250 g glycerol

25 g glucose

100 g α-lactose

Trace elements

Composition for 1 mL final volume

500 µL 0.1 M $FeCl_3$

20 µL 1.0 M $CaCl_2$

10 µL 1.0 M $MnCl_2$

10 µL 1.0 M $ZnSO_4$

10 µL 0.2 M $CoCl_2$

20 µL 0.1 M $CuCl_2$

10 µL 0.2 M $NiCl_2$

20 µL 0.1 M Na_2MoO_4

20 µL 0.1 M Na_2SeO_3

20 µL 0.1 M H_3BO_3

LBNB medium

Composition for 1 L final volume

5 g yeast extract

10 g tryptone

29.2 g NaCl

2 g glucose

117.25 mg betaine

5.4.2 Bacterial transformation protocol for recombinant protein expression

The gene encoding each enzyme was ordered subcloned into a pET28c(+) vector from Eurofins Genomics.

Aliquots of competent *E. coli* BL21(DE3) were thawed prior to transformation. Approximately 50 ng of plasmid DNA were added per aliquot and then gently mixed. The cells were incubated on ice for 20 min, then heated for 90 sec at 42 °C and subsequently cooled on ice again. 1 mL of LB medium was added, and the aliquot was incubated for 1 h at 37 °C. The cells were then centrifuged at 3’000 g for 1 min and 1 mL of the supernatant was discarded. The cell pellet was resuspended in the remaining volume of supernatant for inoculation on LB agar plate supplemented with 50 mg/mL of Kanamycin. All microbiological actions were performed under flame.

5.4.3 Protein expression and purification

Single colonies were picked and inoculated into 20 mL overnight cultures of LB medium supplemented with 50 mg/L Kanamycin. The overnight culture was used to inoculate main cultures (5 x 200 mL).

In the case of RedAm, TeSADH and SyADH: The cells were grown in ZYM auto-inducing medium supplemented with 100 mg/mL Kanamycin at 20 °C, 30 °C or 37 °C (for RedAm, SyADH or TeSADH respectively) for 24 hours.

In the case of FOYE: The cells were grown in LBNB medium supplemented with 50 mg/mL Kanamycin at 37 °C up to OD_{600} = 0.6, protein expression was induced by addition of 0.1 mM IPTG and the cultures were then incubated at 20 °C for 22 hours.

For all: The cells were harvested by centrifugation at 4 °C and 5'000 g and then frozen. The pellet was thawed on ice and was resuspended in wash buffer (see **Table *5.1***) prior to cell lysis by sonication or homogenization. The suspension was centrifuged at 5'000 g for 20 min at 4 °C and the supernatant was collected. In the case of TeSADH was the supernatant heat treated at 70 °C for 15 minutes and subsequently centrifuged at 20'000 for 10 minutes at 4 °C to. For all enzymes were the supernatant filtered through a 0.22 µm filter prior to purification. The cell extract was loaded onto a HisTrap column (Cytiva) and eluted with an imidazole gradient using an ÄKTA FPLC system.

The fractions were analysed with SDS-PAGE to determine purity. The fractions with the protein of interest were pooled together and were then desalted on a HiPrep desalting column (Cytiva). Enzyme concentration was determined with Pierce BCA Protein Assay Kit (ThermoFisher). The enzyme stocks were aliquoted, snap-frozen and then stored at -20 °C. For glycerol concentration during storage see **Table *5.1***. **Table 2.1**

Table 5.1. Buffers for purification and storage of produced enzymes.

	RedAm	TeSADH	SyADH	FOYE
Wash buffer	100 mM Tris-HCl, 300 mM NaCl, 30 mM imidazole, pH 8	50 mM Tris-HCl, 300 mM NaCl, 10 mM imidazole, pH 8	50 mM Tris-HCl, 300 mM NaCl, 20 mM imidazole, pH 7.5	50 mM NaPi, 300 mM NaCl, 20 mM imidazole, pH 7.1
Elution buffer	100 mM Tris-HCl, 300 mM NaCl,	50 mM Tris-HCl, 300 mM NaCl,	50 mM Tris-HCl, 300 mM NaCl,	50 mM NaPi, 300 mM NaCl,

	300 mM imidazole, pH 8	300 mM imidazole, pH 8	300 mM imidazole, pH 7.5	300 mM imidazole, pH 7.1
Storage buffer	10 mM NaPi, pH 8.2	50 mM NaPi, pH 8	50 mM NaPi, pH 7.5	50 mM NaPi, pH 7.1
Glycerol content	40 % glycerol	No glycerol added	No glycerol added	50 % glycerol

5.4.4 Activity assays

For RedAm: The typical reaction mixture for measuring RedAm activity contained 15 mM cyclohexanone, 60 mM methylamine and 0.6 mM of NADPH in 10 mM NaPi pH 8.2. The assay was run with 30 μg/mL of soluble or 60 μg/mL immobilised RedAm. For soluble RedAm was the assay mixture incubated at 25 °C and the increase in absorbance was measured at 340 nm with a plate reader, Synergy H1 (BioTek). For immobilised RedAm were the assay performed at 25 °C for 5 min and for immobilised and shielded for 20 min. The mixture were thereafter centrifuged (20 000 g, 1 min) to pellet the particles. 200 μL from the supernatant was then transferred to a 96 UV well plate and absorbance was measured at 340 nm with a plate reader.

For TeSADH: The typical reaction mixture for measuring TeSADH activity contained 500 mM isopropanol and 1 mM of $NADP^+$ in 50 mM NaPi pH 8. The assay was run at 60 °C with 1 μg/mL of soluble or immobilised TeSADH W110A. The assay was run for 5 minutes, then inhibited with thiourea (final concentration 0.9 M) and the mixture was thereafter centrifuged (20 000 g, 2 min) to pellet the particles. 250 μL from the supernatant was then transferred to a 96 UV well plate and absorbance was measured at 340 nm with a plate reader.

For SyADH: The typical reaction mixture for measuring SyADH activity contained 200 mM isopropanol and 1 mM of $NADP^+$ in 50 mM NaPi pH 7.5. The assay was run at 30 °C with 10 μg/mL of soluble or immobilised SyADH The assay was run for 5 minutes, then inhibited with thiourea (final concentration 0.9 M) and the mixture was thereafter centrifuged (20 000 g, 2 min) to pellet the particles. 250 μL from the supernatant was then transferred to a 96 UV well plate and absorbance was measured at 340 nm with a plate reader.

For FOYE: The typical reaction mixture for measuring FOYE activity contained 10 mM maleimide and 0.5 mM of NADPH in 50 mM NaPi pH 7.1. The assay was run at 30 °C with 1.5 μg/mL of soluble or immobilised FOYE. The assay was incubated at 30 °C and the increase in absorbance was measured at 340 nm with a plate reader.

5.5 Nanobiocatalyst synthesis

5.5.1 MSN surface modifications

5.5.1.1 Aminomodification

The MSN was functionalised with 5.6 mM APTES for 90 min at 20 °C. The washing step to remove the unreacted APTES was then done four times by centrifugation (20'000 g, 15 min) and resuspension of the particles in milli-Q water. The MSN-NH_2 were stored at 4°C.

5.5.1.2 NTA modification

The MSN-NH_2 (3.2 mg/mL MSN-NH_2 in milli-Q water) were functionalised with 21 mM glutaraldehyde for 20 min at 20 °C and 400 rpm stirring to yield MSN_G. The particles were washed by centrifugation (20'000 g, 5 min) and then resuspended in buffer (50 mM NaPi, pH 8). The washing was repeated four times. The MSN_G were then further functionalised with 25 mM N_α,N_α-bis(carboxymethyl)-L-lysine by incubation for 30 min at 20 °C and 400 rpm stirring. 22 mM of $NaBH_4$ was added to reduce the formed imines and the suspension was incubated for 2 hours at room temperature with 400 rpm stirring under nitrogen flux. The particles were washed by centrifugation (20'000 g, 5 min) four times and were then resuspended in 100 mM $NiSO_4$ and incubated for 1 hour at room temperature with 400 rpm stirring. The particles were washed by centrifugation (20'000 g, 5 min) and then resuspended in milli-Q water. The washing was repeated four times. This yielded MSN_{NTA} and they were stored at 4 °C.

5.5.2 Enzyme immobilisation

Enzyme immobilisation with glutaraldehyde: The MSN-NH_2 (3.2 mg/mL MSN-NH_2 in milli-Q water) were functionalised with 21 mM glutaraldehyde for 20 min at 20 °C and 400 rpm stirring to yield MSN_G. The particles were washed by centrifugation (20'000 g, 5 min) and then resuspended in immobilisation buffer (50 mM NaPi, pH 6). The washing was repeated four times. 200 µg/mL of enzyme was used for immobilisation on MSN_G for 30 min at 20 °C and 400 rpm stirring to yield $MSN_{G\text{-}Enz}$. The $MSN_{G\text{-}Enz}$ was washed by centrifugation (1'500 g, 5 min) and then resuspended in layer growth buffer (50 mM NaPi, pH 8). The washing was repeated three times. The immobilisation yield was determined by BCA assay by analysing the protein content in the first supernatant after immobilisation.

Enzyme immobilisation with EGS (or BS(PEG)5): The MSN-NH_2 (3.2 mg/mL MSN-NH_2 in 10 mM NaPi pH 7.5) were functionalised with 0.16 mM EGS for 20 min at 20 °C and 400 rpm stirring to yield MSN_{EGS}. The particles were washed by centrifugation (20'000 g, 5 min) and then resuspended in immobilisation buffer (50 mM NaPi, pH 6). The washing was repeated four times. 200 µg/mL of enzyme was used for immobilisation on MSN_{EGS} for 30 min at 20 °C and 400 rpm stirring to yield $MSN_{EGS\text{-}Enz}$. The $MSN_{EGS\text{-}Enz}$ was washed by centrifugation (1'500 g, 5 min) and then resuspended in layer growth buffer (50 mM NaPi, pH 8). The washing was repeated three times. The immobilisation yield was determined by BCA assay by analysing the protein content in the first supernatant after immobilisation.

Enzyme immobilisation with affinity: 200 µg/mL of enzyme was used for immobilisation on MSN_{NTA} (3.2 mg/mL MSN_{NTA}) in the appropriate storage buffer for each enzyme, see Table 5.1, for 30 min at 20 °C and 400 rpm stirring to yield $MSN_{NTA\text{-}Enz}$. The $MSN_{NTA\text{-}Enz}$ were washed by centrifugation (1'500 g, 5 min) and then resuspended in layer growth buffer (50 mM NaPi, pH 8). The washing was repeated three times. The immobilisation yield was determined by BCA assay by analysing the protein content in the first supernatant after immobilisation. For co-immobilisation on MSN_{NTA} were the immobilisation procedure repeated once more and the enzyme concentration of the first enzyme was decreased to 100 µg/mL.

5.5.3 Growth of protecting organosilica layer

Shielding layer on MSN_{EGS}: 1.5 mM of $NADP^+$ was added to $MSN_{EGS\text{-}Enz}$ and they were incubated for 15 minutes. Then 49.9 mM of TEOS was added and the $MSN_{EGS\text{-}Enz}$ were incubated at 20 °C for 1 h with 400 rpm stirring. 9.4 mM APTES was added and the $MSN_{EGS\text{-}Enz}$ was incubated at 20 °C with 400 rpm stirring for 20 h. After incubation the particles were collected and washed by centrifugation (1'500 g, 5 min). The washing was repeated 3 times. This yielded $MSN_{EGS\text{-}Enz\text{-}OrgS}$ and they were then stored at 20 °C for 14 hours to allow curing before being finally stored at 4 °C.

Shielding layer on MSN_{NTA}: 1.5 mM of $NADP^+$ was added to $MSN_{NTA\text{-}Enz}$ and they were incubated for 15 minutes. Then 26.6 mM of TEOS was added and the $MSN_{NTA\text{-}Enz}$ were incubated at 20 °C for 1 h with 400 rpm stirring. 5 mM APTES was added and the $MSN_{NTA\text{-}Enz}$ was incubated at 10 °C with 400 rpm stirring for 5 h. After incubation the particles were collected and washed by centrifugation (1'500 g, 5 min). The washing was repeated 3 times.

This yielded MSN $_{NTA\text{-}Enz\text{-}OrgS}$ and they were then stored at 20 °C for 14 hours to allow curing before being finally stored at 4 °C.

5.6 Biotransformations in organic solvents

5.6.1 Synthesis of additional substances

Phenylacetone was kindly provided by Dr. Claude Schärer and was synthesised as follows.

Synthesis of phenylacetone: The synthesis was performed analogous to described procedures (*138*). 3-phenylpropan-2-ol (700 µL, 5 mmol) and 2,2,6,6-tetramethylpiperidine-1-oxyl (7.8 mg, 0.05 mmol, 1 mol%) were dissolved in EtOAc (2.5 mL) in an electrolysis vessel (undivided cell, IKA screening kit). Aqueous 25% NaBr, saturated with $NaHCO_3$ was added (5.0 mL). Two graphite electrodes (IKA SK-50,10 mm broad, 3 mm thick) were immersed (21 mm) into the emulsion and the mixture was electrolysed for 4 h 20 min (3 F mol-1) under stirring and under galvanostatic conditions at 93 mA. The reaction was repeated four times. The combined reaction mixtures were extracted with EtOAc. The organic phase was washed with brine, dried (Na_2SO_4) and evaporated under reduced pressure. The crude product was purified by flash chromatography (SiO_2, MTBE/heptane 0-10 % MTBE) to give phenylacetone (1.57 g, 59 %) as a pale yellow oil. ^{1}H- and ^{13}C-NMR spectra were consistent with those reported (*139*).

^{1}H-NMR (400 MHz, $CDCl_3$): δ 7.36-7.32 (m, 2 H, m-Ph-*H*), 7.29-7.25 (m, 1 H, *p-H* Ph), 7.22-7.20 (m, 2 H, *o*-Ph-*H*), 3.70 (s, 2 H, C*H*$_2$), 2.15 (s, 3 H, C*H*$_3$). ^{13}C-NMR (101 MHz, $CDCl_3$): δ 206.4 (*C*=O), 134.4 (aryl *C*-CH$_2$), 129.4 (*o*-aryl *C*), 128.8 (*m*-aryl *C*), 127.1 (*p*-aryl *C*), 51.1 (*C*H$_2$), 29.3 (*C*H$_3$).

Synthesis of 4(4-methoxyphenyl)-2-butanol: The synthesis was performed analogous to described procedures (*140*). 4-(4-Methoxyphenyl)-2-butanone (1.01 g, 5.67 mmol) was dissolved in MeOH (10 mL). $NaBH_4$ (107 mg, 2.82 mmol) was added portion wise over 15 min under stirring at room temperature. The reaction mixture was stirred for 1.5 h, then quenched with H_2O (75 mL) and extracted twice with EtOAc (150 and 50 mL). The organic phases were washed with brine (20 mL), combined, dried (Na_2SO_4) and evaporated under reduced pressure. 4-(4-methoxyphenyl)-2-butanol was obtained as a pale yellow oil. ^{1}H- and ^{13}C-NMR spectra were consistent with those reported (*140, 141*).

^{1}H-NMR (400 MHz, $CDCl_3$): δ 7.13-7.10 (m, 2 H, aryl *H*-3/5), 6.84-6.82 (m, 2 H, aryl *H*-2/4), 3.83-3.78 (m, 1 H, C*H*OH), 3.78 (s, 3 H, OC*H*$_3$), 2.73-2.57 (m, 2 H, ArC*H*$_2$), 1.80-1.67 (m, 2 H, C*H*$_2$CHOH), 1.50 (br s, 1 H, O*H*), 1.22 (d, $^3J_{H,H}$=6.2 Hz, 2 H, CH(OH)C*H*$_3$). ^{13}C-NMR (101

MHz, $CDCl_3$): δ 157.8 (aryl *C*OMe), 134.1 (aryl *C*CH_2), 129.3 (aryl *C*-3/5), 113.8 (aryl *C*-2/4), 67.5 (*C*HOH), 55.3 (O*C*H_3), 41.1 (*C*H_2CHOH), 31.2 (Ar*C*H_2), 23.6 (CH(OH)*C*H_3).

5.6.2 Biotransformations in batch mode

5.6.2.1 Biotransformations using $MSN_{EGS\text{-}TeSADH\text{-}OrgS}$

$MSN_{EGS\text{-}TeSADH\text{-}OrgS}$ was used for biotransformation in organic solvents. 30 mM of substrate and 2 M isopropanol was dissolved in an organic solvent (heptane, ethyl acetate (EA), toluene or methyl *tert*-butyl ether (MTBE)). 1.92 mg of particles were re-suspended in 200 µL reaction mixture and incubated with stirring at 400 rpm for 18 hours at 45 °C. After incubation the reaction mixture were centrifuged to pellet the MSN and the supernatant was collected and analysed with GC-FID to determine the conversion from substrate to product.

5.6.2.2 Recycling experiment with $MSN_{EGS\text{-}TeSADH\text{-}OrgS}$

The recycling experiment with $MSN_{EGS\text{-}TeSADH\text{-}OrgS}$ was performed in a similar fashion as the biotransformations but with addition of the recycling step and an increased incubation time to 24 hours. The substrates used were either benzylacetone or phenylacetone.

For recycling without $NADP^+$ reloading: The $MSN_{EGS\text{-}TeSADH\text{-}OrgS}$ were centrifuged after the first biotransformation and washed twice with 200 µL of MTBE by centrifugation (3'200 g, 5 min) before being resuspended in 200 µL fresh reaction mixture and then incubated for the next biotransformation cycle. The supernatant after each recycling step was collected and analysed with GC-FID.

For recycling with $NADP^+$ reloading: The $MSN_{EGS\text{-}TeSADH\text{-}OrgS}$ were centrifuged after the first biotransformation and washed once with 200 µL of MTBE by centrifugation (3'200 g, 5 min) before being incubated in 200 µL of 1.5 mM $NADP^+$ in 50 mM NaPi, pH 8 for 15 minutes to re-equilibrate the mesopores within $MSN_{EGS\text{-}TeSADH\text{-}OrgS}$. The $MSN_{EGS\text{-}TeSADH\text{-}OrgS}$ were then collected by centrifugation (3'200 g, 5 min), resuspended in 200 µL fresh reaction mixture and then incubated for the next biotransformation cycle. The supernatant after each recycling step was collected and analysed with GC-FID.

5.6.2.3 Biotransformation using co-immobilised TeSADH and FOYE

A reaction mixture of 100 mM 2-cyclohexen-1-one and 500 mM *i*-PrOH in MTBE were prepared. 1.28 mg of $MSN_{Co\text{-}TeSADH/FOYE\text{-}OrgS}$ were resuspended in 400 µL reaction mixture and

incubated with stirring at 400 rpm at 30 °C. Samples were collected after 1 h, 3 h and 24 h. After collection the sample were centrifuged to pellet the MSN and the supernatant was collected and analysed with GC-FID to determine the conversion from substrate to product.

5.6.3 Biotransformation in continuous flow

140 mg of $MSN_{EGS\text{-}TeSADH\text{-}OrgS}$ was packed into a metal column (4.6 mm i.d. × 50 mm length) with steel frits. The column was then rinsed with 1.5 mM $NADP^+$ in 50 mM NaPi, pH 8 for 20 min (flow 300 µL/min). A reaction solution was prepared containing 30 mM benzylacetone, 3 M *i*-PrOH in MTBE. The reaction solution was pumped through the column for 20 min (flow 200 µL/min) to remove the remaining water. The flow was reduced to 10 µL/min, the column was heated to 40 °C and fractions was collected and analysed with GC-FID to determine the conversion from substrate to product. The flow was increased to 20 µL/min and 50 µL/min and the procedure was repeated for these flow rates as well.

5.6.4 GC analysis

The instrument used was a GC-FID, Agilent 7820A.

Column 1: Agilent HP-5 column, 30 m × 0.32 mm i.d.x × d_f 0.25 µm; carrier gas H_2; injector temperature: 290 °C; detector temperature: 300 °C.

Column 2: Chiraldex B-DM, 50 m × 0.25 mm i.d. × d_f 0.12 µm; carrier gas H_2; injector temperature: 200 °C; detector temperature: 220 °C.

Table 5.2. Table with parameters for GC methods.

	GC method 1	GC method 2	GC Method 3	GC method 4	GC method 5
Column	Column 1	Column 1	Column 1	Column 1	Column 2
Start temperature	80 °C	60 °C	80 °C	60 °C	70 °C
Hold time	1 min	7 min	1 min	3 min	45 min
Gradient 1	20 °C/min to 160 °C	30 °C/min to 300 °C	20 °C/min to 150 °C	30 °C/min to 300 °C	10 °C/min to 200 °C
Gradient 2	30 °C/min to 300 °C	No second gradient	50 °C/min to 300 °C	No second gradient	No second gradient
Hold time	2 min	2 min	1 min	2 min	2 min
Flow	1.15 mL/min	1.47 mL/min	1.15 mL/min	1.15 mL/min	2.2 mL/min

Compounds analysed with GC method 1: benzylacetone, 4-phenyl-2-butanol

Compounds analysed with GC method 2: phenylacetone, 1-phenyl-2-propanol

Compounds analysed with GC method 3: cyclohexanone, cyclohexanol, 2-cyclohexen-1-one, 2-cyclohexen-1-ol, 4-phenyl-3-buten-2-one, 4-phenyl-3-buten-2-ol, phenoxy-2-propanone, 1-phenoxy-2-propanol, 4-(4-methoxyphenyl)-2-butanone, 4-(4-methoxyphenyl)-2-butanol, β-tetralone, 1,2,3,4-tetrahydro-2-naphthol.

Compounds analysed with GC method 4: 6-methyl-5-hepten-2-one, 6-methyl-5-hepten-2-ol.

The conversion was determined via product-substrate ratios corrected by standard curves of the pure substances.

GC method 5 was used to determine the ee of 4-phenyl-2-butanol after derivatisation with *N*-methyl-bis(trifluoroacetamide).

Chapter 6

Bibliography

6 Bibliography

1. D. Vasic-Racki, in *Industrial biotransformations*. (2006), pp. 1-36.
2. E. F. Armstrong, Enzymes: A discovery and its consequences. *Nature* **131**, 535-537 (1933).
3. C. M. Heckmann, F. Paradisi, Looking back: A short history of the discovery of enzymes and how they became powerful chemical tools. *ChemCatChem* **12**, 6082-6102 (2020).
4. M. Jaskolski, Z. Dauter, A. Wlodawer, A brief history of macromolecular crystallography, illustrated by a family tree and its nobel fruits. *The FEBS Journal* **281**, 3985-4009 (2014).
5. U. T. Bornscheuer, K. Buchholz, Highlights in biocatalysis – historical landmarks and current trends. *Eng. Life Sci.* **5**, 309-323 (2005).
6. N. Grubhofer, L. Schleith, Modifizierte ionenaustauscher als spezifische adsorbentien. *Naturwissenschaften* **40**, 508-508 (1953).
7. R. Kohler, The background to eduard buchner's discovery of cell-free fermentation. *Journal of the History of Biology* **4**, 35-61 (1971).
8. O. May, in *Industrial enzyme applications*. (Wiley-VCH, 2019), pp. 1-24.
9. H. Gröger, Y. Asano, in *Enzyme catalysis in organic synthesis*. (2012), pp. 1-42.
10. U. T. Bornscheuer *et al.*, Engineering the third wave of biocatalysis. *Nature* **485**, 185-194 (2012).
11. R. A. Sheldon, D. Brady, Broadening the scope of biocatalysis in sustainable organic synthesis. *ChemSusChem* **12**, 2859-2881 (2019).
12. V. Steck, D. M. Carminati, N. R. Johnson, R. Fasan, Enantioselective synthesis of chiral amines via biocatalytic carbene n–h insertion. *ACS Catal.* **10**, 10967-10977 (2020).
13. S. Simić *et al.*, Shortening synthetic routes to small molecule active pharmaceutical ingredients employing biocatalytic methods. *Chem. Rev.* **122**, 1052-1126 (2022).
14. N. J. Turner, E. O'Reilly, Biocatalytic retrosynthesis. *Nat. Chem. Biol.* **9**, 285-288 (2013).
15. U. Hanefeld, F. Hollmann, C. E. Paul, Biocatalysis making waves in organic chemistry. *Chem. Soc. Rev.* **51**, 594-627 (2022).
16. K. Faber, in *Biotransformations in organic chemistry: A textbook*. (Springer International Publishing, Cham, 2018), pp. 1-30.
17. R. A. Sheldon, D. Brady, The limits to biocatalysis: Pushing the envelope. *Chem. Commun.* **54**, 6088-6104 (2018).
18. P. T. Anastas, J. C. Warner, *Green chemistry: Theory and practice*. (Oxford University Press, Oxford, 1998).
19. J. R. Ludwig, C. S. Schindler, Catalyst: Sustainable catalysis. *Chem* **2**, 313-316 (2017).

20. Price pressures on metals. *Nat. Catal.* **2**, 735-735 (2019).

21. E. L. Bell *et al.*, Biocatalysis. *Nat. Rev. Methods Primers* **1**, 46 (2021).

22. P. N. Devine *et al.*, Extending the application of biocatalysis to meet the challenges of drug development. *Nat. Rev. Chem.* **2**, 409-421 (2018).

23. R. A. Sheldon, D. Brady, M. L. Bode, The hitchhiker's guide to biocatalysis: Recent advances in the use of enzymes in organic synthesis. *Chem. Sci.* **11**, 2587-2605 (2020).

24. R. A. Sheldon, in *Green biocatalysis*. (2016), pp. 1-15.

25. A. L. Serdakowski, J. S. Dordick, Enzyme activation for organic solvents made easy. *Trends Biotechnol.* **26**, 48-54 (2008).

26. R. A. Sheldon, J. M. Woodley, Role of biocatalysis in sustainable chemistry. *Chem. Rev.* **118**, 801-838 (2018).

27. S. Kara, A. Liese, in *Industrial enzyme applications*. (Wiley-VCH, 2019), pp. 71-94.

28. A. Petrenz *et al.*, Medium and reaction engineering for the establishment of a chemo-enzymatic dynamic kinetic resolution of rac-benzoin in batch and continuous mode. *J. Mol. Catal. B: Enzym.* **114**, 42-49 (2015).

29. K. Faber, in *Biotransformations in organic chemistry: A textbook*. (Springer International Publishing, Cham, 2018), pp. 315-405.

30. P. Adlercreutz, in *Organic synthesis with enzymes in non-aqueous media*. (2008), pp. 1-24.

31. V. Stepankova *et al.*, Strategies for stabilization of enzymes in organic solvents. *ACS Catal.* **3**, 2823-2836 (2013).

32. L. Sellés Vidal, C. L. Kelly, P. M. Mordaka, J. T. Heap, Review of nad(p)h-dependent oxidoreductases: Properties, engineering and application. *Biochim. Biophys. Acta* **1866**, 327-347 (2018).

33. S. K. Ma *et al.*, A green-by-design biocatalytic process for atorvastatin intermediate. *Green Chem.* **12**, 81-86 (2010).

34. J. Liang *et al.*, Development of a biocatalytic process as an alternative to the (−)-dip-cl-mediated asymmetric reduction of a key intermediate of montelukast. *Organic Process Research & Development* **14**, 193-198 (2010).

35. T. Knaus, W. Böhmer, F. G. Mutti, Amine dehydrogenases: Efficient biocatalysts for the reductive amination of carbonyl compounds. *Green Chem.* **19**, 453-463 (2017).

36. D. Dascier, S. Kambourakis, L. Hua, J. D. Rozzell, J. D. Stewart, Influence of cofactor regeneration strategies on preparative-scale, asymmetric carbonyl reductions by engineered escherichia coli. *Organic Process Research & Development* **18**, 793-800 (2014).

37. F. G. Mutti, T. Knaus, N. S. Scrutton, M. Breuer, N. J. Turner, Conversion of alcohols to enantiopure amines through dual-enzyme hydrogen-borrowing cascades. *Science* **349**, 1525-1529 (2015).

38. S. L. Montgomery *et al.*, Direct alkylation of amines with primary and secondary alcohols through biocatalytic hydrogen borrowing. *Angew. Chem. Int. Ed.* **56**, 10491-10494 (2017).

39. A. Zaparucha, V. de Berardinis, C. Vaxelaire-Vergne, in *Modern biocatalysis: Advances towards synthetic biological systems*. (The Royal Society of Chemistry, 2018), pp. 1-27.

40. A. Scholtissek *et al.*, A thermophilic-like ene-reductase originating from an acidophilic iron oxidizer. *Appl. Microbiol. Biotechnol.* **101**, 609-619 (2017).

41. S. Yoshida *et al.*, A bacterium that degrades and assimilates poly(ethylene terephthalate). *Science* **351**, 1196-1199 (2016).

42. G. A. Aleku *et al.*, A reductive aminase from aspergillus oryzae. *Nature Chemistry* **9**, 961-969 (2017).

43. R. Chen, Enzyme engineering: Rational redesign versus directed evolution. *Trends Biotechnol.* **19**, 13-14 (2001).

44. J. L. Porter, R. A. Rusli, D. L. Ollis, Directed evolution of enzymes for industrial biocatalysis. *ChemBioChem* **17**, 197-203 (2016).

45. K. I. Ziegelmann-Fjeld, M. M. Musa, R. S. Phillips, J. G. Zeikus, C. Vieille, A thermoanaerobacter ethanolicus secondary alcohol dehydrogenase mutant derivative highly active and stereoselective on phenylacetone and benzylacetone. *Protein Eng. Des. Sel.* **20**, 47-55 (2007).

46. M. M. Musa *et al.*, A single point mutation reverses the enantiopreference of thermoanaerobacter ethanolicus secondary alcohol dehydrogenase. *ChemCatChem* **1**, 89-93 (2009).

47. H. Cui *et al.*, Enzyme hydration determines resistance in organic cosolvents. *ACS Catal.* **10**, 14847-14856 (2020).

48. O. Kuchner, F. H. Arnold, Directed evolution of enzyme catalysts. *Trends Biotechnol.* **15**, 523-530 (1997).

49. C. C. Farwell, R. K. Zhang, J. A. McIntosh, T. K. Hyster, F. H. Arnold, Enantioselective enzyme-catalyzed aziridination enabled by active-site evolution of a cytochrome p450. *ACS Central Science* **1**, 89-93 (2015).

50. C. C. Farwell, J. A. McIntosh, T. K. Hyster, Z. J. Wang, F. H. Arnold, Enantioselective imidation of sulfides via enzyme-catalyzed intermolecular nitrogen-atom transfer. *J. Am. Chem. Soc.* **136**, 8766-8771 (2014).

51. T. Seng Wong, F. H. Arnold, U. Schwaneberg, Laboratory evolution of cytochrome p450 bm-3 monooxygenase for organic cosolvents. *Biotechnol. Bioeng.* **85**, 351-358 (2004).

52. C. J. Hartley *et al.*, Engineered enzymes that retain and regenerate their cofactors enable continuous-flow biocatalysis. *Nat. Catal.* **2**, 1006-1015 (2019).

53. R. A. Sheldon, S. van Pelt, Enzyme immobilisation in biocatalysis: Why, what and how. *Chem. Soc. Rev.* **42**, 6223-6235 (2013).

54. R. A. Sheldon, Enzyme immobilization: The quest for optimum performance. *Adv. Synth. Catal.* **349**, 1289-1307 (2007).

55. U. Hanefeld, L. Gardossi, E. Magner, Understanding enzyme immobilisation. *Chem. Soc. Rev.* **38**, 453-468 (2009).

56. C. Mateo, J. M. Palomo, G. Fernandez-Lorente, J. M. Guisan, R. Fernandez-Lafuente, Improvement of enzyme activity, stability and selectivity via immobilization techniques. *Enzyme Microb. Technol.* **40**, 1451-1463 (2007).

57. R. C. Rodrigues, C. Ortiz, Á. Berenguer-Murcia, R. Torres, R. Fernández-Lafuente, Modifying enzyme activity and selectivity by immobilization. *Chem. Soc. Rev.* **42**, 6290-6307 (2013).

58. M. P. Thompson, I. Peñafiel, S. C. Cosgrove, N. J. Turner, Biocatalysis using immobilized enzymes in continuous flow for the synthesis of fine chemicals. *Organic Process Research & Development* **23**, 9-18 (2019).

59. L. Cao, L. v. Langen, R. A. Sheldon, Immobilised enzymes: Carrier-bound or carrier-free? *Curr. Opin. Biotechnol.* **14**, 387-394 (2003).

60. F. A. Quiocho, F. M. Richards, Intermolecular cross linking of a protein in the crystalline state: Carboxypeptidase-a. *Proceedings of the National Academy of Sciences* **52**, 833-839 (1964).

61. A. L. Margolin, M. A. Navia, Protein crystals as novel catalytic materials. *Angew. Chem. Int. Ed.* **40**, 2204-2222 (2001).

62. N. L. St. Clair, M. A. Navia, Cross-linked enzyme crystals as robust biocatalysts. *J. Am. Chem. Soc.* **114**, 7314-7316 (1992).

63. R. A. Sheldon, Cross-linked enzyme aggregates as industrial biocatalysts. *Organic Process Research & Development* **15**, 213-223 (2011).

64. L. Cao, F. van Rantwijk, R. A. Sheldon, Cross-linked enzyme aggregates: A simple and effective method for the immobilization of penicillin acylase. *Org. Lett.* **2**, 1361-1364 (2000).

65. L. Cao, L. M. van Langen, F. van Rantwijk, R. A. Sheldon, Cross-linked aggregates of penicillin acylase: Robust catalysts for the synthesis of β-lactam antibiotics. *J. Mol. Catal. B: Enzym.* **11**, 665-670 (2001).

66. L. Wilson, A. Illanes, L. Soler, M. J. Henríquez, Effect of the degree of cross-linking on the properties of different cleas of penicillin acylase. *Process Biochem.* **44**, 322-326 (2009).

67. R. A. Sheldon, Cross-linked enzyme aggregates (clea®s): Stable and recyclable biocatalysts. *Biochem. Soc. Trans.* **35**, 1583-1587 (2007).

68. R. Schoevaart *et al.*, Preparation, optimization, and structures of cross-linked enzyme aggregates (cleas). *Biotechnol. Bioeng.* **87**, 754-762 (2004).

69. C. Garcia-Galan, Á. Berenguer-Murcia, R. Fernandez-Lafuente, R. C. Rodrigues, Potential of different enzyme immobilization strategies to improve enzyme performance. *Adv. Synth. Catal.* **353**, 2885-2904 (2011).

70. N. R. Mohamad, N. H. C. Marzuki, N. A. Buang, F. Huyop, R. A. Wahab, An overview of technologies for immobilization of enzymes and surface analysis techniques for immobilized enzymes. *Biotechnology & Biotechnological Equipment* **29**, 205-220 (2015).

71. R. A. Sheldon, A. Basso, D. Brady, New frontiers in enzyme immobilisation: Robust biocatalysts for a circular bio-based economy. *Chem. Soc. Rev.* **50**, 5850-5862 (2021).

72. H. T. Imam, P. C. Marr, A. C. Marr, Enzyme entrapment, biocatalyst immobilization without covalent attachment. *Green Chem.* **23**, 4980-5005 (2021).

73. D. M.-R. D. Temiño, W. Hartmeier, M. B. Ansorge-Schumacher, Entrapment of the alcohol dehydrogenase from lactobacillus kefir in polyvinyl alcohol for the synthesis of chiral hydrophobic alcohols in organic solvents. *Enzyme Microb. Technol.* **36**, 3-9 (2005).

74. M. M. Musa, K. I. Ziegelmann-Fjeld, C. Vieille, J. G. Zeikus, R. S. Phillips, Xerogel-encapsulated w110a secondary alcohol dehydrogenase from thermoanaerobacter ethanolicus performs asymmetric reduction of hydrophobic ketones in organic solvents. *Angew. Chem. Int. Ed.* **46**, 3091-3094 (2007).

75. S. A. Nazemi *et al.*, Immobilisation and stabilisation of glycosylated enzymes on boronic acid-functionalised silica nanoparticles. *Chem. Commun.* **57**, 11960-11963 (2021).

76. M. R. Correro *et al.*, Enzyme shielding in an enzyme-thin and soft organosilica layer. *Angew. Chem. Int. Ed.* **55**, 6285-6289 (2016).

77. G. T. Hermanson, in *Bioconjugate techniques (third edition)*, G. T. Hermanson, Ed. (Academic Press, Boston, 2013), pp. 549-587.

78. G. T. Hermanson, in *Bioconjugate techniques (third edition)*, G. T. Hermanson, Ed. (Academic Press, Boston, 2013), pp. 275-298.

79. O. Barbosa *et al.*, Heterofunctional supports in enzyme immobilization: From traditional immobilization protocols to opportunities in tuning enzyme properties. *Biomacromolecules* **14**, 2433-2462 (2013).

80. A. A. Homaei, R. Sariri, F. Vianello, R. Stevanato, Enzyme immobilization: An update. *J Chem Biol* **6**, 185-205 (2013).

81. R. C. Rodrigues, Á. Berenguer-Murcia, D. Carballares, R. Morellon-Sterling, R. Fernandez-Lafuente, Stabilization of enzymes via immobilization: Multipoint covalent attachment and other stabilization strategies. *Biotechnol. Adv.* **52**, 107821 (2021).

82. C. P. R. Hackenberger, D. Schwarzer, Chemoselective ligation and modification strategies for peptides and proteins. *Angew. Chem. Int. Ed.* **47**, 10030-10074 (2008).

83. E. M. Sletten, C. R. Bertozzi, Bioorthogonal chemistry: Fishing for selectivity in a sea of functionality. *Angew. Chem. Int. Ed.* **48**, 6974-6998 (2009).

84. O. Boutureira, G. J. L. Bernardes, Advances in chemical protein modification. *Chem. Rev.* **115**, 2174-2195 (2015).

85. J. N. deGruyter, L. R. Malins, P. S. Baran, Residue-specific peptide modification: A chemist's guide. *Biochemistry* **56**, 3863-3873 (2017).

86. J. C. Vantourout *et al.*, Serine-selective bioconjugation. *J. Am. Chem. Soc.* **142**, 17236-17242 (2020).

87. R. Fernandez-Lafuente, P. Armisén, P. Sabuquillo, G. Fernández-Lorente, J. M. Guisán, Immobilization of lipases by selective adsorption on hydrophobic supports. *Chem. Phys. Lipids* **93**, 185-197 (1998).

88. C. Ortiz *et al.*, Novozym 435: The "perfect" lipase immobilized biocatalyst? *Catalysis Science & Technology* **9**, 2380-2420 (2019).

89. L. Veum, M. Kuster, S. Telalovic, U. Hanefeld, T. Maschmeyer, Enantioselective synthesis of protected cyanohydrins. *Eur. J. Org. Chem.* **2002**, 1516-1522 (2002).

90. B. M. Brena, F. Batista-Viera, in *Immobilization of enzymes and cells*, J. M. Guisan, Ed. (Humana Press, Totowa, NJ, 2006), pp. 15-30.

91. S. Fornera, T. E. Balmer, B. Zhang, A. D. Schlüter, P. Walde, Immobilization of peroxidase on sio2 surfaces with the help of a dendronized polymer and the avidin-biotin system. *Macromol. Biosci.* **11**, 1052-1067 (2011).

92. K. Holland-Nell, A. G. Beck-Sickinger, Specifically immobilised aldo/keto reductase akr1a1 shows a dramatic increase in activity relative to the randomly immobilised enzyme. *ChemBioChem* **8**, 1071-1076 (2007).

93. L. Zhou *et al.*, Facile oriented immobilization and purification of his-tagged organophosphohydrolase on viruslike mesoporous silica nanoparticles for organophosphate bioremediation. *ACS Sustainable Chemistry & Engineering* **6**, 13588-13598 (2018).

94. D. Quaglia *et al.*, His-tagged horse liver alcohol dehydrogenase: Immobilization and application in the bio-based enantioselective synthesis of (s)-arylpropanols. *Process Biochem.* **48**, 810-818 (2013).

95. G. E. Jeromin, Superabsorbed alcohol dehydrogenase—a new catalyst for asymmetric reductions. *Biotechnology Letters* **31**, 1717 (2009).

96. M. Heidlindemann, G. Rulli, A. Berkessel, W. Hummel, H. Gröger, Combination of asymmetric organo- and biocatalytic reactions in organic media using immobilized catalysts in different compartments. *ACS Catal.* **4**, 1099-1103 (2014).

97. M. L. Contente, F. Paradisi, Self-sustaining closed-loop multienzyme-mediated conversion of amines into alcohols in continuous reactions. *Nat. Catal.* **1**, 452-459 (2018).

98. S. Velasco-Lozano, A. I. Benítez-Mateos, F. López-Gallego, Co-immobilized phosphorylated cofactors and enzymes as self-sufficient heterogeneous biocatalysts for chemical processes. *Angew. Chem. Int. Ed.* **56**, 771-775 (2017).

99. A. I. Benítez-Mateos *et al.*, Asymmetric reduction of prochiral ketones by using self-sufficient heterogeneous biocatalysts based on nadph-dependent ketoreductases. *Chemistry – A European Journal* **23**, 16843-16852 (2017).

100. H. Seelajaroen, A. Bakandritsos, M. Otyepka, R. Zbořil, N. S. Sariciftci, Immobilized enzymes on graphene as nanobiocatalyst. *ACS Appl. Mater. Interfaces* **12**, 250-259 (2020).

101. X. Wang, P. C. Lan, S. Ma, Metal–organic frameworks for enzyme immobilization: Beyond host matrix materials. *ACS Central Science* **6**, 1497-1506 (2020).

102. W.-H. Chen, M. Vázquez-González, A. Zoabi, R. Abu-Reziq, I. Willner, Biocatalytic cascades driven by enzymes encapsulated in metal–organic framework nanoparticles. *Nat. Catal.* **1**, 689-695 (2018).

103. T. Man *et al.*, Hierarchically encapsulating enzymes with multi-shelled metal-organic frameworks for tandem biocatalytic reactions. *Nat. Commun.* **13**, 305 (2022).

104. F. Lyu, Y. Zhang, R. N. Zare, J. Ge, Z. Liu, One-pot synthesis of protein-embedded metal–organic frameworks with enhanced biological activities. *Nano Lett.* **14**, 5761-5765 (2014).

105. C. Hou *et al.*, Facile synthesis of enzyme-embedded magnetic metal–organic frameworks as a reusable mimic multi-enzyme system: Mimetic peroxidase properties and colorimetric sensor. *Nanoscale* **7**, 18770-18779 (2015).

106. F.-K. Shieh *et al.*, Imparting functionality to biocatalysts via embedding enzymes into nanoporous materials by a de novo approach: Size-selective sheltering of catalase in metal–organic framework microcrystals. *J. Am. Chem. Soc.* **137**, 4276-4279 (2015).

107. K. Würges, P. H. Pfromm, M. E. Rezac, P. Czermak, Activation of subtilisin carlsberg in hexane by lyophilization in the presence of fumed silica. *J. Mol. Catal. B: Enzym.* **34**, 18-24 (2005).

108. J. C. Cruz, P. H. Pfromm, M. E. Rezac, Immobilization of candida antarctica lipase b on fumed silica. *Process Biochem.* **44**, 62-69 (2009).

109. A. E. David, N. S. Wang, V. C. Yang, A. J. Yang, Chemically surface modified gel (csmg): An excellent enzyme-immobilization matrix for industrial processes. *J. Biotechnol.* **125**, 395-407 (2006).

110. W. Stöber, A. Fink, E. Bohn, Controlled growth of monodisperse silica spheres in the micron size range. *J. Colloid Interface Sci.* **26**, 62-69 (1968).

111. K. Möller, T. Bein, Talented mesoporous silica nanoparticles. *Chem. Mater.* **29**, 371-388 (2017).

112. C.-Y. Lai *et al.*, A mesoporous silica nanosphere-based carrier system with chemically removable cds nanoparticle caps for stimuli-responsive controlled release of neurotransmitters and drug molecules. *J. Am. Chem. Soc.* **125**, 4451-4459 (2003).

113. C.-H. Lee, T.-S. Lin, C.-Y. Mou, Mesoporous materials for encapsulating enzymes. *Nano Today* **4**, 165-179 (2009).

114. P. S. Nabavi Zadeh, B. Åkerman, Immobilization of enzymes in mesoporous silica particles: Protein concentration and rotational mobility in the pores. *The Journal of Physical Chemistry B* **121**, 2575-2583 (2017).

115. L. Bayne, R. V. Ulijn, P. J. Halling, Effect of pore size on the performance of immobilised enzymes. *Chem. Soc. Rev.* **42**, 9000-9010 (2013).

116. R. A. Sheldon, Characteristic features and biotechnological applications of cross-linked enzyme aggregates (cleas). *Appl. Microbiol. Biotechnol.* **92**, 467-477 (2011).

117. J. Cui, S. Jia, L. Liang, Y. Zhao, Y. Feng, Mesoporous cleas-silica composite microparticles with high activity and enhanced stability. *Sci. Rep.* **5**, 14203 (2015).

118. M. L. Briand, M. Bikaki, C. Puorger, P. F. X. Corvini, P. Shahgaldian, A proteolytic nanobiocatalyst with built-in disulphide reducing properties. *RSC Advances* **11**, 810-816 (2021).

119. M. R. Correro, M. Takacs, S. Sykora, P. F. X. Corvini, P. Shahgaldian, Supramolecular enzyme engineering in complex nanometer-thin biomimetic organosilica layers. *RSC Advances* **6**, 89966-89971 (2016).

120. C. I. Giunta *et al.*, Tuning the properties of natural promiscuous enzymes by engineering their nano-environment. *ACS Nano* **14**, 17652-17664 (2020).

121. M. L. Briand *et al.*, Partially shielded enzymes capable of processing large protein substrates. *Chem. Commun.* **56**, 5170-5173 (2020).

122. I. I. Slowing, J. L. Vivero-Escoto, C.-W. Wu, V. S. Y. Lin, Mesoporous silica nanoparticles as controlled release drug delivery and gene transfection carriers. *Adv. Drug Del. Rev.* **60**, 1278-1288 (2008).

123. E. Caponetti, A. Minoja, M. L. Saladino, A. Spinella, Characterization of nd–mcm-41 obtained by impregnation. *Microporous Mesoporous Mater.* **113**, 490-498 (2008).

124. A. Stein, B. J. Melde, R. C. Schroden, Hybrid inorganic–organic mesoporous silicates—nanoscopic reactors coming of age. *Adv. Mater.* **12**, 1403-1419 (2000).

125. D. R. Radu *et al.*, A polyamidoamine dendrimer-capped mesoporous silica nanosphere-based gene transfection reagent. *J. Am. Chem. Soc.* **126**, 13216-13217 (2004).

126. D. Shen *et al.*, Biphase stratification approach to three-dimensional dendritic biodegradable mesoporous silica nanospheres. *Nano Lett.* **14**, 923-932 (2014).

127. E. Gasteiger *et al.*, in *The proteomics protocols handbook*, J. M. Walker, Ed. (Humana Press, Totowa, NJ, 2005), pp. 571-607.

128. M. M. Musa, K. I. Ziegelmann-Fjeld, C. Vieille, J. G. Zeikus, R. S. Phillips, Asymmetric reduction and oxidation of aromatic ketones and alcohols using w110a secondary alcohol dehydrogenase from thermoanaerobacter ethanolicus. *J. Org. Chem.* **72**, 30-34 (2007).

129. M. M. Musa *et al.*, Racemization of enantiopure secondary alcohols by thermoanaerobacter ethanolicus secondary alcohol dehydrogenase. *Org. Biomol. Chem.* **11**, 2911-2915 (2013).

130. H. Man *et al.*, Structures of alcohol dehydrogenases from ralstonia and sphingobium spp. Reveal the molecular basis for their recognition of 'bulky–bulky' ketones. *Top. Catal.* **57**, 356-365 (2014).

131. I. Lavandera *et al.*, One-way biohydrogen transfer for oxidation of sec-alcohols. *Org. Lett.* **10**, 2155-2158 (2008).

132. D. Tischler *et al.*, Asymmetric reduction of (r)-carvone through a thermostable and organic-solvent-tolerant ene-reductase. *ChemBioChem* **21**, 1217-1225 (2020).

133. D. J. Opperman, Structural investigation into the c-terminal extension of the ene-reductase from ralstonia (cupriavidus) metallidurans. *Proteins: Structure, Function, and Bioinformatics* **85**, 2252-2257 (2017).

134. F. W. Studier, Protein production by auto-induction in high-density shaking cultures. *Protein Expression Purif.* **41**, 207-234 (2005).

135. A. Kumar, C. K. Dixit, in *Advances in nanomedicine for the delivery of therapeutic nucleic acids*, S. Nimesh, R. Chandra, N. Gupta, Eds. (Woodhead Publishing, 2017), pp. 43-58.

136. Y. Liu *et al.*, Molecular orientation of enzymes attached to surfaces through defined chemical linkages at the solid–liquid interface. *J. Am. Chem. Soc.* **135**, 12660-12669 (2013).

137. R. L. Policarpo *et al.*, Flow-based enzymatic ligation by sortase a. *Angew. Chem. Int. Ed.* **53**, 9203-9208 (2014).

138. T. Inokuchi, S. Matsumoto, S. Torii, Indirect electrooxidation of alcohols by a double mediatory system with two redox couples of [r2n+:O]/r2no.Cntdot. And [br.Cntdot. Or br+]/br- in an organic-aqueous two-phase solution. *J. Org. Chem.* **56**, 2416-2421 (1991).

139. G. Zhang *et al.*, Anti-markovnikov oxidation of β-alkyl styrenes with h2o as the terminal oxidant. *J. Am. Chem. Soc.* **138**, 12037-12040 (2016).

140. T. C. Atack, S. P. Cook, Manganese-catalyzed borylation of unactivated alkyl chlorides. *J. Am. Chem. Soc.* **138**, 6139-6142 (2016).

141. S. Rezazadeh, V. Devannah, D. A. Watson, Nickel-catalyzed c-alkylation of nitroalkanes with unactivated alkyl iodides. *J. Am. Chem. Soc.* **139**, 8110-8113 (2017).